ABSTRACT

Title of Document: RESOURCE ALLOCATION IN RELAY-BASED SATELLITE AND WIRELESS COMMUNICATION NETWORKS

Hui Zeng, Doctor of Philosophy, 2008

Directed By: Professor John S. Baras, Department of Electrical and Computer Engineering

A two-level bandwidth allocation scheme is proposed for a slotted Time-Division Multiple Access high data rate relay satellite communication link to provide efficient and fair channel utilization. The long-term allocation is implemented to provide per-flow/per-user Quality-of-Service guarantees and shape the average behavior. The time-varying short-term allocation is determined by solving an optimal timeslot scheduling problem based on the requests and other parameters. Through extensive simulations, the performance of a suitable MAC protocol with two-level bandwidth allocation is analyzed and compared with that of the existing static fixed-assignment scheme in terms of end-to-end delay and successful throughput. It is also shown that pseudo-proportional fairness is achieved for our hybrid protocol.

We study rate control systems with heterogeneous time-varying propagation delays, based on analytic fluid flow models composed of first-order delay-differential equations. Both single-flow and multi-flow system models are analyzed, with special

attention paid to the Mitra-Seery algorithm. The stationary solutions are investigated. For the fluctuating solutions, their dynamic behavior is analyzed in detail, analytically and numerically, in terms of amplitude, transient behavior, fairness and adaptability, etc.. Especially the effects of heterogeneous time-varying delays are investigated. It is shown that with proper parameter design the system can achieve stable behavior with close to pointwise proportional fairness among flows.

Finally we investigate the resource allocation in 802.16j multi-hop relay systems with rate fairness constraints for two mutually exclusive options: transparent and non-transparent relay systems (T-RS and NT-RS). Single-Input Single-Output and Multi-Input Multi-Output antenna systems are considered in the links between the Base Station (BS) and Relay Stations (RS). 1 and 3 RSs per sector are considered. The Mobile Station (MS) association rule, which determines the access station (BS or RS) for each MS, is also studied. Two rules: *Highest MCS scheme* with the highest modulation and coding rate, and *Highest* (*Mod*) *ESE scheme* with the highest (modified) effective spectrum efficiency, are studied along with the optimal rule that maximizes system capacity with rate fairness constraints. Our simulation results show that the highest capacity is always achieved by NT-RS with 3 RSs per sector in distributed scheduling mode, and that the *Highest* (*Mod*) *ESE scheme* performs closely to the optimal rule in terms of system capacity.

RESOURCE ALLOCATION IN RELAY-BASED SATELLITE AND WIRELESS COMMUNICATION NETWORKS

By

Hui Zeng

Dissertation submitted to the Faculty of the Graduate School of the
University of Maryland, College Park, in partial fulfillment
of the requirements for the degree of
Doctor of Philosophy
2008

Advisory Committee:
Professor John S. Baras, Chair
Professor Prakash Narayan
Professor Richard J. La
Professor Raymond E. Miller
Professor Paul J. Smith

DEDICATION

To my Parents, my wife Hong and our daughter Sophia

ACKNOWLEDGEMENTS

First and foremost, I would like to thank my advisor, Professor John S. Baras, for his encouragement and support during my studies. Without his academic guidance and support, the completion of this dissertation would not have been possible. The knowledge and experience I have acquired from working with him have been invaluable to me. I am also grateful to Doctor Michael Hadjitheodosiou for his academic co-advising and help during the first half of my studies till 2006.

I would also like to thank my committee members, Professors Prakash Narayan, Richard J. La, Raymond E. Miller and Paul J. Smith, for kindly reviewing my dissertation and serving on my dissertation committee despite their busy schedules.

My thanks also go to the staff of the Institute for Systems Research (ISR) and the Maryland Hybrid Networks Center (HyNet). Special thanks go to Kimberly Edwards, Althia Kirlew, Diane Hicks and Alexis Jenkins. I am also grateful for the financial support of my research and studies from HyNet under the National Aeronautics and Space Administration (NASA) cooperative agreement NCC8-235 and NASA cooperative agreement NAG3-2844.

I am also thankful for the financial support from Fujitsu Laboratories of America (FLA) of my research in areas of analysis and design for WiMAX 802.16 networks. My thanks especially go to Doctor Chenxi Zhu and Vice President Jonathan Agre for their excellent supervision and great help in so many ways. I have gained so much from working with them for the past fifteen months.

I extend my gratitude to my colleagues, officemates and friends for their companionship, academic support and help in many ways: Yadong Shang, Xiaoming Zhou, Huigang Chen, Shaoxiong Hua, Tao Jiang, Georgios Papageorgiou, Ayan Roy-Chowdhury, Pedram Hovareshti, Nicolas Rentz and Yingyong Chen.

Last, but not the least, I express my sincere gratitude to my family. I want to thank my parents for their spiritual support throughout my education and my life. I am especially thankful to my lovely wife, Hong Wang, for her constant love, support and patience during all these years. This dissertation is dedicated to them.

TABLE OF CONTENTS

LIST OF FIGURES

1. Introduction

Intermediate relay nodes have been widely used in both satellite and wireless communication networks, generally for the purposes of coverage extension, capacity enhancement, fast or temporary service provision, or any combination of the above. In this dissertation, two types of relay-based systems are investigated: relay-based satellite systems where the spacecraft (or any other ground users) communicate with a centralized ground station through a broadband relay satellite; and IEEE 802.16j multi-hop relay systems, also known as Worldwide Interoperability for Microwave Access (WiMAX) Mobile Multi-hop Relay (MMR) systems.

1.1. Broadband Relay-Based Satellite Communication Networks

Satellite systems have a key role to play as a global integrated services provider, due to the wide coverage of satellite footprints together with their broadcasting capability [1]. High-capacity satellite links are a promising medium for transporting not only voice and bulk data traffic, but also high-speed Internet content, virtually to everywhere in the world without the extra cost of cabling and maintenance.

Satellites can be in different orbits, such as low earth orbit (LEO), medium earth orbit (MEO) and geo-synchronous orbit (GEO). Also satellites can be classified as bent-pipe satellites and on-board process (OBP) satellites. Bent-pipe satellites are simply signal repeaters which merely receive, amplify and send traffic without extra processing. Bent pipe point-to-point and star topologies are shown in Figure 1.1. The

remote sites could be on the ground like Very Small Aperture Terminals (VSAT), or in space like spacecraft, which only affects the complexity of the implementation.

Satellite systems are moving in a new direction from their traditional voice service to emerging data communication services, due to the growth in data and video applications. Being compatible with Internet-based terrestrial networks, the next generation of satellite systems will support both connection-oriented and connectionless traffic over a broadband channel, particularly using the Internet protocol (IP). In addition, satellite systems often need to provide dynamic support and guarantees of different quality-of-service (QoS) upon user demands, sometimes under a bursty error environment. To achieve this, the underlying medium access control (MAC) protocol plays an important role and therefore needs suitable designs.

Clearly, the ability to utilize all the recent advances in communication technologies could allow investigators on Earth to enjoy a virtual presence in space, but this generates a need to provide high quality communication support that will enable cost effective global access to experimental data from future space missions, and an efficient way to disseminate these data to a large and diverse pool of users. For all these reasons, it might be beneficial to consider an approach that gradually facilitates broadband Internet services throughout future space missions, eventually leading to a scenario where every spacecraft and instrument can be an addressable node and has a direct connection to the Internet. NASA is already exploring several evolutionary approaches that will enable the gradual transition of today's operational scenario into a more flexible, IP-compatible environment in the near future, utilizing technology available today [2]. A key to improving the cost-effectiveness of future

space missions is to adopt (where possible) available industry standards and off-the-shelf software & hardware. Technically, the Internet Protocol IP can work in space. Recent studies demonstrated that this is possible [3,4,5] and outlined the functional building blocks and the system engineering work that remains to be done.

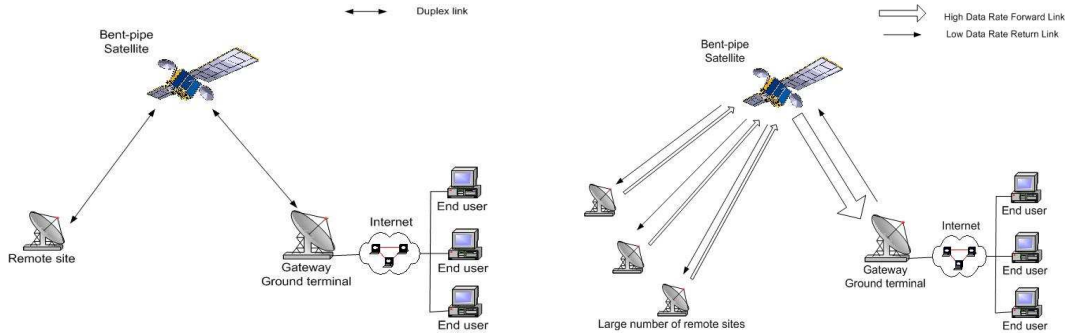

(a) Bent pipe point-to-point topology (b) Bent pipe star topology

Figure 1.1: Satellite Communication Network Topologies

Several aspects of extending IP-in-Space have already been demonstrated:

- IP in small spacecraft: The 1994 CCSDS STRV Dera (U.K. DoD spacecraft) and the 1999 UoSat-12 are some early examples of small spacecraft with IP functionality. The UoSat-12 satellite has demonstrated a working IP-stack and more IP-enabled spacecraft are now operational or in development [6].
- The CANDOS payload (Feb 2003) demonstrated UDP, Mobile IP and other protocol performance from the Space Shuttle, connecting via NASAs TDRS relay satellite [7].
- The first Mobile Router demonstration in space involved a CISCO Mobile Access Router (MAR3251) demonstration on one of the UK-DMC Satellites that was launched Sept 2003 [8].

An end-to-end communication architecture for future space missions, using the Internet Protocol (IP) as the "glue" that connects everything together is clearly

feasible. IP provides a basic standardized mechanism for end-to-end communication between applications across a network. This will lead to an environment where most spacecraft could have an IP router on board and instruments on the spacecraft can become addressable nodes, connected with an on-board LAN. Spacecraft environments still pose numerous specific challenges but most of these have direct analogs in the ground-based mobile IP and wireless networking industries, such as:

- Intermittent communication links.
- Highly asymmetric or unidirectional communication links.
- Bit error rates higher than most terrestrial wired links.
- Multiple mobile nodes forming a dynamic network topology.
- High mobility (velocity), but often very predictable, since most spacecraft move along pre-defined orbits and their locations may be easily predicted.

In order to use IP in space, the basic Internet datagram delivery service over the space RF links need to be established first. We assume that issues related to the lower layers such as FEC, Reed-Solomon coding, antenna and power issues and all related challenges in delivering bits at a needed rate across the space link can be solved with current State-of-the-Art techniques or enhancements that will soon be available for even more efficient performance.

Resource Allocation in Broadband Relay-Based Satellite Systems

The round-trip transmission (up and down) to a GEO satellite (one hop), roughly 36,000 km above the earth, is approximately 0.24 sec if the satellite is directly overhead, and is roughly 0.27 sec if the satellite is near the horizon. Our primary concern is to dynamically allocate the resources to all users in the system in a fair and

efficient way with QoS guarantees. The main problems are the limited resources and the time-varying long propagation delays.

We focus on resource allocation in space communications with bent pipe satellites, where a number of IP-addressable spacecraft (LEO, MEO, space shuttle, ISS, etc.) are sharing the broadband downlink channel of GEO relay systems (TDRSS or other commercial systems). Each relay satellite is a bent pipe satellite with a direct link to a specific ground terminal. Highly asymmetric links, the long propagation delay, the mobility of spacecraft and the limitation of buffer space on-board the spacecraft make it difficult and unique to achieve the following requirements:

1) High resource utilization or efficiency: Satellite capacity is a scarce resource and therefore efficiency is very important.
2) Good Admission Control algorithm and QoS framework: They must be well-coupled to provide different QoS guarantees for the users (spacecraft) and all the flows. It must be compatible with the terrestrial IP QoS framework.
3) Variable service classes: This is also a must for providing different QoS guarantees for different types of users or flows. In addition, it provides a possibility to prefer some service classes to others.
4) Fairness: Although there are different definitions of fairness, the basic principle is to avoid systematical unfair resource allocation among users. And the resource allocation management should be flexible. One important consideration is the queue management on-board the spacecraft.

The errors or channel fading mainly occur in the link between the relay satellite and the ground terminals, which is the common path for the users sharing the same

downlink channel. A simple way to model this fading channel is bandwidth reduction [9]. Basically, a factor β_m, a real number in the interval [0, 1], is defined according to a certain fading level m. This parameter exactly represents the bandwidth reduction due to the adoption of a Forward Error Correction (FEC) scheme. Hence, the relation between the actual bandwidth (BW_m) and the nominal bandwidth (BW) is:

$$BW_m = \beta_m * BW \tag{1.1}$$

The results can be extended to any planetary communication network (Moon vicinity network, Mars vicinity network, Earth-Moon communication network and Earth-Mars communication network, etc.) [10].

Flexible Dynamic Communication Architecture for Lunar Exploration

The new phase of space exploration involves a growing number of human and robotic missions with varying communication and service requirements. These will include continuous, maximum coverage of areas of concentrated activities, such as in the vicinity of in-space planetary outposts and orbiting missions (single spacecraft or constellations) around the Earth, Moon or Mars. These nodes would be connected back to Earth through a broadband backbone and relay infrastructure. This Space Information Highway would serve the dual role of providing virtual presence to space, mission telemetry and control and coordination between missions but also broadband capability to download collected data back to Earth.

Several network topologies that involve a space component are possible. Most of the proposed topologies are for scientific interplanetary communications, with satellites acting as relays to connect remote networks on distant planets to networks on Earth. The resulting networks form hierarchical hybrid meshes and present

interesting challenges to overcome the constraint of long propagation delay, ensure robustness against fluctuations in satellite channel conditions due to atmospheric changes.

Our work in this dissertation on resource allocation in space communication networks is also related to communication network design for lunar exploration. This network shares similarities with terrestrial wireless network and sensor network architectures. However, the issues related to performance and robustness are different due to the long delay over the inter-satellite links, the limited power of the space nodes, the special hardware required to support functionality in space, and very different conditions on the lunar surface. Therefore solutions that are geared towards terrestrial wireless networks might not be suitable for the interplanetary network we consider; instead, our study of space communication networks around Earth can be extended to the communication network for lunar exploration.

In our view, a space network for lunar exploration consists of one or more small clusters of wireless networks on the remote planetary surface, which are connected by long-distance broadband links to heterogeneous terrestrial networks. Some important design considerations for such a space exploration network are listed as follows:

- The number of missions might grow and any mission might evolve, with varying communication and service requirements. Evolution of a mission would impact the size and/or topology of the network.
- On the remote planetary surface, the areas of concentrated activities would require continuous coverage by the satellites.
- There might be orbiting missions of single spacecraft or constellations.

- The long-distance broadband backbone should have the capability to upload mission telemetry and control data to the remote outposts, and download collected mission data to the command centers on Earth. There might also be the requirement for coordination between different missions using the satellite broadband backbone.
- The network backbone should be capable of supporting a wide range of data rates – from a few *kilobits per second* (Kbps) in the case of command and telemetry traffic, to several *gigabits per second* (Gbps) in the case of collected science data downloaded to Earth centers.
- The utilization of the network links would be variable in time – there would be periods of idle time or low keep-alive interchanges, followed by periods of full utilization.
- The link delays would vary from a few milliseconds (for example, in the case of surface wired/wireless links) to a few seconds or minutes (for example, in the case of an inter-planetary link between Earth and a remote planet).

1.2. IEEE 802.16j Multi-hop Relay Systems

Broadband wireless network technologies attract increasing attentions for providing flexible broadband access to the Internet while moving. As one of the latest wireless technologies with high data rate and large coverage area, IEEE 802.16 [11] has been proposed to serve as a promising alternative to broadband wireline networks. IEEE 802.16e Orthogonal Frequency-Division Multiple Access (OFDMA) introduces support for mobility, amongst other things and is therefore also referred to mobile WiMAX [12]. With the rapid growth of wireless data services and multimedia

applications, it is expected that IEEE 802.16e systems will provide QoS differentiation and guarantees for different classes.

Initial field trials of mobile WiMAX products showed that the IEEE 802.16e system has limited coverage and provides poor QoS for indoor users as well as users at cell boundaries. To address this issue, since 2006 IEEE 802.16j Multihop Relay (MR) Task Group has been working to define a new relay station (RS) which can be used as an extension to the Base Station (BS) and relay traffic between the BS and the mobile station (MS). A RS communicates with the BS through a wireless channel and can operate without additional carrier frequencies. This eliminates the need for a wired or a dedicated wireless connection to the backhaul network and significantly reduces the installation and operation cost compared with using micro-BS to cover these areas. By replacing the direct link between a BS and a MS in a poor coverage area with two links (the link from BS to RS is called relay link, and the link from RS to MS is called access link) with better channel quality, the network capacity may be increased. Additional functions to support relay is needed in the BS, and a BS which incorporates these new functions are called a MR-BS. The 802.16j RS is fully backward compatible to an 802.16e MS, meaning an MS can be supported by an 802.16j relay network without any change.

In the 802.16j standard draft D2, two types of RS are defined from the PHY point of view. The first type of RS, non-transparent RS (NT-RS), transmits all the control signals as well as data packets like a normal BS to the MS. The coverage area of a non-transparent RS is the same as that of a micro-BS with similar transmission power, so deployment of non-transparent RSs in a cell may extend the coverage area

of the MR-BS as well as enhancing the cell capacity. The second type of RS, transparent RS (T-RS), does not transmit control signals including frame-start preamble (used by MS for network synchronization and BS identification), FCH and MAP (received by MS for transmission scheduling); instead, a MS depends on these control signals transmitted by the MR-BS. The control signals are usually transmitted with a more robust modulation and coding scheme (MCS) and determine the network coverage. Consequently a transparent RS can not be used to extend cell coverage but only to increase network capacity. The two different types of RS also have different and incompatible frame structures and offer different network capacities. In centralized scheduling mode, a MR-BS generates the transmission schedule for its associated RS. While in distributed scheduling mode, a RS generates its own transmission schedule to its MSs. Because a T-RS does not transmit control signals, its transmission schedule is generated by the MR-BS. A non-transparent RS can operate in either centralized or distributed scheduling mode.

System Design and Resource Allocation in 802.16j Multi-hop Relay Systems

It is worthwhile to conduct a detailed comparison study of these options to understand the benefits and limits of each option. For each option, a system design approach is necessary to determine the frame partition for the usage of different links among the BS, RSs and MSs. Special attention also needs to be paid to the MS association rule in determining the access station between the MR-BS and the RSs. The effect of increasing the number of deployed RSs per sector, and the usage of Single-Input Single-Output (SISO) or Multi-Input Multi-Output (MIMO) in the relay

links also need to be investigated. All the above studies have to be considered in a framework with a certain fairness constraint among all users (MSs).

1.3. Contributions of the Dissertation

The contributions of the dissertation are listed below within three different areas:

***Flexible Access for the Downlink of Relay-based Space Communication Networks*:**

- A two-level bandwidth allocation scheme is proposed in a slotted TDMA protocol in a space relay topology with the high data rate downlink. Through simulation results, it is shown that our scheme outperforms the existing fixed-assignment TDMA scheme in terms of end-to-end delay, throughput and fairness.
- Novel communication architectures for lunar exploration are considered for the design and evaluation of our hybrid TDMA scheme. Special attention is paid to the important requirements for future space missions that influence the design of this network.

***Dynamic Behavior of the Rate Control Systems with Heterogeneous Time-varying Propagation Delays*:**

- Analytic fluid models composed of first-order delay-differential equations are formulated with consideration of heterogeneous time-varying propagation delays for the systems with single flow and multiple flows, respectively.
- Stationary solutions including their existence conditions and convergence speed are presented for the single-flow and multi-flow systems, respectively.
- The system dynamic behavior (rate and queue size) of fluctuating solutions are analyzed and shown to be bounded although aperiodic.

- The effect of delays and parameter design are investigated in terms of fairness, fluctuation amplitude and period, transient time and adaptability, etc.

***System Design and Resource Allocation in Multi-hop Relay WiMAX Systems*:**

- A detailed system level performance evaluation and system design analysis for different types of multi-hop relay WiMAX systems has been carried out.
- A system design approach is proposed to evaluate the per-user throughput and total system capacity in two mutually exclusive options of multi-hop relay WiMAX systems: transparent relay system (T-RS) and non-transparent relay system (NT-RS).
- The optimal mobile station (MS) association rules are derived in T-RS and NT-RS, respectively. Two heuristic MS association rules are proposed and compared along with the optimal rules.
- One of two heuristic MS association rules, *Highest (Modified) ESE Scheme* has been shown to be optimal for the T-RS. Although it is suboptimal for the NT-RS, it has the system capacity close to the optimal rule with much less information exchange and computation time required.

1.4. Organization of the Dissertation

Brief literature overviews are given in Chapter 2 in areas of MAC protocols and scheduling algorithms in communication networks, including satellite, wireline and wireless systems.

In Chapters 3 – 4, we present the details of our dynamic resource allocation problems and proposed solutions in the context of broadband IP-based satellite communication networks.

Chapter 3 first investigates the traffic characteristics in satellite communication networks considered. Different types of traffic sources have different statistics and QoS requirements, and hence need different treatment. Constant Bit Rate (CBR) and on/off traffic sources are two general types to be considered. According to the different requirements, each traffic source provides its bandwidth triple request: LR (Lower Resource), TR (Targeted Resource) and UR (Upper Resource), and its priority level and weight when trying to get access to the broadband satellite network. A fact that needs to be emphasized is that the users (spacecraft or earth stations) need to have advanced algorithms to provide estimates of their resource requirements. In addition, Chapter 3 also presents a suitable slotted hybrid-mode Time-Division Multiple Access (TDMA) scheme to achieve the efficient, dynamic and fair utilization of the broadband channel of a bent-pipe relay GEO satellite.

Chapter 4 proposes a two-level bandwidth allocation scheme for the slotted TDMA broadband relay-based satellite communication link. The long-term allocation is implemented to provide per-flow/per-user QoS guarantees and shape the average behavior. The time-varying short-term allocation is determined by solving an optimal timeslot scheduling problem based on the requests and other parameters. Some ideas from recent work [13, 14] are incorporated to formulate the timeslot assignment problem and find its optimal solution. The bandwidth allocation is performed on a per-frame or multi-frame base. After guaranteeing CBR traffic, we want to take advantage of the on/off nature of most traffic sources. In many applications like voice or video and data communications, if a source transmits a packet to a destination in a frame, it is very possible that it will also transmit a packet to the same destination in

the next frame. So it is not necessary to schedule incoming packets for every frame if we can preserve all the switching patterns for the nearest scheduled frame and update the patterns appropriately according to the changes of traffic demands. Through extensive simulations, the performance of our MAC protocol with two-level bandwidth allocation is analyzed and compared with that of the existing static fixed-assignment scheme in terms of end-to-end delay and successful throughput. It is also shown that pseudo-proportional fairness is achieved by our hybrid protocol.

Chapter 5 studies rate control systems with heterogeneous time-varying propagation delays, based on analytic fluid flow models composed of first-order delay-differential equations. Both single-flow and multi-flow system models are analyzed, with special attention paid to the Mitra-Seery algorithm. The stationary solutions are investigated. For the fluctuating solutions, the dynamic behavior is analyzed in detail, analytically and numerically, in terms of amplitude, transient behavior, fairness and adaptability, etc.. Especially the effect of heterogeneous time-varying delays is investigated. It is shown that with the proper parameter design the system can achieve stable behavior with close to pointwise proportional fairness among flows.

Chapter 6 investigates resource allocation in 802.16j multi-hop relay systems under the user (MS) rate fairness constraint for two mutually exclusive options: transparent relay system (T-RS) and non-transparent relay system (NT-RS). SISO and MIMO antenna systems are considered in the links between the BS and RS. 1 and 3 RSs per sector are considered. Our simulation results show that the highest capacity is always achieved by NT-RS with 3 RSs per sector in distributed scheduling mode.

Furthermore, the MS association rule, which determines the access station (BS or RS) for each MS, is also studied. Two rules: *Highest MCS scheme* with the highest modulation and coding rate, and *Highest* (*Mod*) *ESE scheme* with the highest (modified) effective spectrum efficiency, are studied along with the optimal rule that maximizes system capacity with rate fairness constraints. It is shown that the *Highest* (*Mod*) *ESE scheme* performs closely to the optimal rule in terms of system capacity.

2. Overview of Resource Allocation in Communication Networks

The multiple access issue arises from the necessity of sharing a single link or channel among a number of users, whether geographically distributed or not. The sharing algorithm is called MAC protocol. Based on techniques and domains, there are basically three forms of multiple access schemes: [15]

- Frequency-Division Multiple Access (FDMA)
- Time-Division Multiple Access (TDMA)
- Code-Division Multiple Access (CDMA)

In FDMA, there is no interference among different users since the assigned frequency bands are well separated by guard bands. Also, it is simple to implement and allows the use of smaller antennas at earth stations when compared with ordinary TDMA and CDMA. However, it provides little flexibility for dynamic resource management and has some implementation difficulties in dealing with inter-modulation (IM) products during the amplification process in the satellite gateway transponder due to the non-linear power amplifiers [16].

TDMA systems divide the radio spectrum into time slots, where each user gets the total link capacity for limited time intervals. The data are transmitted in a buffer-and-burst method; therefore for any user the transmission is non-continuous. Thus, digital data and digital modulation must be used with TDMA, unlike accommodating analog FM in FDMA. The advances in digital communication give TDMA systems the advantage of highly flexible dynamic bandwidth allocation and hence efficient usage

of the channel. Bandwidth can be supplied on demand to different users by concatenating or reassigning time slots based on priority and fairness. Also, discontinuous transmissions result in low power consumption, since the user transmitter can be turned off when not in use. Moreover, no IM products are presented due to the exclusive use of the whole channel in a given time duration. However, TDMA has its own disadvantages. High synchronization overhead is necessary because of the burst nature of TDMA transmissions, and guard times or slots are also required to separate users. Both of them result in larger overhead in TDMA systems as compared with FDMA. In addition, each user has to have sufficiently high transmission power and large antennas fit for the high channel capacity when exclusively using it. To combat this problem, a hybrid of FDMA and TDMA, Multi-Frequency TDMA (MF-TDMA), is in usage for broadband IP-based satellite networks. In MF-TDMA systems, the total capacity is divided into different frequency bands and each of them is used in the sense of TDMA. Each user can transmit data in one of these frequency bands in a specific time slot. Since the whole channel is segmented into smaller bands, the size of antenna and the level of transmission power are reduced in each user.

In CDMA systems, the narrowband message signal is multiplied by a very large bandwidth signal called the spreading signal, and many users share the same frequency. Unlike TDMA or FDMA, CDMA has a soft capacity limit, i.e., no absolute limit on the number of users. However, the performance for all users gradually degrades as the number is increased. Moreover, since the signal is spread over a large spectrum, multi-path fading may be substantially reduced. In addition,

timing synchronization is merely required between the transmitter of source and the receiver of destination, unlike in TDMA systems. But CDMA has several inherent problems: self-jamming, near-far problem, lower spectral efficiency. Self-jamming arises from the practically non-orthogonal spreading sequences of different users and results in the interference of transmissions with each other. The near-far problem occurs when stronger received signal levels decrease the probability that weaker signals will be received, and therefore need complex power control. CDMA systems basically have lower spectral efficiency as compared with TDMA and FDMA.

According to the qualitative nature of the transmission discipline, MAC protocols can also be classified into three general categories:

- Fixed Assignment Multiple Access (FAMA)
- Demand Assignment Multiple Access (DAMA) or Reservation Access
- Random Access (RA) or Contention Access

Every category is further divided into some sub-categories and has many variations. Hybrid multiple access protocols are the combination of the above three. FAMA works in a static and pre-scheduled way, which is relatively simple and inexpensive, but results in inefficient usage of bandwidth and difficulty to scale as the number of possible users increases. Therefore, satellite communications used to adopt FAMA systems in the early development stage, and FAMA protocols are still in good use with scenarios of small number of users (earth stations or spacecraft) and light load now. In addition, FAMA systems do not need synchronization, and easily provide QoS guarantee, especially for traffic with relatively smooth characteristics like CBR sources. However, pure FAMA doesn't quite meet the requirements of the

infrastructure to support a large number of IP-based users with bursty and dynamic traffic nowadays.

Instead of statically sharing the channel, DAMA assigns the channel to the users by using reservation or polling techniques. Both FAMA and DAMA protocols are contention-free, in the sense that every scheduled data transmission is guaranteed unless transmission errors occur. In DAMA systems, the reservation process may be collision-based (e.g. ALOHA) or collision-free (pre-assigned control slots for each user). In either case, every user needs to go through the following reservation process to obtain its own portion of the channel: request => approval and allocation => reservation establishment => channel usage. According to the time scale during which the allocated capacity is constant, two types of DAMA protocols are used: fixed-rate DAMA and variable-rate DAMA. In fixed-rate DAMA, a fixed amount of capacity is allocated to each user for the lifetime of the connection. While in variable-rate DAMA, the bandwidth allocation to each user is variable for the connection's lifetime. DAMA protocols improve the efficiency of the channel usage and the overall system performance, and are fit for networks with variable traffic loads, compared with FAMA protocols. However, DAMA protocols introduce an extra delay for the reservation process in the amount of at least one Round Trip Delay (RTD), which is very significant in the space communications environment. Pure DAMA protocols are not fit for real-time applications or other applications bounded by end-to-end delay requirements. In order to circumvent this extra delay and provide high maximum channel utilization for bursty traffic, DAMA combined with alternative techniques such as FAMA, are often used.

Contention-based access protocols, also known as Random Access (RA) protocols, include many variations of slotted or unslotted ALOHA and Carrier-Sense Multiple Access (CSMA). RA protocols enable each user to attempt to send their own traffic through the common channel without avoiding collisions. Once a collision happens, users back off their attempts or certain Collision Resolution Algorithms (CRA) are used to deal with the retransmission. RA protocols are more effective for networks with bursty but light traffic load. Define β as the ratio of propagation delay to packet transmission time. For $\beta << 1$, CSMA can decrease delay and increase throughput significantly over the basic RA protocols [17]. CSMA with Collision Detection (CSMA-CD) or CSMA with Collision Avoidance (CSMA-CA) are two variations of CSMA, which requires users to sense the channel before use attempts in order to reduce the collision probability. In communication networks involved with satellites, however, the interesting feature is dealing with $\beta >> 1$. CSMA also introduces an extra delay for the carrier sensing. Therefore, it is not as useful for space communications with long propagation delays as for networks with small delays. In addition, the longer the propagation delay is, and the more dispersed the users are, the less effective the carrier sensing will be. Another problem with the RA protocols is throughput. Even RA protocols with most the sophisticated collision resolution techniques can just provide limited throughputs around 0.5 [17]. Furthermore, to achieve throughput close to such an upper bound, the RA system has to endure a significantly long delay. So, to avoid the unbearable delay, the successful throughput in practice is even less than the nominal bound for the RA system.

Scheduling, or service discipline, is always conducted within the MAC schemes, since it is necessary for providing end-to-end per-user or per-connection guaranteed performance service to heterogeneous and bursty traffic. In addition, the service disciplines must be simple so that they can be fit for high-speed broadband communication networks. The scheduling and associated performance problems have first been widely studied in the contexts of hard real-time systems and queueing systems, and then in QoS provisioning for wire-line packet-switching networks. Research has also been conducted in wireless communication networks with bursty and location-dependent errors environment. Zhang [18] presented an overview of the proposed service disciplines and discussed the tradeoffs in scheduling designs to provide QoS guarantees in packet-switching networks.

The following two sections present detailed literature overviews in the areas of MAC protocols and scheduling algorithms, respectively, within the framework of satellite, wireline and wireless communication networks.

2.1. Related Work on Medium Access Control Protocols

To reduce the delay while providing QoS guarantees, hybrid MAC protocols – the combinations of free assignment, fixed assignment, demand assignment and random access have been often proposed in the literature.

A reservation protocol, which partitions the multi-access channel into reservation and data sub-frames by means of time division, was proposed in [19]. An analysis of this protocol is presented by considering the case where the channel partition is fixed from frame to frame [20]. It is well known that such reservation protocols provide

efficient channel access when propagation delays are long, as in satellite channels, and the user data messages are relatively long compared with the overhead for reservation requests. Their variations are widely used in wireless IP networks [21, 22, 23] and satellite communication networks [24, 25, 26]. These dynamic-assignment or hybrid schemes no longer need to allocate bandwidth based on the requests in advance. Despite that they are more difficult to implement and complicated to meet QoS guarantees, the schemes can enable multiple users to dynamically share the common link for different types of heavy traffic.

Le-Ngoc et al. presented the Combined Free/Demand Assignment Multiple Access (CFDAMA) protocol in [27] for integrated voice/data satellite communication networks. As a hybrid centralized TDMA scheme, CFDAMA first assigns data slots to reservation requests of all the users (earth stations) based on the fixed-rate or variable-rate demand-assignment principles. These requests can be made in a fixed manner (pre-assigned reservation slots), random access manner (RA reservation slots) or piggy-backed manner (PB in data slots) by each earth station. After assigning the requested bandwidth, the remaining data slots (free channels) are allocated to all the earth stations in a round-robin manner. This way, the extra request-allocation process, which is exactly equal to one round-trip propagation delay, is avoided for the free assignments. Hence, with light load and small number of earth stations, the probability of obtaining free assignments is very high for each earth station, and then a transmission delay close to one round-trip propagation delay could be achieved. Besides, the realization of this round-robin free assignment scheme is simple and therefore consumes little space, electrical power and time. However, by allocating the

free capacity to earth stations simply in a round-robin manner, the central scheduler (either in satellite or in a main earth station) possibly assigns precious channel bandwidth to some stations without the wait-to-send data. With the increase of traffic load and/or number of earth stations, the possibility of this kind of waste will be highly increased, which leads to inefficient usage of system resources.

Hung et al. proposed a hybrid DAMA protocol in [28]. Denote ρ_i^{fx} as the allocated bandwidth for fixed-rate demand to connection i, ρ_i^{v} as the allocated bandwidth for variable-rate demand to connection i, and $\rho_i = \rho_i^{fx} + \rho_i^{v}$ as the total allocated bandwidth to connection i. Let B represent the total uplink bandwidth and N be the number of earth stations. Then the main issue is to assign the rest of the available bandwidth $B - \sum_{i=1}^{N} \rho_i^{fx}$ to the earth stations to fulfill their variable-rate demands. In each TDMA frame, each earth station transmits its current queue size in its control slot. The central scheduler estimates the current backlogged queue sizes according to the queue sizes information inserted in the control slots, previous bandwidth assignments and ρ_i^{v}. Based on these estimations, the new bandwidth assignments for the variable-rate demands are made. This scheme is a combination of fixed bandwidth allocation and demand assignment multiple access with estimation. Under certain load conditions, it will provide better performances than pure DAMA and FAMA since one round-trip delay is avoided for some variable-rate demands. However, it has several disadvantages. First, this scheme attempts to estimate the current demands based on the previous one-step instantaneous queue sizes, which change rapidly. The long round-trip propagation delay makes it even worse. Second,

the assigned slots for a certain earth station are possibly partially wasted if its actual queue size is less than the estimated. And this situation happens with high possibility due to the simple estimation technique used in this scheme. Third, the measure and transmission of queue sizes need to be achieved every frame at both the satellite and earth stations, which inevitably wastes the uplink bandwidth and electric power.

Movable boundary Random/DAMA Access, a scheme which can support video, voice and file transfer, is proposed by Nguyen and Suda in [29]. The frame is divided in three subframes by movable boundaries: a reservation subframe, a Slotted Aloha channel for bursty data traffic, and a DAMA channel for all other traffic. DAMA allocation is done first and the remaining bandwidth is available for Slotted Aloha access, which gives DAMA higher priority and determines the moveable boundary accordingly. UBR traffic can be sent using random access because no QoS guarantees are provided for this service class. This scheme performs like the fixed-rate DAMA when voice and CBR video traffic is dominant, while it functions like a random access protocol when most traffic in the network is bursty data traffic.

Anticipated Reservation scheme is presented by Zein et al. in [30]. In this hybrid TDMA scheme for fixed-rate and variable-rate demand assignment, the frame is divided into three parts: reservation subframe, bursty subframe and stream subframe with movable boundaries among them. The stream subframe is reserved for delay sensitive traffic using fixed-rate DAMA, while the bursty subframe is reserved for delay insensitive bursty traffic using a variable-rate DAMA, anticipated reservation protocol. Anticipated reservation means that the initial request for bursty traffic is sent right after the terminal receives the first cell instead of the typical store &

forward approach. After the complete burst is received, another request has to be made to reserve the necessary bandwidth. Hence one drawback is that a portion of capacity is lost if the burst duration is smaller than the reservation cycle.

Combined Fixed Reservation Assignment (CFRA), a modified version of the Anticipated Reservation scheme, is proposed by Zein et al. in [31] in order to reduce the capacity loss. This scheme is a combination of the anticipated reservation protocol and the buffer threshold method. It distinguishes between short and long bursts and implements different reservation schemes accordingly. At the beginning of each burst, a fixed rate-DAMA assignment of $R_{\min}$ is made. An extra portion of capacity is requested if a burst is longer than a certain number of cells. If no more cells arrive in the station after a time-out interval, one request is sent to the scheduler for capacity de-allocation. Fixed-rate DAMA is still used for stream traffic without modification.

In [32] and [33], Rosenberg and Acar proposed the Bandwidth on Demand (BoD) process, a combination of fixed-rate and variable-rate demand-assignment MF-TDMA protocol. This adaptive scheme allocates an amount of Static Resource (SR) and Booked Resource (BR) to each connection per MF-TDMA frame. Here, SR represents the fixed assigned transmission resources, while BR represents the booked transmission resources which will be really allocated only if the connection requests them in the Resource Request (RR). Active earth stations send their RRs within the users' time slots by piggybacking (i.e., in-band request signaling). For each connection: if its RR is less than its BR, it will be allocated exactly the RR; if its RR is greater than its BR, it will be allocated the BR and a share from the rest of the bandwidth. An optimization problem derived from game theory is solved to

determine the sharing of the remaining bandwidth among those connections whose RRs are greater than BRs. The BoD process also introduces a connection admission control based on the (SR, BR) pair of new connections, with consideration of an OBP satellite network without on-board buffer. Due to their different QoS requirements, CBR connections are assigned SRs only, VBR connections are assigned (SR, BR) pairs and UBR connections are not assigned SRs/BRs. The performance of this scheme depends on how to set the (SR, BR) pairs and the parameters in the optimization problem formulation.

Connors et al. presented a combined Random Access/Demand Assigned Multiple Access (RA/DAMA) for medium quality interactive video in [34]. This scheme takes advantage of two facts: first, some real-time multimedia applications can tolerate light to moderate packet loss. Second, source coded video, like MPEG, can be thought as a slow time process (STP) modulating a fast time process (FTP). RA/DAMA tracks the behavior of STP by determining the time when a scene change occurred. The random access channel and the DAMA channel are partitioned in a logical manner. In each earth terminal, the channel selection algorithm estimates the delays of the last packet in the DAMA queue and the RA queue, respectively, and chooses the channel for the new arriving packet based on the estimations. So, the basic idea of this scheme is to achieve less packet delay while baring some tolerable packet loss and insignificant standard deviation of delays. In RA/DAMA, the RA channel is not based on the ARQ (Automatic Repeat-reQuest); hence packet loss is inevitable when two users choose the same RA slot. Furthermore, no guarantee for the delay can be provided although packet delay estimates are always made for channel selection.

Burst Targeted DAMA (BTDAMA), a DAMA to support on/off type traffic over GEO satellite links, was proposed by Mitchell et al. in [35]. BTDAMA is designed to support packet-train traffic sources identified by a series of bursts and inter-burst gaps. Each terminal only requests the satellite capacity at the beginning of one burst and subsequently receives a continuous allocation of bandwidth during this burst as long as required, which enables an end-to-end delay close to one round-trip time (RTT) for variable rate DAMA. The request slots are allocated to terminals in a round-robin manner for contention free DAMA requests on a burst-by-burst basis. BTDAMA is very suitable for the traffic sources mainly consisting of bursts with length longer than the RTT. An analytical model of BTDAMA is also introduced for the performance evaluation of BTDAMA with free and demand assignments.

Chan et al. presented a dynamic reservation protocol for LEO satellite systems in [36]. This scheme is aiming for the emerging MPLS/ATM (Multiprotocol Label Switching and Asynchronous Transfer Mode) –based LEO satellite system with both connection-oriented and connectionless traffic. The contribution of this scheme is to maximize the number of successful terminals by varying the access probabilities of the contending terminals and the number of reservation minislots. The frame-based and minislot-based approaches of varying the access probabilities are proposed. Most importantly, a novel contention-pattern-analysis algorithm is adopted to estimate the number of contending terminals, which is a must for operating either of the above approaches. Simulations demonstrate the effectiveness and efficiency of this scheme. This scheme can adaptively handle a variety of different combinations of traffic sources with the complex computation and protocol operation.

2.2. Related Work on Scheduling Algorithms

Packet scheduling has been one of the most important issues in the context of wireline, wireless and satellite communication networks. A general introduction and analysis of varieties of packet scheduling mechanisms in wireline systems can be found in [18].

Unlike a wireline system, a wireless system has several different characteristics: (1) error-prone environment, (2) bursty and location dependent error, (3) time-varying and location dependent capacity, (4) mobile users. So compared with a wireline system, it is more challenging to provide efficient and effective scheduling algorithms for a wireless system. A general introduction of packet scheduling mechanisms in wireless systems can be found in [37]. Basically, scheduling mechanisms are considered to achieve tradeoffs between system performance, in terms of throughput, end-to-end delay, jitter, etc., and fairness, i.e., degrade in system performance while improving fairness among users and vice versa [38, 39, 40, 41, 42].

Generally, the proposed schedulers for wireless systems are derived from their wireline counterparts. So it is acceptable and beneficial to study schedulers originally designed for wireline systems, while leaving some tunable parameters and interfaces for new components.

In the rest of this section, we review and compare several widely used scheduling algorithms in wireline systems, and then present analysis and review on scheduling algorithms in wireless systems.

Scheduling Mechanisms in Wireline Systems

A scheduling mechanism is the manner in which queued packets are selected for transmission on the link. General scheduling mechanisms used or proposed in wireline systems can be found in [18] and its references.

Scheduling mechanisms are classified into two groups: Work-Conserving schemes and Non-Work-Conserving schemes. For Work-Conserving schemes, the server is never idle when a packet is to be sent. While for Non-Work-Conserving schemes, the server could be idle even when a packet is waiting to be sent, as long as its assigned eligibility time is not ready yet. Traffic pattern distortions are generated by Work-Conserving schemes, while controlled by Non-Work-Conserving schemes.

Several widely used schemes in the Work-Conserving group are Virtual Clock (VC), Weighted Fair Queueing (WFQ), Worst-case Fair Weighted Fair Queueing (WF^2Q), Self-Clocked Fair Queueing (SCFQ) and Earliest-Due-Date (EDD). The comparison of them follows.

- *Virtual Clock (VC)*: uses the virtual time that emulates the Time-Division Multiplexing (TDM) system.
    - Simple, easy to implement
    - VC and WFQ have same delay bounds for flows with leaky bucket
    - Refer to the static TDM
    - Virtual time is independent of the behavior of other connections
- *Weighted Fair Queueing (WFQ)*: using finish times, picks the 1st packet at current time that would complete service in Fluid Fair Queueing (FFQ).
    - At any given time, the total amount of bits transmitted never falls behind the FFQ system by more than one packet size

- Needs to emulate a FFQ system for reference and keep track of active connections at any time
- In Rate-Proportional Processor Sharing (RPPS), a special case of WFQ, the delay bound is inversely proportional to the allocated rate

- *Worst-case Fair Weighted Fair Queueing (WF^2Q)*: considers only packets that started receiving service at the current time in FFQ, and picks the 1st packet at the current time that would complete service in FFQ.
  - At any given time, the difference between the services provided by WF^2Q and FFQ is always less than one packet size
  - Needs to emulate a FFQ system for reference and keep track of active connections at any time
  - Needs more calculations and operations
- *Self-Clocked Fair Queueing (SCFQ)*: may use the Virtual time estimated from the virtual service time of the packet currently being serviced.
  - Uses a simpler algorithm by calculating virtual time rather than keeping the computationally expensive reference FFQ server
  - The inaccuracy incurred can make the SCFQ perform much worse than WFQ
  - Does not provide end-to-end delay bounds
- *Earliest-Due-Date (EDD)*: uses (expected) arrival time plus delay bound as its deadline, when a source obeys its contract.
  - Two state variables allow Delay-EDD to solve the problem of coupling between the allocation of delay bound and bandwidth

- The update of state variables depends only on per connection parameters instead of system load

Several widely used schemes in Non-Work-Conserving group are Jitter Earliest-Due-Date (Jitter-EDD), Stop-and-Go and Rate-Controlled Static Priority (RCSP). The comparison of them follows.

- *Jitter-EDD*: uses the time difference between the deadline of a packet and its actual finish time, stamped in a field of its header.
  - Provides flexible delay bounds and bandwidth allocation
  - The update of state variables depends only on per connection parameters instead of system load
  - Has implementation issues
- *Stop-and-Go*: maps the arriving frame into the departing frame by introducing a constant delay α, $0 < \alpha < T$, where T is the length of the fixed-size frame.
  - An arrival packet is postponed for transmission until the beginning of the next frame (the traffic that satisfies (r, T) specification keeps its property)
  - Provides a bound for both the delay and Jitter
  - Introduces a coupling problem between the delay bound and bandwidth allocation granularity
- *RCSP*: consists of a rate-controller, which performs traffic shaping, eligibility time calculation and assignment, and a static priority scheduler.
  - Achieves flexibility in the allocation of delay and bandwidth as well as simplicity of implementation

- Delay-jitter (DJ) regulators keep all traffic characteristics by completely reconstructing traffic pattern, while rate-jitter (RJ) regulators only keep certain characteristics
- Although optimizing for guaranteed performance service, RCSP may negatively affect the performance of other packets (e.g., best-effort service packets)
- A client is always punished when it sends more than specified

Scheduling Mechanisms in Wireless Systems

Four required objectives for a fair wireless scheduler are clearly specified in [43] and quoted below:

- *Delay and throughput guarantees*: delay bound and throughput for error-free flows should be guaranteed, and not affected by other flows in error state.
- *Long-term fairness*: after a flow exits from link error, as long as it has enough service demand, it should be compensated, over a sufficiently long period, for all of its lost service while it was in error.
- *Short-term fairness*: the difference between the normalized services received by any two error-free flows that are continuously backlogged and are in the same state (i.e., leading, lagging or satisfied) during a time interval should be bounded.
- *Graceful degradation for leading flows*: during any interval while it is error free, a leading backlogged flow should be guaranteed to receive at least a minimum fraction of the service it would receive in an error-free system.

According to these objectives, several popular wireless scheduling algorithms are discussed below.

Channel State Dependent Packet Scheduling (CSDPS): Channel State Dependent Packet Scheduling (CSDPS) is proposed in [44] as one of the first wireless scheduling algorithms to address problems of location-dependent and bursty errors. In CSDPS, each queue executes First-In-First-Out (FIFO). A Link Status Monitor (LSM) monitors the link states, determines whether a link is in a good or bad state, and marks queues with bad links accordingly. The marked queues will be unmarked after a time-out period. The basic idea is that the server does not serve the marked queue. As shown in [44], CSDPS achieves much higher throughput and channel utilization and also smaller average delay, compared with a purely FIFO mechanism. However, CSDPS does not provide guarantees on bandwidth and delay. Also, there is no limitation on the exceeded portion from the fair share of service time for the users in good state.

CSDPS combined with Class-Based Queueing (CBQ): CSDPS, combined with Class-Based Queueing (CBQ) [45], is proposed in [46] to solve the problem of unfairness in CSDPS. CBQ is used to provide fairness in sharing the wireless channel. In [45], CBQ restricts a class from receiving more service when it is allocated bandwidth more than its fair share. Some modifications on CBQ are made in [46]. First, effective throughput (successful throughput or goodput) replaces fair share in the original CBQ scheme. Second, as an exception, a class with more-than-fair-share allocated bandwidth is still allowed to receive more service if it has a good link and all unsatisfied classes have bad links. There are also some modifications on

the signaling for link monitoring in the original CSDPS. In summary, CSDPS combined with CBQ (CSDPS + CBQ) implements a fairness mechanism on top of CSDPS, so it could provide fairness in some sense while trying to maintain high throughput. However, no explicit mechanism is provided to compensate the lagging user due to link error.

Idealized Wireless Fair Queueing (IWFQ): Wireless Fluid Fair Queueing (WFFQ) and Idealized Wireless Fair Queueing (IWFQ) are proposed in [47] as a variant of FFQ and WFQ, respectively. Like the relation between FFQ and WFQ, IWFQ is a packet-wise approximation of WFFQ with practical considerations. Basically, IWFQ is a lead-and-lag version defined with reference to an error-free WFQ. A flow is called leading, lagging, or in sync at any time if its queue size is smaller than, larger than, or equal to the queue size in the reference error-free WFQ system.

IWFQ works exactly like ordinary WFQ if no link suffers from errors. When link errors happen, if the chosen packet has a bad link state, the packet with the next smallest finish time and good link state will be served. This way, when the link turns from bad state to good state, this omitted packet will definitely be served first because it always has the smallest finish time. So compensation is guaranteed. In IWFQ, leading and lagging of all flows are also bounded with respect to error-free WFQ service. In [47], some analyses of delay and throughput guarantee are given in terms of deterministic bounds for error-free and error-prone links, respectively.

To fight bursty and location-dependent errors, the implementation of this policy adopts spreading to reduce worst-case packet loss for an arbitrary user, and uses swapping based on prediction of the channel state to avoid waste of slots. Extensive

simulation results show that performance in terms of delay (average, maximum) and packet loss is better than common policies without spreading and swapping. However, IWFQ also has its limitations. First, it is complicated and sometimes even impractical to have the finish times of all packets in the uplink scheduler. Second, one of its parameters reflects a conflict between delay and fairness. Hence delay and throughput are coupled together.

Channel-condition Independent packet Fair Queueing (CIF-Q): Channel-condition Independent packet Fair Queueing (CIF-Q) is proposed in [48] to address the fairness issue. Similar to IWFQ, a flow is called leading, lagging or satisfied at any time if it receives more, less or exactly the same amount of service corresponding to an error-free fair queueing reference system. Start-time Fair Queueing (SFQ) [49] is chosen to be the reference system as an example.

In CIF-Q, each arrived packet is put into two queues: one in a real error-prone system and the other in an error-free reference system. Normal SFQ is performed in the reference system and the virtual time of the packet is updated even when this packet is not served in the real system due to link error. For any specific flow, the difference between the service in the real system and the service in the reference system is tracked. When a packet is chosen in the reference system, its corresponding packet in the real system is transmitted unless its link state is bad or it belongs to a leading flow which reaches the upper bound of received service. Lagging flows have higher priority to receive additional service from leading flows giving up lead or flows not being able to send because of bad link state. The additional service is distributed among the lagging flows proportionally to their allocated service rates. If

no lagging flow can send packets due to bad link state, the additional service is distributed among the other flows proportionally to their allocated service rates.

CIF-Q provides both long-term and short-term fairness guarantees. Also packet delay and throughput guarantees are provided for flows with error-free links. However, it is complicated and sometimes even impractical to have the virtual time of all packets in the uplink scheduler.

Opportunistic Scheduling (OS): In [50], a general background of Opportunistic Scheduling (OS) schemes is presented. And then an OS scheme is also proposed to achieve an optimal trade-off between throughput and fairness in [50]. The major difference between OS and the other schemes is that OS uses a more practical channel model instead of a two-state channel (good or bad) model.

OS is an emerging cross-layer design approach over fading wireless channels. Basically it exploits channel variations, in terms of estimated instantaneous carrier-to-interference ratios, supportable data rates, received signal strength indications, or bit error rates of users' links, to maximize wireless throughput. Proportional Fair sharing (PF) scheduler [51], 1xEV scheduler [52], and Best Link Lowest Throughput First (BLOT) scheduler [50] are examples of OS schemes.

More on Scheduling Mechanisms

Store-and-Forward queueing is proposed in [53] and is based on a network-wide slot structure. A finite number of connection types are predefined. The delay and buffer size guarantees are made by executing an admission policy with upper bound of submitted bits in a certain period. This service discipline offers two advantages over others for packet-switching networks: better delay jitter and easier

implementation, especially for certain types of traffic with delay jitter requirements. Also, due to the long propagation delay in satellite communication networks, it is better to place the scheduler on-board the satellite (gateway) to significantly reduce the end-to-end delay, which leads to easy implementation and quick response time for efficient usage of limited space on-board. However, this discipline has inflexibility due to predefined connection types and increases extra delay for the packet delivery.

Round Robin (RR) is analyzed by Mitchell et al. in [54] for a GEO satellite system. RR and its modified version Weighted Round Robin (WRR) are widely employed in TDMA-based communication networks because of its simplicity and straightforward fairness among users. Also RR maintains traffic smoothness inside the network. Under the assumptions of Poisson traffic, infinite buffer capacity at the terminals and the satellite, this paper models the system as a discrete-time Markov process, and finds numerical/analytic results, which conform to simulation results. The performance in term of end-to-end delay degrades with the number of terminals, especially when channel load is higher than 0.7.

Packetized Generalized Processor Sharing (PGPS), also called WFQ, is proposed by Parekh and Gallager in [55]. It is a policy that tries to approximate the same FFQ or Generalized Processor Sharing (GPS) policy. This scheme is flexible since different users can be assigned widely different QoS guarantees, and is efficient since the slot will be allocated to another connection if the current connection has no packet. It also provides a wide range of worst-case performance guarantees on delay and throughput. This is a very popular model for fair resource allocation to fluid flow sources in wireline communication networks. However, due to the bursty and

location-dependent errors in wireless communication networks, scheduling policies good in wireline networks are not necessarily the best policies in wireless networks, including satellite communication networks.

Shakkottai and Srikant proposed Feasible Earlier Due Date (FEDD) policy, a version of EDD, for real-time traffic with deadlines over a wireless channel [56]. The basic idea of this policy is to choose the packet which has the earliest time to expire from the set of queues whose channels are "good". The analytical results have shown that for Markovian channels and strict delay constraints, the policy is optimal for two queues with one packet in each queue. For the issue of fairness, the paper chooses WRR in combination with FEDD to provide some degree of isolation among queues. However, this policy is not necessarily optimal for the other types of real-time traffic and/or more than two queues.

3. Flexible Access for Satellite Communication Networks

3.1. Traffic Modeling

We next turn our attention to the steps that need to be taken in order to enable this dynamic mission operation concept. It is critical to start by understanding the traffic characteristics at the sources of this network (science instruments on the spacecraft) and the statistics of traffic at different points as it flows through the current and future NASA network infrastructure. It is important to:

- *Establish a baseline set of mathematical/statistical models of communication traffic, currently being carried on NASA networks*. These models are to provide a 'holistic' view of NASA networks and will, likely, employ switched-circuit concepts of communication networks. The models need to be driven by actual usage statistics collected by NASA operational communications relay sites.
- *Develop mathematical/statistical models for future NASA communications traffic*. Projections of future traffic are to be based on future missions' communications requirements and extrapolations of models developed to represent the existing traffic and projections of the nature of future NASA networks. Thus, models portraying future NASA traffic will, likely, be based on switched packed concepts.
- *Employ models representing current and planned communications traffic to analyze NASA communication networks*. A small number of candidate

architectures, will be evaluated in terms of overall throughput, quality of service and cost. Models representing current and future communications traffic will be used in the analysis.

3.1.1. Architecture

The space communication networks are evolving to use Internet Protocols to take advantage of the software and hardware popular in the commercial network world. However, one of the major challenges is to use a proper data link framing mechanism to support IP along with good performance over radio frequency (RF) links.

There are several combinations for usage in space communications, such as TDM, Consultative Committee for Space Data Systems (CCSDS), Frame Relay, Point-to-Point and ATM. A standard mapping of IP packets over frame relay is defined in the IETF and widely supported by standard routers [57]. Hence, the combination of Frame Relay over high-level data link control (HDLC) framing may be the most suitable one for the future IP-environment space communication networks. However, as the traditional framing mechanisms, TDM and CCSDS frames are currently widely used in the space communications. And because our MAC protocol with dynamic bandwidth allocation scheme is not dependent on the detailed framing mechanisms, it would not be a problem to switch to the combination of Frame Relay over HDLC framing in the future. So, TDM and CCSDS are used in this Chapter to present our MAC protocol with dynamic bandwidth allocation.

3.1.2. Understanding Mission Traffic Characteristics

First we study the existing traffic on NASA networks, and then develop models to represent the existing and planned traffic. The models include traffic generation,

organization and transmission. By using the Packet Telemetry Data System standard from CCSDS, we define two data structures—Source Packets and Transfer Frames, and a multiplexing process to interleave Source Packets from various Application processes into Transfer Frames [58]. The packet telemetry data system is illustrated in Figure 3.1.

According to CCSDS, the source packet consists of packet primary header (6 bytes) and packet data field (1 to 65536 bytes). The length of the source packet may be variable. In this case, we fix the length at 512 bytes to simplify the MAC issues. Otherwise they can be decomposed or aggregated to form packets of constant length.

Figure 3.1: CCSDS Packet Telemetry Data System

The format of a transfer frame is more complicated. It consists of two headers, data field (variable) and two control fields in tail. However, it shall be of constant length throughout a specific mission phase. In our case, since the duration during which the spacecraft are in the coverage zone is considerably short, it is reasonable to assume that they keep the same mission phase. So, the frame length is fixed. This will have a desirable feature: if some users make errors in one frame, they will not lose track of the next frame.

Note that we assume CCSDS framing because we start by considering legacy systems that are using this frame structure. However, as we move to an IP-environment and possibly adopt commercial standards or relays, High-level Data Link Control (HDLC) or other formats could become more common.

One standard type and also an important type of spacecraft data is real-time data containing spacecraft housekeeping information and science instrument telemetry. The requirements for this kind of data are reliability and fast delivery. To model the above real-time traffic, we selected TERRA, a typical current Earth Science mission spacecraft with five instruments on-board. ASTER, a typical instrument on-board TERRA, is selected as our example for traffic modeling.

	Mission Mode	Data Rate
Day	Full Mode	89.2 Mbps
	VNIR Mode	62.038 Mbps
	TIR Mode	4.109 Mbps
	Stereo Mode	31.019 Mbps
Night	TIR Mode	4.109 Mbps
	SWIR+TIR Mode	27.162 Mbps

Table 3.1: ASTER Observation Modes

As shown in Table 3.1, ASTER operates in different modes, basically in Full mode during daytime and in SWIR + TIR mode during night. Therefore, for simplification and in order to study bandwidth optimization, it is appropriate to model the ASTER instrument as a 2-state, 4-mode traffic generator: in Full or VNIR mode in one state and in SWIR + TIR or TIR Mode in the other. In a specific state, at the beginning of each small period, the active data rate is randomly chosen from two modes by their active probabilities. Then the generator keeps generating source packets in this active data rate during the following period. All these parameters can be set or changed.

We model the other instruments in a similar way. The five traffic sources are using a common queue with priority queuing. The priority levels are assigned according to their data rate, and the instrument with the highest data rate has the

highest priority. Of course the priority levels can also be assigned by other rules, for example, the importance of data. We assume that the traffic (source packets) generated from TERRA is relatively bursty. Simulation results showing a 10s instance of the traffic from TERRA are shown in Figure 3.2.

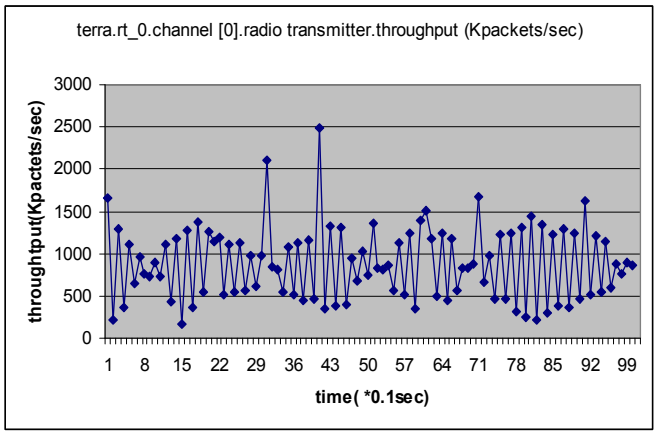

Figure 3.2: Simulation Results of TERRA Output Packets

We also consider other types of traffic models for real-time or non real-time data, including voice, video and bulk image files. For example, because some on-board instruments only generate traffic at constant rate and for part of the time, we could use a Constant Bit Rate (CBR) traffic generator model for some instruments. A CBR traffic generator model is also fit for the command & data handling traffic and voice traffic from the space shuttle. We are using our own multi-state-multi-mode (MSMM) traffic generators to emulate this instrument traffic that includes a Poisson-distributed traffic generator and a CBR traffic generator. And also, a MSMM traffic generator model with on/off switch, where the on/off periods are exponentially distributed, is proposed to better model the active/inactive durations of the sources. We call it Markov Modulated MSMM (MM-MSMM) traffic model.

3.1.3. Triple Request Model

Every traffic source will be provided with the guaranteed QoS in terms of its triple request: LR (Lower Resource), TR (Targeted Resource) and UR (Upper Resource). Intuitively, the LRs and URs are the minimum and maximum bandwidth assignments to fulfill the data delivery for every connection according to the different requirements. And the TRs are the expected bandwidths to "better" satisfy the QoS requirements of the connections in some sense based on the estimation of the traffic behaviors. Here "better" means: below its TR, the traffic source is very eager to get more bandwidth assignment if the price is affordable; while some way beyond the TR, more bandwidth assignment is not that much in need any more considering the price. In other words, the TR is a measure to describe the starting point of the turning zone for the tradeoff between resource demand and utilization price.

The reasons why we introduce the triple request model are as follows: first, it fits better the traffic sources in our scenario, which generally have expected performance and lower/upper bounds. Second, it allows us to use a unified framework to provide long-term average QoS guarantees for the traffic sources for a variety of basic traffic models, e.g., (Min, Max), (Static, Best-effort), or (SR, BR) etc. Third, this parameterized model could provide more flexible and adaptive control for the bandwidth allocation in broadband satellite communication networks with long propagation delays. We will describe how our adaptive bandwidth allocation fits the triple request model in Chapter 4.

According to their different types, the traffic sources may or may not need all the three parameters. CBR traffics are only assigned LRs because they demand fast

delivery with zero tolerance of transfer delays. So LR = TR = UR. Real-time (rt) and non real-time (nrt) Variable Bit Rate (VBR) traffic flows with minimum QoS guarantees are assigned different LRs and URs for their requirements, while different TRs by considering the transfer delay they can tolerate and the price they want to pay. For example, if these traffic flows are modeled as (Min, Avg, Max), then (LR, TR, UR) can be seen as a mapping, where LR is a function of Min, UR is a function of Max, and TR is a function of LR, TR and UR. Certainly the simplest mapping is LR = Min, TR = Avg, UR = Max. For rt-VBR and nrt-VBR traffic flows without minimum QoS guarantees, LR = 0, while the TR and UR are similar as before. Here we have discussed three general types of traffic sources: guaranteed bandwidth traffic, best-effort traffic and mixed-type traffic. In Chapter 4, we will show that our triple request model allows the scheduler to treat users/flows differently during both the constant-rate and the variable-rate resource allocation process.

3.2. Flexible Bandwidth Allocation

For the paradigm shift that will enable the transition of operations from "pre-planned" to "on demand" mode, another key requirement would be the development of a new multiple access technique to support on demand space to ground communications, that takes into account the novel network topologies that need to be supported and introduces a new, unique QoS requirement. Users (spacecraft) are visible by a ground station for a limited time window. Therefore, we have another dimension added to the traditional dynamic resource allocation problem: dynamic allocation of capacity under a time constraint.

We are trying to define a detailed scenario and evaluation criteria for suitable multiple access techniques for this operation, where:

- A priori bandwidth allocations are still based on advance requests/scheduled passes over certain position.
- There is an option for dynamically assigned additional bandwidth, either piggy-bagged to a priori reservation or available on demand as spacecraft enters coverage of the ground station.

A suitable Multiple Access protocol must satisfy the following requirements:

- Provide required QoS/availability guarantees for different classes of traffic (TT&C, Scientific Data Request, other priorities);
- Support multiple spacecraft sharing a common link to the same ground station;
- Enable multiplexing of various traffic streams on-board for delivery to multiple destinations (multiple scientists);
- Accommodate several scientists sending commands/download requests to various instruments on-board the same spacecraft;
- Does not impose significant cost or complexity demands on hardware on-board the spacecraft;
- Handle the mobility of spacecraft ("mobile platform").

A potential solution to the multiple access issues would be to implement a scheme utilizing a movable boundary concept (Figure 3.3), where transmission is organized in fixed size, slotted frames. The slots in the first part of the frame are dedicated for transmission of information on the user status, while the rest N slots are used for

information transmission. Movable boundaries exist between the different types of service. The objective here is to optimize the boundary positions, and for an optimal solution this could be done on a frame-by-frame basis [59].

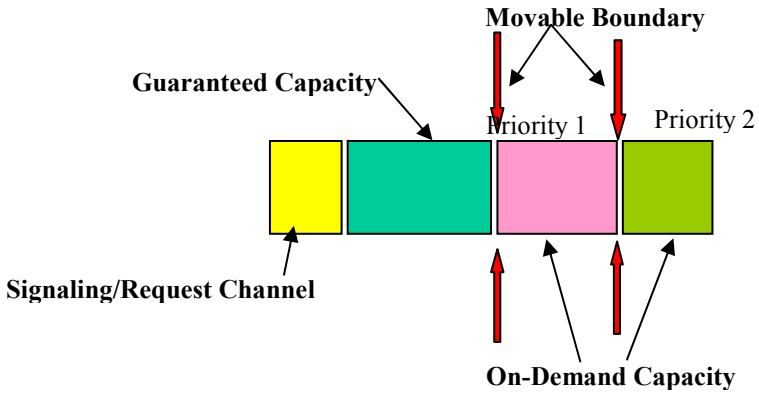

Figure 3.3: Dynamic Access Scheme - Movable Boundary Concept

3.2.1. Network Architecture

Most Earth Science Enterprise (ESE) missions either use the NASA Tracking and Data Relay Satellite System (TDRSS) [60] for relaying data to the ground or can communicate directly with certain NASA (or other) ground terminals. TDRSS consists of 7 GEO satellites around the globe that relay data from satellites in LEO and MEO to ground facilities at the White Sands Complex in New Mexico, and Guam. The GEO satellites have the capability to forward and return data in the S and Ku bands at speeds of up to 300 Mbps in the Ku band. These systems were developed in the 1970's and have been heavily used over the past two decades. A new generation of TDRS satellites (called TDRS-H, TDRS-I, and TDRS-J) was recently initiated to augment the older system and provide additional capacity for users. This new generation TDRS satellite has the additional capability to relay data in Ka-band at up to 300 Mbps without modifications to the ground stations, and up to 800 Mbps

with ground station modifications. A new tunable, wideband, high frequency service offered by the 15-foot antennas provides for the capability of these high data rates.

In the architecture, large numbers of spacecraft share the downlink channel of TDRS to the ground station, which can provide single access for high data rate channel (up to hundreds Mbps) per TDRS satellite. TDRSS has a Single Access (SA) and Multiple Access (MA) Capability using Spatial Diversity. The total end-to-end architecture is known as the Space Network (SN). Further details about the TDRSS operation and SN can be found in the Space Network Users Guide [61], and it is beyond the scope of this dissertation.

It is important to note that we are not focusing on the details of the current TDRSS nor are we trying to modify or improve on that design, although we start by considering a GEO relay satellite similar in architecture to TDRSS. We are looking into the concept of optimizing future relay systems which could be the next generation of NASA owned relays or other systems that share NASA but also commercial traffic. For simplification, we consider only one GEO relay satellite to avoid the issues of handover and routing.

To simplify our analysis, we consider the network architecture shown in Figure 4.4. This system consists of a number of LEO satellites, one GEO relay satellite and one ground station. The ground station receives the scientific data from all the spacecraft via the relay link but also acts as Network Control Center (NCC) performing the bandwidth allocation under certain QoS guarantees by collecting reservation/dynamic access and statistical information from the data transmission link. We mainly consider LEO spacecraft in orbits common to Earth Observation

Science (EOS) missions, and only consider the zone where the spacecraft are in the coverage of the relay. Since the orbits of mission spacecraft are known, we know the exact time they "join" (enter the coverage zone) and "depart" (leave the coverage zone) the zone.

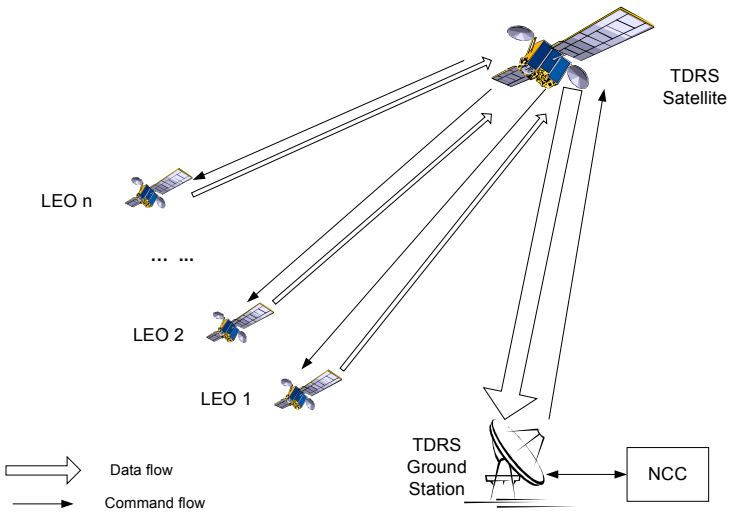

Figure 3.4: Network Architecture

The uplink is from the ground station to spacecraft through the relay satellite, operated in TDM broadcasting mode. The downlink is the data link, from the users (spacecraft) to the ground station through the relay satellite. The uplink is used by the ground station to notify all users of the bandwidth allocation for downlink, which has much larger bandwidth. We focus on how the spacecraft can share the downlink dynamically. In the current mode of operation this is done using a static-TDMA process using a priori reservations.

The current TDRSS system (with all satellites) provides extended view times for LEO satellites and is capable of transmitting to and receiving data from any LEO spacecraft over at least 85% of its orbit via S/Ku-band service. Currently, missions

are using the downlink channel of TDRSS in a mainly static and pre-scheduled way, which is relatively simple and inexpensive, but results in inefficient usage of bandwidth and difficulty to scale as the number of possible users (spacecraft) increases. Therefore, we need a new infrastructure to support a large number of spacecraft, which could eventually have IP-addressable instruments and could exhibit more bursty and dynamic traffic.

A simple, Reservation-based Demand TDMA protocol has been proposed to address the above problems [62]. In this operational scenario, spacecraft share access to NASA ground stations based on advance requests but there is also an option for dynamically assigning additional bandwidth on demand. Simulation results have shown that this solution outperforms pre-planned mode in most cases under unevenly distributed traffic load conditions in terms of delay and throughput. However, this was based on a number of simplifying assumptions and did not provide a complete on-demand scheme or use of realistic traffic models, corresponding to the traffic generated by the relevant mission instruments.

3.2.2. Medium Access Control Protocol Design

As mentioned earlier, FAMA protocols have very good performance for predictable and regular traffic, but are inflexible and inefficient for unpredictable dynamic traffic. Random access protocols can solve the problem of inflexibility and are suitable for light traffic, but have bandwidth inefficiency and long access delay for heavy traffic load. Reservation access protocols are on-demand mode, not completely dynamic schemes, but once the reservation requests are granted to users, the protocols will operate as fixed assigned protocols. Therefore, to overcome the

obvious shortcomings of each class, we design a hybrid-mode MAC protocol. And since reservation-based and random access protocols both need transmit request and feedback information, hybrid reservation-based protocols will inevitably share the bandwidth for control. So our scheme should be simple to implement and lower the overhead as much as possible. Before we propose our hybrid-mode protocol, we first discuss two issues: delay and time synchronization, which are significant for our protocol in satellite communication networks.

Delay

In a TDMA protocol with reservation, the bandwidth allocation could be optimized on a frame-by-frame or multi-frame basis. This will solve the problems of inflexibility and inefficiency, but also add some extra delay and more complexity for frame structure due to the need for reservation requests in advance.

The total delay T for the static mode and the reservation mode are:

$$T_{\text{static}} = T_{\text{transmission}} + T_{\text{queueing}} + T_{\text{propagation}}$$

$$T_{\text{reservation}} = T_{\text{transmission}} + T_{\text{queueing}} + T_{\text{propagation}} + T_{\text{reservation-process}}$$

There is an additional item, reservation delay, in the total delay for reservation mode. The spacecraft need to send reservation requests to the ground station and get the allocation from the feedback before acquiring extra bandwidth. Therefore, the reservation delay is equal or larger than twice the Round Trip Delay (RTD).

For satellites in LEO, the RTD is in the order of 10ms. In GEO orbits, it is 270-350ms. And the RTD between GEO and LEO is also in the range of 150-350ms. Therefore, in our scenario, the RTD of the system is around 480ms or more. This relatively long delay (i.e. delay > 100ms) may cause long access delay and seriously

damage the medium access control policy of our system. So in our proposed protocol we should carefully address this issue in evaluating its suitability.

Time synchronization

Another important issue is time synchronization among the spacecraft and ground station. Whether centralized or distributed algorithms, the system using a MAC protocol must perform one of them to complete the synchronization. Otherwise, there is a danger that durations of the data slots would overlap.

When the NCC and all users are stationary, it is easy to do this by computing and storing the time differences at the initiation phase of the system. The time difference of every user is constant. In our case, however, the spacecraft are orbiting the earth in high velocities. The time difference between every spacecraft and the ground station and thus the position of the frame would be variable due to the variation of their relative distance. Thus, synchronization would be more complicated. We would show the variation of the time difference in our simulation results.

Since the orbits of the spacecraft are known in advance, at any given time we know the exact position of spacecraft and therefore can compute the relative distances between the spacecraft and the ground station, and we can take advantage of this fact. There are two approaches in performing the synchronization: (i) When the spacecraft gets system time from the ground station, it computes the time difference and stores the adjusted own time. Then the spacecraft keeps computing the new time difference, and considering the time elapsed from getting the adjusted own time, it restores a list of adjusted own time. Alternatively, (ii) The spacecraft only computes the adjusted own time when getting system time from the ground station regularly. Then between

the adjacent two synchronizations, the spacecraft just uses this "out-of-date" adjusted own time. This will cause some errors and lead to time slots overlapping. So a guard time needs to be added in the frame structure to avoid the overlapping.

For the first approach, in our case, it is very difficult to decide how fast we should compute the time difference to provide updated adjusted own time for every spacecraft. When the spacecraft needs to send a packet in its assigned slot, but the adjusted own time is not updated yet, the overlapping will occur. Compared with this approach, the second approach is more practical and reasonable for our scenario. Note that although GPS information could be available to most spacecraft, the problem is not simply about getting the precise time, but how to synchronize the spacecraft and the ground terminal in the sense of frames to avoid packet collisions. On top of that, orbital timing skew could be a potential problem for high speed data transfers and could possibly aggravate the synchronization problem, and this must be considered during implementation.

3.2.3. Hybrid-Mode Medium Access Control Protocol

As shown in Figure 3.5, we are using a simple hybrid-mode MAC protocol in our scenario. All active spacecraft are using the common downlink channel to send packets to the ground station with NCC. There are request sub-channels in this downlink channel and feedback in the control link for bandwidth reservations.

The whole channel is divided into a number of identical sub-channels. A fixed number of these sub-channels are allocated for the static slots and the rest are used for reservation-based slots. This hybrid-mode can guarantee the minimal bandwidth for

each user (spacecraft) while assigning reservation channels dynamically for optimum performance.

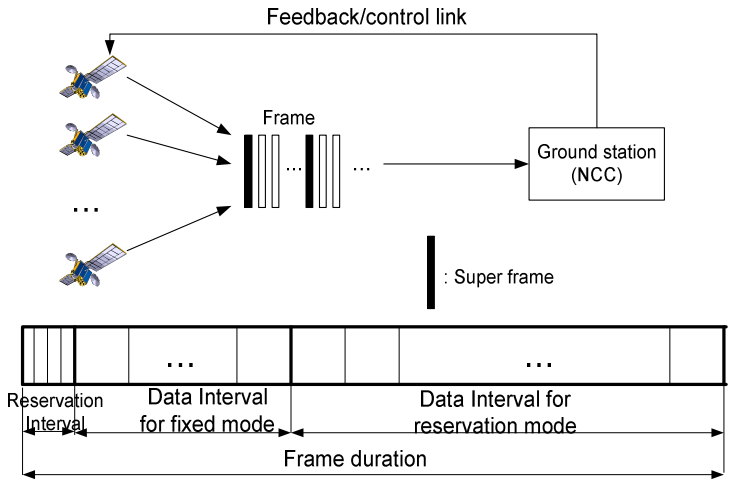

Figure 3.5: Hybrid-mode Access Protocol

Access Control Algorithm

Reservation minislots are used for access requests from new users. The access request contains the source (spacecraft) ID (MAC address) and the demands including average, minimal and maximal traffic loads from the new user. According to the different requirements, in the demands, every traffic source provides its triple request: LR (Lower Resource), TR (Targeted Resource) and UR (Upper Resource), and its priority level and weight when trying to get access to the broadband satellite network. Certainly for some types of traffic sources, the three parameters might be redundant and therefore could be combined. This framework is similar to the studies presented by Hung [28] and BoD protocol [33], but has a different parameter model. A fact that needs to be emphasized is that the users need to have advanced algorithms to provide estimates of their resource requirements.

The access control algorithm is performed as follows: the new user (or new connection) will be admitted only if the sum of the LRs of all active users is less than or equal to the total bandwidth of the broadband channel, which could be written as follows:

$$\sum_i LR_i \leq B,$$

where B is the total bandwidth. After admitted to the network, every stream will be assigned a new triple: LR, PR (Projected Resource) and UR. In other words, LR must be guaranteed for every admitted stream. The stream will be allocated its PR as a sum of LR and a best-effort share from the rest of the available bandwidth. The best-effort share will be assigned according to fairness and efficiency by solving an optimization problem. However, the assigned bandwidth could not exceed the requested maximum bandwidth. We will present the detailed problem formulation and results in Chapter 4.

Bandwidth Request Track

The estimation of "future" traffic demands from users, employs one-step forward linear estimation based on n-step previous and current information.

Since, the RTD is approximately 480ms or more it cannot be ignored. We chose RTD as the maximum round trip delay during the whole operating time. Typically the frame duration T_f is set to be equal to RTD in communication systems. In our case, however, to support data rates as high as 200Mbps while satisfying the requirements for frame length in CCSDS, it is impossible to let T_f = RTD. According to CCSDS, the transfer frame has mandatory Primary Header (48bits) and Data Field (variable), and also optional Secondary Header (16, 24, … 512bits), Operational Control Field

(32bits) and Error Control Field (16bits). The length shall not be longer than 16384 bits, which gives us a number of choices.

We can set $M \cdot T_f$ = RTD, where M is a given integer. Then, when a user sends a request or makes a transmission attempt in a specific frame, say the frame k, it will know the feedback from the uplink before the same slot in the frame ($k + M$).

The ground station with NCC broadcasts the feedback packets to spacecraft immediately after processing the incoming frame. And for every M frames, it sends a "super packet" including system time along with the feedback information. When a "super packet" arrives, the spacecraft will perform time synchronization, and we call the following frame a "super frame". We note that frames and slots are using guard times to avoid overlapping.

Suppose a frame has N data slots. N_1 slots are used for static slots, while N_2 data slots are used for reservation-based slots; $N_1 + N_2 = N$. Since the data rates and capacities of all spacecraft are predictable, these N_1 static data slots are allocated to them based on the expected traffic loads and the minimal bandwidth requirements. One reservation request is piggybacked in the first assigned data slot for each user per frame. A reservation request contains the source (spacecraft) ID (MAC address) and the current size of the on-board queue. The NCC keeps storing two statistics: the size of the on-board queue in the previous adjacent request, and that in the latest super frame. The NCC collects these requests from all the spacecraft and then determines the allocation of the rest N_2 data slots based on these statistics. The NCC assigns the weights to every spacecraft by certain rules (for example, nominal data rate, or importance), and then using the products of weights and queue sizes to determine the

portions of reserved slots assigned to each spacecraft. The obvious benefit is that the ground station considers the behavior of traffic not only in a very short range (T_f) but also in a relatively long range (RTD). This helps the ground station to make a more fair and optimal decision and decrease the opportunity to waste bandwidth, and therefore approach the bandwidth-efficiency. Our hybrid-mode protocol performs bandwidth optimization on a frame-by-frame basis although the collected information is M frames "out-of-date".

Another option is to send reservation requests in the "super frame" only and operate as a static TDMA protocol based on the previous granted bandwidth allocations. This option can decrease the computing complexity and lower the overhead, but now the optimization must be done on a multi-frame basis.

In the next chapter, we propose our two-level dynamic bandwidth allocation scheme in our hybrid TDMA protocol and present simulation results on its performance.

4. Two-Level Dynamic Bandwidth Allocation

The work presented here can be applied to both space communication networks around the Earth, and to novel communication network architectures for lunar exploration. Special attention is paid to the important requirements for future space missions that influence the design of this network. To provide per-user/per-flow QoS guarantees for different users with fairness consideration in communication networks, a well-performed bandwidth allocation process along with a good admission control algorithm is necessary. Due to significant propagation delays, space communication networks even need a much more adaptive bandwidth allocation and a more systematic admission control. To efficiently use the available channel, it is shown later on that a well-design time-varying bandwidth allocation scheme based on the instantaneous or statistical traffic of all users/flows performs better. However, only short-term (instantaneous) bandwidth allocation may cause instabilities and will have difficulties in providing QoS guarantees and managing the long-term (average) behavior of all the users/flows. Besides, the instantaneous and average behavior managements need to be well-coupled with each other. Therefore, we propose a two-level bandwidth allocation in our implemented MAC scheme.

As shown in Figure 4.1, the two-level bandwidth allocation is performed by the scheduler at the ground station with Network Control Center (NCC). To access the channel, a new user or new flow first sends a request to the scheduler. After executing the admission control algorithm mentioned in Chapter 3, the scheduler will broadcast

its decision to the users. If the user/flow is accepted, a static initial bandwidth allocation, which will be described further in section 4.1, is made by the long-term bandwidth allocator. Then the initial allocations will be delivered to the short-term bandwidth allocator as control parameters for the next-level scheduling. Under some other conditions, the long-term bandwidth allocation might be performed and updated to the next level. In the short-term scheduler, according to the continuous bandwidth requests from users/flows, the time-varying bandwidth allocation (or slots assignments) will be obtained and broadcast. This is another reason why we use a triple request model, which gives us more controls for bandwidth management.

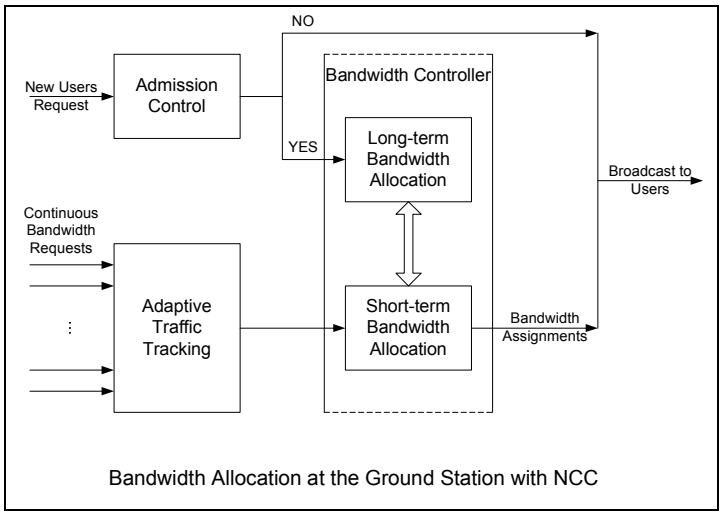

Figure 4.1: Two-level Bandwidth Allocation at the Ground Station

The long-term bandwidth allocation shapes the average behavior of all the traffic by assigning relatively static fair shares and appropriate bounds of the fluctuations to all users/flows, according to the long-term statistics of the traffic. On the other hand, the short-term bandwidth allocation shapes the instantaneous behavior and takes advantage of the time-varying properties of the traffic by allowing fluctuations of the allocations within designated bounds for all users/flows, adaptive to the available

collected statistics of their traffic. The computational complexity and response time are critical components affecting the performance of the dynamic bandwidth allocation algorithm, and need to be minimized. For dynamic short-term bandwidth allocation, the nominal optimal bandwidth allocation for all users/flows packet-wise or frame-wise is impractical to be achieved here due to the long feedback delay and large amounts of control information otherwise. Hence, we try to find a near-optimal solution for a multi-frame allocation instead. The parameters and collected statistics for calculation of every short-term bandwidth allocation are time-varying due to the characteristics of traffic and propagation delays, and our objective is to adaptively and efficiently take full use of this information while avoiding inappropriate fluctuations. We will present our simulation results after the presentation of our models in the following sections.

4.1. Long-term Bandwidth Allocation

To provide certain per-steam (and per-user) QoS guarantees, for access request from a new stream (or new user), the central scheduler will execute the admission control algorithm to ensure the sum of the contracted bandwidths (rates) of all the streams/users is less than or equal to the targeted bandwidth (data rate) of the broadband channel. After being admitted to the network, each stream is assigned a new triple: LR, PR (Projected Resource) and UR. In other words, LR must be guaranteed for each admitted stream. If UR can also be satisfied, then it's projected to the flow and we have PR = UR. If not, then the stream will be allocated its PR as a sum of LR and a best-effort share from the rest of the available bandwidth. The best-

effort share is assigned according to fairness and efficiency by solving an optimization problem.

This long-term optimal bandwidth allocation will be conducted not only when a new user or new connection is requesting the admission to broadband satellite communication networks ("joining"), but also when an active user turns to be inactive or changes to another relay satellite ("leaving"). It could be performed on a fixed or event-driven schedule. Here, long-term is referring to a relatively long time range compared with the dynamic bandwidth allocation, which is performed per frame or on a multi-frame basis.

Our long-term optimization problem is derived from Kelly's model [63], so we will first briefly introduce the original framework in the following subsection, and then propose our formulation and solution thereafter.

4.1.1. Kelly's Model

In this section, we briefly describe Kelly's basic model as background. Some notations and definitions are changed here. Details of the original framework can be found in [63].

Consider a network with a set L of resources or links and a set I of users (or flows). Let B_l denote the finite capacity of link $l \in L$. Each user has a route r, which is a non-empty subset of L. Define a 0-1 matrix A, where $A_{l,r} = 1$ if $l \in r$, and $A_{l,r} = 0$ otherwise. Suppose that if a rate (bandwidth) x_i is allocated to the user then $U_i(x_i)$ represents its utility. Here, the utility $U_i(x_i)$ is an increasing, strictly concave and continuously differentiable function of x_i over the range $x_i \geq 0$ (i.e., elastic traffic). Also, utilities are additive so that the aggregate utility of rate allocation $x = (x_i, i \in I)$ is

$\sum_{i \in I} U_i(x_i)$. Let $B = (B_l,\ l \in L)$, $U = \left(U_i(\cdot),\ i \in I\right)$, and the rate-control optimization problem is formulated as follows:

$$\begin{aligned} &\text{SYSTEM}(U, A, B): \\ &\max \sum_{i \in I} U_i(x_i) \\ &\text{subject to } Ax \le B,\ x \ge 0. \end{aligned} \tag{4.1}$$

Instead of solving the problem (4.1) directly, which is especially difficult for large networks, two simpler problems are also proposed in [63]. We will discuss the similarly decomposed rate-control problems later in this chapter.

Also, a vector of rates $x = (x_i,\ i \in I)$ is *proportionally fair* if it is feasible and for any other feasible vector x^*, the aggregate of proportional changes is zero or negative, or in other words, x satisfies:

$$\begin{aligned} &x \ge 0 \text{ and } Ax \le B; \\ &\sum_{i \in I} \frac{\delta x_i}{x_i} \;=\; \sum_{i \in I} \frac{x_i^* - x_i}{x_i} \;\le\; 0. \end{aligned} \tag{4.2}$$

Clearly, for the utility function $U_i(\cdot) = \log x$, its derivative is $1/x$. From the convexity of the feasible region for x and the strict concavity of the logarithmic function, it follows that the solution of the problem (4.1) is unique and proportionally fair. Later in Rosenberg's work [64], it is shown that the optimum solution associated with the logarithmic utility function is also a Nash Bargaining Solution. We are interested in proportional fairness or its variations because of its simplicity and popularity, although there are also other fairness criteria.

4.1.2. Utility Functions Discussion

In Kelly's model, there are no definitions for lower resource guarantee (LR), upper resource bound (UR) or targeted resource (TR). To formulate the optimum problem in our case, we need to modify the utility function and the constraints to incorporate all these parameters. For simplicity, we denote c = LR, b = UR, a = TR. To investigate the alternative utility functions, consider a small feasible perturbation of x, $x = (x_i, i \in I) \rightarrow x + \delta x = (x_i + \delta x_i, i \in I)$ in problem (4.1). The objective function will be increased provided

$$\sum_{i \in I} U_i'(x_i) \cdot \delta x_i > 0 . \tag{4.3}$$

Therefore, the optimal point x has the property that for any perturbation,

$$\sum_{i \in I} U_i'(x_i) \cdot \delta x_i \leq 0 . \tag{4.4}$$

To incorporate the minimum bandwidth c and also maintain proportional fairness, we modify the utility function to $\log(x - c)$, for which the optimal point x has the property

$$\sum_{i \in I} \frac{\delta x_i}{x_i - c_i} \leq 0 \text{ for any perturbation,} \tag{4.5}$$

which is exactly proportional fair in a truncated sense.

Considering TR (or in our notation a), we want the optimal solution associated with the modified utility function to have the following property: below its TR, the traffic source is very likely to get more bandwidth assignment if the price is affordable; while some way beyond the TR, more bandwidth assignment is not that much in need any more considering the price. In other words, the TR is a measure

describing the starting point of the turning zone for the tradeoff between resource demand and utilization price. Considering the variations of logarithmic functions, we list some candidates in Table 4.1, where k, $k > 0$, is the desired attenuation parameter for the designated source. Note that the utility functions can be written as logarithmic functions: $\log[(x-c)\cdot\exp(-(x-a)/k)]$, $\log[(x-c)\cdot\exp(-(x-a)^2/k)]$ and $\log[(x-c)\cdot\exp(-|x-a|/k)]$, respectively.

Recall that the utility function $U(x)$ is an increasing, strictly concave and continuously differentiable function of x over the range $x \in (c, b]$ for the elastic traffic. So, to keep the strict concavity, the second derivative of $U(x)$ needs to be negative, which is clearly correct except at one point ($x = a$) for the 3rd candidate utility function. To keep the utility function to be increasing, the first derivative of $U(x)$ is nonnegative over the range $x \in (c, b]$, which leads to the regions specified in Table 4.1 respectively.

$U(x)$	$U'(x)$	$U''(x)$	Region
$\log(x-c)-\frac{x-a}{k}$	$\frac{1}{x-c}-\frac{1}{k}$	$-\frac{1}{(x-c)^2}$	$k \geq b-c$
$\log(x-c)-\frac{(x-a)^2}{k}$	$\frac{1}{x-c}-\frac{2(x-a)}{k}$	$-\frac{1}{(x-c)^2}-\frac{2}{k}$	$k \geq 2(b-a)(b-c)$
$\log(x-c)-\frac{\lvert x-a\rvert}{k}$	$\frac{1}{x-c}-\frac{1}{k}$	$-\frac{1}{(x-c)^2}$ except $x = a$	$k \geq b-c$

Table 4.1: Comparison of Utility Functions

For detailed comparison amongst the above utility functions, we draw all of them and the truncated logarithmic function in Figure 4.2, with $c = 1$, $b = 8$, $a = 6$. As shown in Figure 4.2, before the point $x = a$, the 2nd line is the most steep one among all the utility functions; while after the point $x = a$, it is the most flat one except the

3rd one. However, the 3rd line is the least steep one before the point $x = a$. Therefore we take the 2nd one, which is associated with the utility function

$$\log[(x-c)\cdot\exp(-(x-a)/k)] = \log(x-c)-(x-a)/k\ . \qquad (4.6)$$

Also note that after the point $x = a$, the 2nd line and the 4th line coincide with each other.

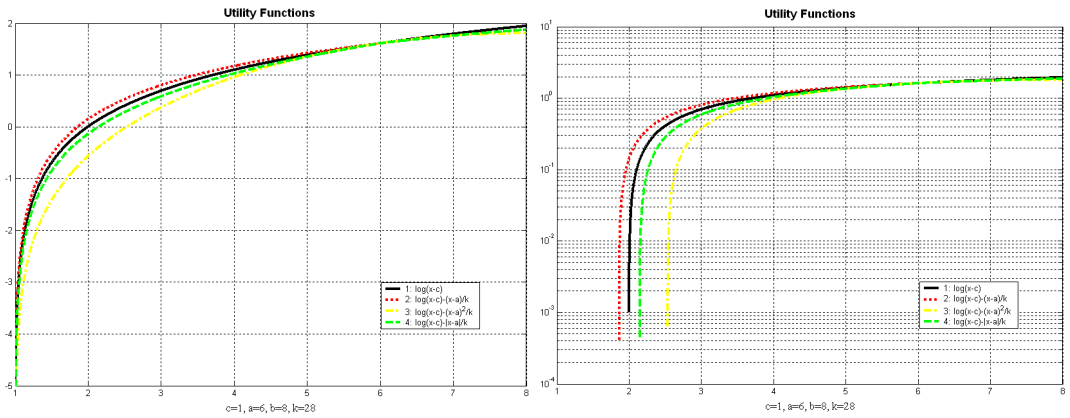

Figure 4.2: Comparison of Utility Functions

Left: linear scales, Right: semi-logarithmic scales.
1st: log(x-c), 2nd: log(x-c)-(x-a)/k, 3rd: log(x-c)-(x-a)^2/k, 4th: log(x-c)-|x-a|/k.

In the next section, we will present the problem formulation with the chosen utility function and show an interesting property associated with the optimal solution.

4.1.3. Problem Formulation

In this section, we will use the utility function chosen in the previous section to formulate the long-term static centralized bandwidth allocation problem. Consider N users or flows and L links or nodes in a network that compete with each other for use of the broadband channel. In the following discussion, we will generally use users to refer to users or flows. Each user is associated with a minimum bandwidth LR to be guaranteed by the network, maximum bandwidth UR and targeted bandwidth TR. According to the framework presented in the previous sections, the feasible rate set X

is defined by the finite capacity B and the triple parameters of the users, and could be defined as:

$$X = \left\{ x: x \in R^N, x \geq LR, x \leq UR \text{ and } Ax \leq B \right\}.$$

Where $LR = [LR_1, LR_2, \ldots, LR_N]^T$ is the vector of lower resource requests of the N users, $UR = [UR_1, UR_2, \ldots, UR_N]$ is the vector of upper resource requests of the N users, A is the $L \times N$, 0-1 matrix and B is the vector defined as before. Recall that for simplicity we will use c, a, b to denote LR, TR, UR in equations respectively.

We make the assumption that the available bandwidth for each node is greater than the sum of the LRs in the same node. If for one specific node this assumption does not hold, the long-term bandwidth allocation problem is trivial, i.e., $x = LR$. We are only interested in the subset of nodes for which the assumption holds in the network. So our assumption is reasonable. Now with our assumption, the feasible rate set X is:

$$X = \left\{ x: x \in R^N, x > LR, x \leq UR \text{ and } Ax \leq B \right\},$$

and has at least one nonempty interior point.

Now we can formulate our centralized bandwidth allocation problem as follows:

$$\begin{aligned} &\max \sum_{i=1}^{N} \left[m_i \cdot \log(x_i - c_i) - \frac{x_i - a_i}{k_i} \right] \\ &\text{subject to}: x_i \geq c_i, x_i \leq b_i, i = 1, 2, ..., N. \\ &\qquad Ax \leq B \end{aligned} \tag{4.7}$$

with the assumption that $Ax_c < B$, where $x_c = [c_1, c_2, \ldots, c_N]^T$. Due to the concavity and injective properties are invariant under the mapping of the logarithmic function [64], the objective function in the problem (4.7) is equivalent to the following one:

$$\max \prod_{i=1}^{N} (x_i - c_i)^{m_i} \cdot e^{-\frac{x_i - a_i}{k_i}} . \tag{4.8}$$

In this problem, m_i is the weight for the source i, x_i is the allocated bandwidth for the source i, c_i is the minimum bandwidth for the source i, a_i is the targeted bandwidth for the source i, b_i is the maximum bandwidth for the source i, k_i is the desired attenuation parameter for the source i, and A, B represent the other constraints for the capacity.

Before solving this problem, we will first investigate the objective function, or namely our chosen utility function. According to the previous discussion, the optimal point x of the above problem has the property that for any perturbation,

$$\sum_{i \in I} U_i'(x_i) \cdot \delta x_i \leq 0,$$

or equivalently, when $m_i = 1$,

$$\sum_{i \in I} \delta x_i \cdot \left(\frac{1}{x_i - c_i} - \frac{1}{k_i} \right) \leq 0 .$$

Therefore, the solution will have a similar property as proportional fairness:

$$\sum_{i \in I} \frac{\delta x_i}{x_i - c_i} \leq \sum_{i \in I} \frac{\delta x_i}{k_i}, \tag{4.9}$$

i.e., nearby the optimum point, the aggregation of the relative changes of all the sources will be upper-bounded, although not zero. We call this property "pseudo-proportional fairness". When (k_i, $i \in I$) are large enough, the upper bound will be small, even close to zero. We will see that this property is well-coupled with the short-term time-varying bandwidth allocation in section 4.2. For arbitrary (m_i, $i \in I$), the property becomes:

$$\sum_{i\in I}\frac{m_i\cdot\delta x_i}{x_i-c_i}\ \le\ \sum_{i\in I}\frac{\delta x_i}{k_i} \tag{4.10}$$

and we call it "weighted pseudo-proportional fairness".

4.1.4. Problem Solution

Under our assumptions, the feasible rate set X has nonempty interior, and the chosen utility function is an increasing, strictly concave and continuously differentiable function of x over the designated range. Then clearly, in the problem (4.7), the objective function is increasing, strictly concave and continuously differentiable, and the constraints are linear. Therefore, the first-order Kuhn-Tucker conditions are the sufficient and necessary conditions for optimality [65].

Now we consider the Lagrangian form:

$$\begin{aligned} L(x,\lambda,\beta,\mu) &= \sum_{i=1}^{N}\left[m_i\cdot\log(x_i-c_i)-\frac{x_i-a_i}{k_i}\right]-\sum_{i=1}^{N}\lambda_i(c_i-x_i) \\ &-\sum_{i=1}^{N}\beta_i(x_i-b_i)-\sum_{l=1}^{L}\mu_l\cdot\left[(Ax)_l-B_l\right],\ \ x_i\ge 0,\ \lambda_i\ge 0,\ \beta_i\ge 0,\ \mu_i\ge 0,\ i=1,\ ...,\ N \end{aligned} \tag{4.11}$$

where λ_i, μ_i, β_i, $i = 1, \ldots, N$, are Lagrange multipliers associated with the LRs, URs and capacity constraints.

Consequently the sufficient and necessary conditions are:

$$\frac{\partial L}{\partial x_i}=\frac{m_i}{x_i-c_i}-\frac{1}{k_i}+\lambda_i-\beta_i-\sum_{l=1}^{L}\mu_l A_{l,i}=0;$$

$$\begin{cases}\dfrac{\partial L}{\partial \lambda_i}=x_i-c_i=0 \ \text{ if } \lambda_i>0\\ \dfrac{\partial L}{\partial \lambda_i}=x_i-c_i\ge 0 \ \text{ if } \lambda_i=0\end{cases},\ i=1,\ \ldots,\ N;$$

$$\begin{cases} \dfrac{\partial L}{\partial \beta_i} = b_i - x_i = 0 \text{ if } \beta_i > 0 \\ \dfrac{\partial L}{\partial \beta_i} = b_i - x_i \geq 0 \text{ if } \beta_i = 0 \end{cases}, i = 1, \ldots, N; \tag{4.12}$$

$$\begin{cases} \dfrac{\partial L}{\partial \mu_l} = B_l - (Ax)_l = 0 \text{ if } \mu_l > 0 \\ \dfrac{\partial L}{\partial \mu_l} = B_l - (Ax)_l \geq 0 \text{ if } \mu_l = 0 \end{cases}, l = 1, \ldots, L.$$

Note that the first equation of (4.12) is equivalent to

$$m_i = (x_i - c_i)\left[\frac{1}{k_i} - \lambda_i + \beta_i + \sum_{l=1}^{L} \mu_l A_{l,i}\right]. \tag{4.13}$$

Under our assumption that the available bandwidth for each node is greater than the sum of the LRs in the same node, the constraints $x_i - c_i \geq 0$ are always inactive and then $\lambda_i = 0$ for $i = 1, \ldots, N$. Hence, for all i, we consider the two cases $\beta_i > 0$ and $\beta_i = 0$ separately. We obtain the unique solution, which is given by:

$$\begin{aligned} &\forall i = 1, \ldots, N, \quad \forall l = 1, \ldots, L, \\ &x_i = c_i + \min\left[(b_i - c_i), \ \frac{m_i}{\dfrac{1}{k_i} + \sum_{l=1}^{L} \mu_l A_{l,i}}\right] \\ &Ax \leq B, \ (Ax - B)_l \cdot \mu_l = 0, \ \mu_l \geq 0. \end{aligned} \tag{4.14}$$

We have several useful remarks for the obtained optimal solution:

1. The Lagrange multiplier μ_l is the implied cost of unit flow through link l, or the shadow price of an additional unit capacity for link l.
2. For one specific user, the assigned bandwidth is explicitly dependent on the link costs and its own parameters, while implicitly dependent on the users in other nodes.

3. m_i is the weight for the user i. The user with higher m_i has better opportunity to get more bandwidth than the user with lower one in the same node.
4. k_i is the desired attenuation parameter for the source i. Assume that k is proportional to $(a - c)$ and $(b - c)$, while inversely proportional to $(b - a)$, we have that $k \propto \frac{a-c}{b-a}(b-c)$. Again, the user with higher k_i has better opportunity to get more bandwidth than the user with lower one.

From these remarks, we see that our framework has one more parameter (TR) which models the turning point of a user's request. By increasing the utility function before TR while decreasing it after TR, we make the bandwidth allocation more reasonable among all the users/flows while maintaining a property similar to proportional fairness. At the same time, the importance of TR is modeled by k_i. With higher k_i, the effect of TR on our framework is smaller.

Now consider the asymptotic property of k_i, and the difference between our model and the model associated with proportional fairness. Recall that $k_i \geq b_i - c_i, \forall i = 1,..., N$. As all k_i go to ∞, it follows that our objective function

$$\max \sum_{i=1}^{N}\left[m_i \cdot \log(x_i - c_i) - \frac{x_i - a_i}{k_i} \right] \rightarrow \max \sum_{i=1}^{N}\left[m_i \cdot \log(x_i - c_i)\right],$$

which is exactly the one with proportional fairness discussed in [63, 64] when $m_i = 1$. As a result, our optimal solution here is exactly the one in [64] as all k_i go to ∞. Also, with k_i increasing, the attenuation for the source i is decreased, and then the possibility for the source i to get more bandwidth after certain point is increased. This observation illustrates the relation between our model associated with pseudo-proportional fairness with the one associated with proportional fairness.

4.2. *Short-term Dynamic Bandwidth Allocation*

In this section we formulate the general time-varying dynamic bandwidth allocation problem for a slotted TDMA protocol in space communication networks based on the parameters determined by the long-term bandwidth allocation, and find its solution to be used in our proposed hybrid MAC protocol.

4.2.1. Model Description

As shown in Figure 4.3, the system model includes a number of mobile spacecraft (MS) in LEO, a GEO relay system and the ground network consisting of several ground stations (GS). The downlink channel of the relay satellite is shared by the spacecraft, which we model as streams with different priority levels going through a common queue and a router. The data will be delivered to the ground station through this relay, and then arrive at the end user, which could be either at a NASA facility or at the edge of a public/private network.

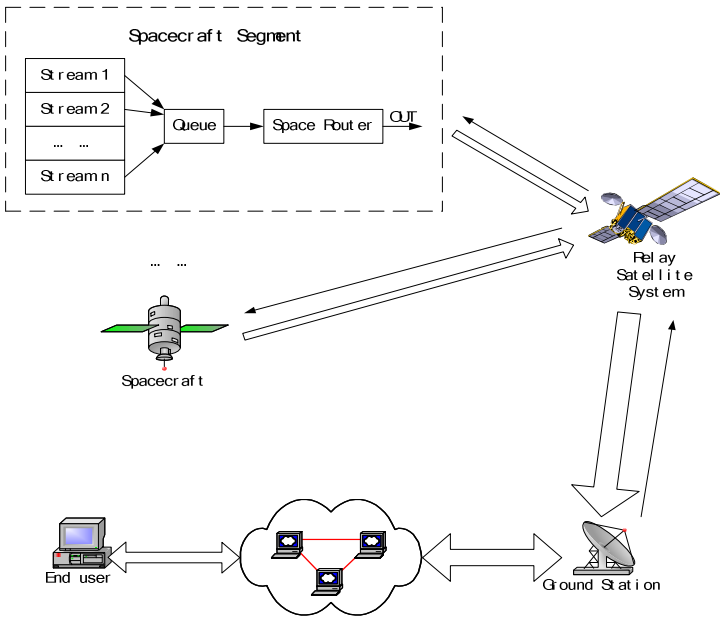

Figure 4.3: Architecture of Multi-access for the Downlink Channel of TDRSS

The multiple-access scheme in the downlink channel is based on a TDMA protocol. The frame with duration T_f consists of control slots and data slots. Let M denote the complete set of all MS, and M_a denote the set of active MS (i.e. the spacecraft with generating traffic). MS $k \in M_a$ sends a bandwidth request (BR) packet to the scheduler in the central ground station. There are two different levels of scheduling for dynamic bandwidth allocation: burst-level scheduling and packet-level scheduling. For burst-level scheduling, the central ground station performs the scheduling only once during each frame and allocates timeslots to a stream within a frame in a contiguous fashion. While for packet-level scheduling, the scheduling is performed during each timeslot and one timeslot is assigned at a time. Here we consider burst-level scheduling only. According to all the BR packets, the scheduler generates a bandwidth allocation table (BAT) and sends it back to all the MS in the set M_a. Then each active MS knows its assigned timeslots after reading the BAT. A BAT contains information including User_ID that defines the identifier of the MS, and the fields that specify the timeslots assigned to this specific MS.

4.2.2. Problem Definition

The resources to be assigned in our TDMA downlink channel are the total available data slots. Let N denote the number of the total available data slots. Here we focus on the optimal scheduling problem for assigning the N timeslots for all the active MS. The MS now represent the different streams on-board itself.

We consider the penalty weights ν_{kl}, $k \in M_a$, $l \in C$ for the service class l of the MS k to reflect the QoS and different requirements in our optimal scheduling problem.

The penalty weights are determined by the QoS, average waiting time and the amount of waiting packets in queues.

For priority queuing, the packets with higher priority level must be delivered earlier than those with lower priority level. Thus we can decompose the optimization problem into several sub-problems, each of which deals with the scheduling among the MS with the same priority level. Certainly the sub-problems must be solved in the descending order of the priority levels. We also can reflect the different priority levels in the penalty weights instead of using priority queuing.

For different slots assignment, the total penalty can be calculated with the definition of these penalty weights and the utility function (which will be defined in the following section). Our objective for the optimal scheduling is to find the solution for minimizing the total penalty. It is very convenient to change the penalty weights and utility function to achieve different optimization problems.

4.2.3. Input Parameters and Utility Function

Every time before determining the BAT, the scheduler collects the updated information including the number of MS (M) and active MS (M_a), the bandwidth demands (D) of active MS and those for calculating the penalty weights. To present the different types of traffic, we let C denote the set of service classes. Thus, D is a two dimensional matrix $\{D_{kl}\}$, $k \in M_a$, $l \in C$. The demands (D) could be directly given by the MS or estimated by the collected information from the MS. The latter is more practical while more complicated since an estimation step is mandatory. The PR, i.e., (x_i, $i = 1, \ldots, N$), are used as parameters for estimation. We will discuss this later.

We use a matrix $s = \{s_{kl}\}$ to denote the amount of assigned data slots for service class $l \in C$ of the MS $k \in M_a$. Therefore, the throughput for MS k is $\sum_{l \in C} S_{kl}$.

We use the proportional utility function with the proportion of 1.

4.2.4. Problem Formulation

$$\begin{aligned} &\text{Minimize} \quad \sum_{k \in M_a} \sum_{l \in C} v_{kl} \cdot (D_{kl} - s_{kl})^+ \\ &\text{subject to:} \\ &\qquad s_{kl} \le \min(U_{kl}, D_{kl}), \qquad k \in M_a,\ l \in C \\ &\qquad s_{kl} \ge L_{kl}, \qquad k \in M_a,\ l \in C \\ &\qquad \sum_{k \in M_a} \sum_{l \in C} s_{kl} \le N, \\ &\qquad\qquad \forall\ s_{kl} \in \{0, 1, 2, ..., N\} \end{aligned} \tag{4.15}$$

If a MS requests more timeslots than the available ones, which can be assigned to it, only a portion of its requested slots will be actually admitted and the residual packets must wait for the next scheduling. Let U_{kl} and L_{kl} denote the upper bound and lower bound of capacity for the service class $l \in C$ of MS $\in M_a$, respectively. The LR and UR from the user via long-term bandwidth could be used directly here. Some mappings from LR and UR are also allowed. The PR, i.e., (x_i, i = 1, …, N), are used as parameters for bounded assignment. The upper bound of waiting time (delay) for the service class $l \in C$ of MS $k \in M_a$ is set and used in the assignment of penalty weights to guarantee the maximum delay if necessary.

4.2.5. Problem Solution

The solution can be found by these steps (as shown in Figure 4.4):

1. **Sorting:** Sort the penalty weights matrix $\{v_{kl}\}$ and re-list them in a vector V in descending order.

2. **Lower Bound assignment:** Determine the number of data slots for the active MS to satisfy the lower bound requirements.
3. **Additional Amount assignment:** After the 2nd step, assign the available slots to the active MS according to their order in the vector *V* until the demand or upper bound is fulfilled.
4. **Final assignment:** Allocate timeslots to each stream within a frame in a contiguous fashion.
5. **Create the BAT**.

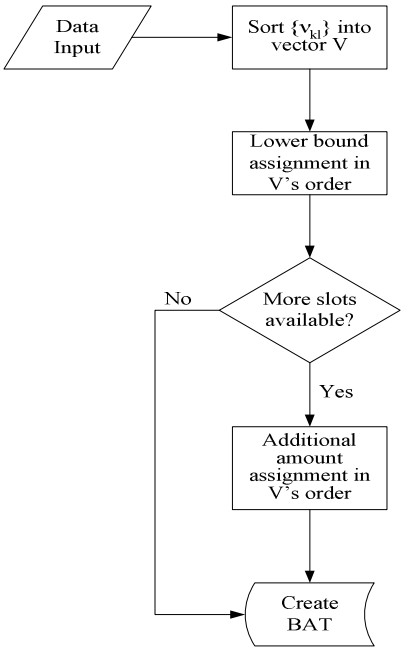

Figure 4.4: Job Flow Diagram of Bandwidth Allocation

Our problem formulation is based on two assumptions: 1) The demands D_{kl}, upper bounds U_{kl} and lower bounds L_{kl} are known or could be determined by the scheduler. 2) The penalty weights v_{kl} are very important and distinct. Another concern is that our problem should consider the multi-frame condition in space communication networks with long propagation delay.

We make some improvements for allowing for these concerns. Usually the U_{kl} and L_{kl} can be assigned according to the service requirements of the streams and the practical condition of the whole channel, and can be viewed as two adjustable parameters. Let t_0 and t denote the time the request was created in the MS and processed in the scheduler respectively. Between t_0 and t, the total assigned timeslots for the service class l of the MS k is called "credit" and denoted by $Ct_{kl}(t_0, t)$. Similarly, the total incoming packets between t_0 and t plus the number of packets in queue at time t_0 for the service class l of the MS k is called "debit" and denoted by $Dt_{kl}(t_0, t)$. Then, the "balance", defined as $\left[Dt_{kl}(t_0, t) - Ct_{kl}(t_0, t)\right]^+$, is a very practical determination of the demand D_{kl}. The cumulative bandwidth assignment for one user is upper bounded by its (TR * frames + U) and lower bounded by its (TR * frames – L). Notice that this approach considers the multi-frame condition for the long propagation delay. The penalty weights ν_{kl} are assigned discrete values based on the relations between the "balance" and some prescribed thresholds. When the ν_{kl} of some streams are the same, the calculated demands D_{kl} are used to determine their order in the first step.

One important advantage of this approach is that emergency traffic demands due to spacecraft anomalies or missed access opportunities or even science events that create a sudden, atypical traffic burst to cover high-entropy events can also be accommodated by such a hybrid MAC protocol approach. With dynamic bandwidth allocation, which can dynamically adjust the allocation to meet the varying requirements of each spacecraft and also allow them to send emergency traffic by using a lower bound for bandwidth, this can be achieved.

We present the simulation results by using our dynamic bandwidth allocation in the framework of our hybrid TDMA protocol in the next section.

4.3. Simulation Results of Relay-based Satellite Systems

4.3.1. Network Configuration

We use the Satellite Tool Kit (STK) software to create nine orbits of existing LEOs in the NASA network: TERRA, LEO1, LEO2, LEO3, LEO4, LEO5, LEO6, LEO7, LEO8 and LEO9. These spacecraft are using traffic models similar to those in the TERRA but with completely different parameters just for comparison purposes.

We use OPNET to import the above satellite network, and model the MAC protocol and network scenario. Once again, for simplification, we do not consider the issue of handover; therefore we will use only one relay satellite. And we only consider the spacecraft in the coverage zone of a relay satellite in the current location of TDRS_EAST [longitude of 319 degree, latitude of 0 degree, and altitude of 35,787 km]. As shown in Figure 4.5, only TERRA, LEO2, LEO3 and LEO4 are in the coverage zone. These four LEOs have the altitude range of 701–716 km. The White Sands Ground Terminal (WSGT) is located at longitude of –106 degrees west, latitude of 34.5 degree.

Because the number of LEOs in the coverage zone is predictable, we can determine the length of frame and time slot in advance. The calculated RTD is more than 0.66 seconds. We set $M \cdot T_f = 0.68$ seconds according to the analysis in the previous chapter. We set the number of data slots per frame as 64 ($N = 64$). The data rate of 200Mbps is assumed to be supported by this common link. However, to simplify the simulation, we do the following transformation: lower the channel

capacity to 2Mbps and accordingly take 1/100 of the data rate of all spacecraft. For example, the peak data rate of TERRA is taken as 1.08Mbps. Therefore, by combining these parameters and the length of source packet (512 bytes), we set M = 5, and get T_f = 0.1372 sec. Considering the use of guard time, we can assume that the downlink channel is an error-free TDMA common link.

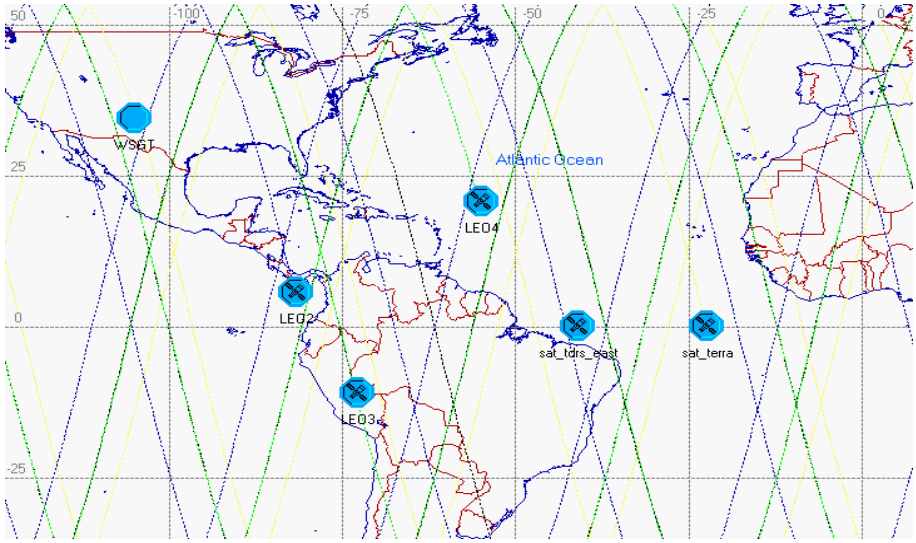

Figure 4.5: Network Model in OPNET

We are particularly interested in the system throughput, defined as the total amount of traffic arrived at the ground station in a given unit of time. This measure, in a sense, provides an indicator of the level of bandwidth-efficiency. Another performance of interest is end-to-end (ETE) delay. By the ETE delay of a packet, we mean the time interval between its generation on-board the spacecraft and its arrival at the ground station. For our hybrid-mode TDMA, in the initial phase, the ETE delay includes the reservation delay, which is more than twice the propagation delay. However, once the system is stable, the packet may not endure this type of long delay by using the allocated data slots.

We assume that the network traffic is diverse, i.e., the traffic loads are unevenly distributed among the spacecraft. Also, as mentioned earlier, the source traffic generating rate in a specific spacecraft varies considerably. Those properties match the unpredictable and dynamic traffic pattern in this environment. There would be times when a spacecraft could be completely inactive for a period of time, and an adaptive protocol would be capable to accommodate that. In practice, the inactive spacecraft can notify the ground station of this special status by sending a "negative" reservation request, i.e., set a negative number in the field of queue size. Then the ground station will exclude the assignment of reservation slots to this inactive spacecraft, and free all the reservation slots assigned to it before, except the statically assigned data slots. This may improve the bandwidth-efficiency by assigning the waste slots to the active spacecraft.

4.3.2. Performance Results and Discussion

Our simulation is run for around 10 minutes to reach steady-state. We try to adjust the simulation time so as to be within the limits corresponding to having the spacecraft inside the common coverage zone under one TDRS relay satellite is limited. Note that the spacecraft are orbiting rapidly (typically their orbit periods are around 95 minutes). Also note that these LEOs have an altitude range of 701–716 km. The propagation delay would vary from 0.24s to 0.30s. The variation of the propagation could be 0.06s, almost half the length of one frame.

The time difference or propagation delay between a spacecraft and the ground station includes two parts: 1) the time difference between spacecraft and relay satellite, which is variable, 2) the time difference between the relay satellite and the

ground station, which is fixed. Based on the orbit of the spacecraft and the positions of the relay satellite and the ground station, we could calculate the relative distances and therefore obtain the time difference. The computation result for the deterministic time difference between the spacecraft TERRA and the ground station WSGT is shown in Figure 4.6, where we use 6400km as the approximate radius of the Earth.

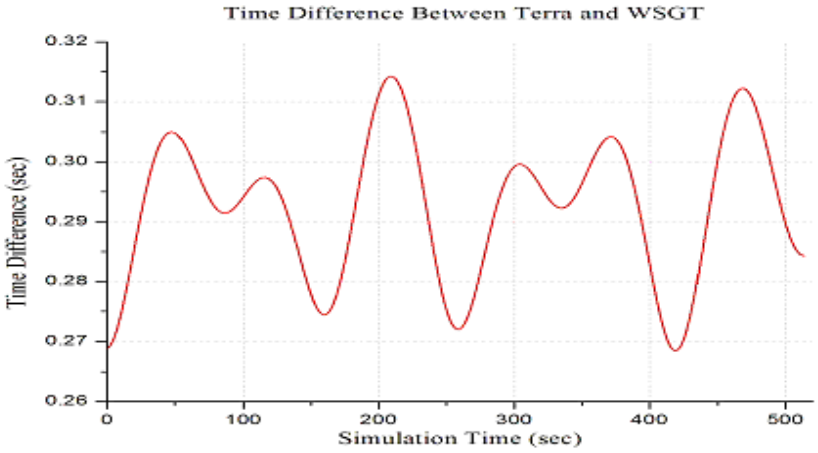

Figure 4.6: Time Difference between TERRA and WSGT

In all simulations we use probability-based traffic generators, MSMM (multi-state-multi-mode) and MM-MSMM (Markov Modulated MSMM), which introduce statistical variations to our simulation. We are collecting the statistical mean of the simulation results for the throughput and delay performance. The other statistics (for example, standard deviation, ranges, etc.) are beyond the scope of this chapter.

We first present the performance of our hybrid protocol under unevenly distributed traffic load. Then the ETE-delay and successful throughput performances of a conventional (static) TDMA solution will be compared with this protocol.

As shown in Figure 4.7, the ETE delay is ranging from 0.26 seconds to less than 0.5 seconds under different traffic loads with different numbers of active spacecraft. Considering the large propagation delay and its large variation due to spacecraft

mobility, this is very good. A major portion of the ETE delay in this case is introduced by the error in time synchronization. Suppose when the spacecraft has packets to transmit, it will calculate the propagation delay, say t_1, and determine whether it owns the current data slot (or control slot). If the answer is yes then it sends the packet, otherwise it determines the time for its data slot, say t. However, at time t, the propagation delay is t_2, not t_1. The direct result is that the spacecraft misses its data slot. And when the packets are delayed inappropriately in the spacecraft, the ETE delay and the throughput would be affected obviously. From Figure 4.7, we can obviously see that, the less active spacecraft, the better the protocol performs.

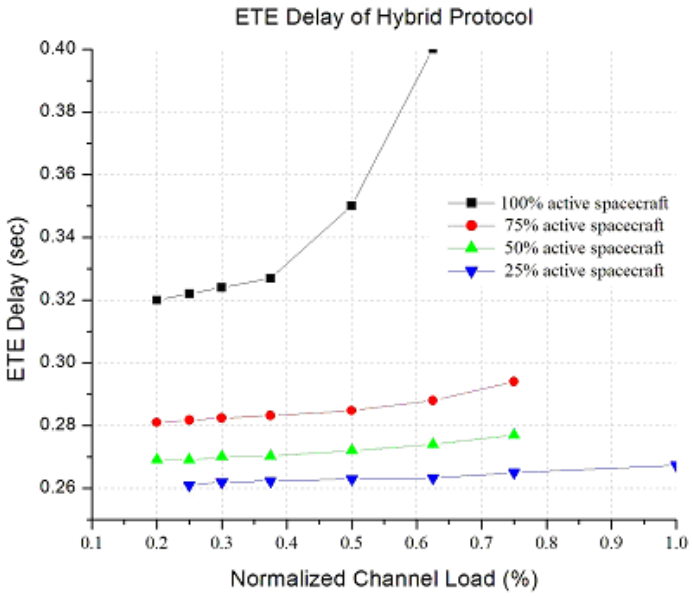

Figure 4.7: ETE Delay of Hybrid Protocol

As shown in Figure 4.8, the hybrid protocol outperforms the fixed TDMA in terms of ETE delay and successful throughput. This is because the hybrid protocol can utilize the data slots once belonging to the inactive spacecraft or spacecraft at low data rates in a short range, while in the fixed TDMA, these data slots are just wasted. Another reason is that in the hybrid protocol, the data slots are dynamically assigned

based on the behavior of their traffic, and therefore achieve the better bandwidth utilization. The more bursty and unpredictable the traffic sources are, the more the hybrid protocol will outperform a fixed TDMA solution.

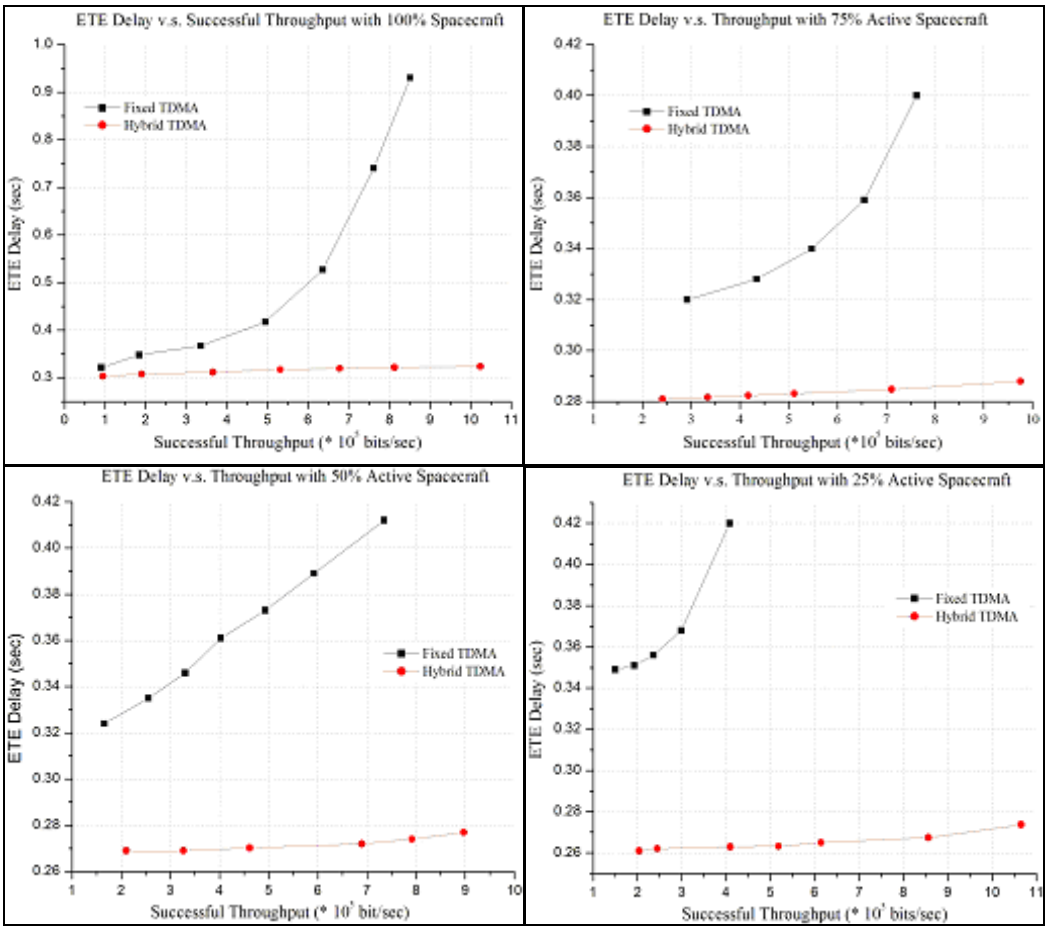

Figure 4.8: ETE Delay vs. Throughput with Different Number of Active Users

To further study the performance of our proposed hybrid protocol, we consider the queuing delay on-board a specific spacecraft (because of the size of exporting data, we only show the results in 5 minutes). The time-varying queuing delay curves for the same mission spacecraft in fixed TDMA mode and in hybrid TDMA mode are presented in Figure 4.9 (a 5-minute instance). As shown in the left figure, the queuing delay on-board a specific spacecraft presents similar behavior no matter how many spacecraft are active during the simulation time. This makes sense because for the

fixed TDMA mode, the assigned bandwidth (timeslots) for a specific user (spacecraft) is always the same regardless of the traffic variations affecting the other users. For the hybrid TDMA mode, the behavior exhibits significant improvements. As shown in the right figure, when there is an inactive spacecraft, the bandwidth re-allocation rapidly reduces the queuing delay on-board this specific spacecraft. When all the spacecraft are active, and competing for the same bandwidth, the queuing delay builds up but is still much shorter than the equivalent case in the fixed TDMA mode.

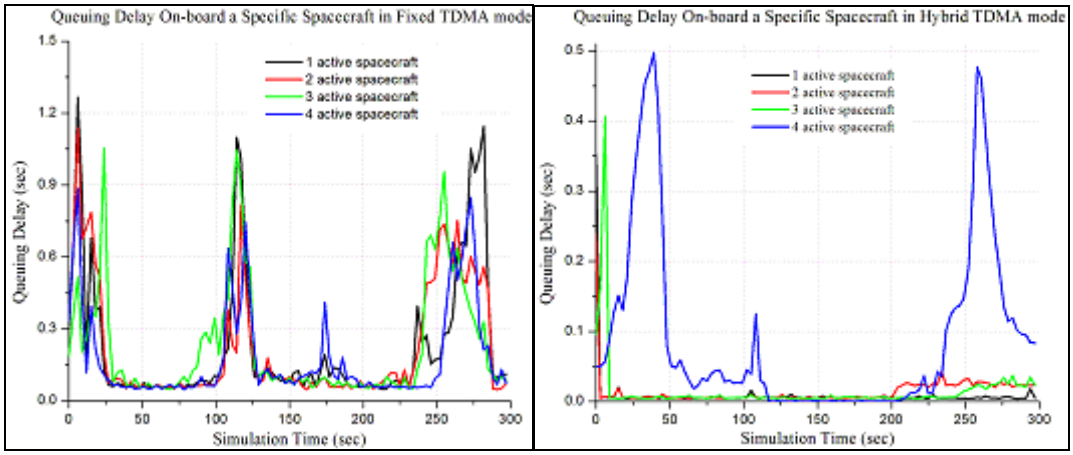

Figure 4.9: Queuing Delay On-board a Specific Spacecraft

Now we fix the ratio of expectations of traffic loads of four users (spacecraft) as 3:2:2:1, and study the performance of our hybrid protocol in terms of ETE delay, successful throughput and the fairness under this special scenario. As shown in Figure 4.10, the hybrid protocol outperforms the fixed TDMA in terms of ETE delay and successful throughput. This is because the hybrid protocol can utilize the data slots once belonging to the inactive spacecraft or spacecraft at low data rate in a short range, while in the fixed TDMA, these data slots are just wasted. Another reason is that in the hybrid protocol, the data slots are dynamically assigned based on the behavior of their traffic, and therefore achieve the better bandwidth utilization. The

more bursty and unpredictable the traffic sources are, the more the hybrid protocol will outperform a fixed TDMA solution.

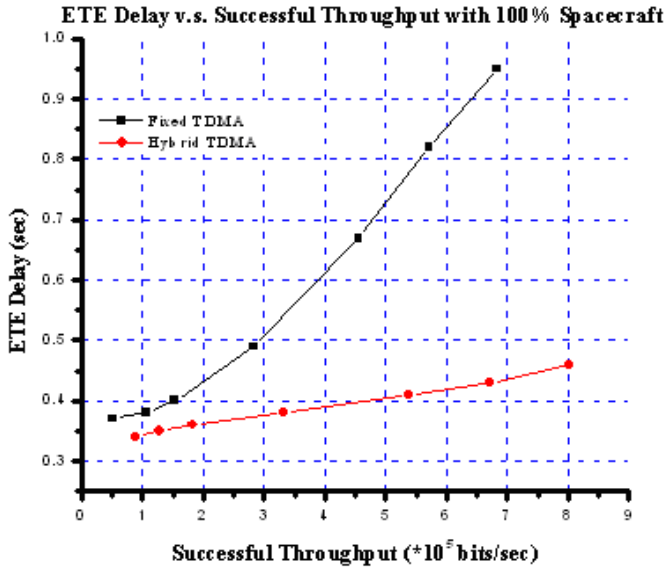

Figure 4.10: ETE Delay vs. Throughput

To study (long-term) fairness among all the users, the successful average throughputs of the total channel and every individual user are shown in Figure 4.11.

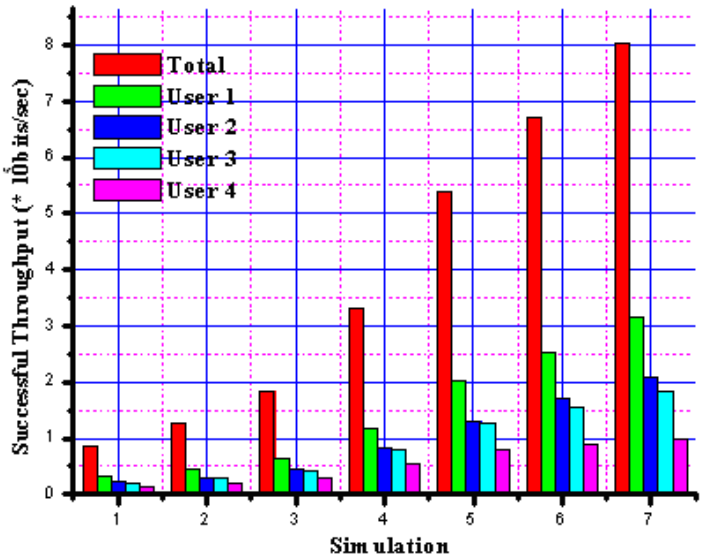

Figure 4.11: Fairness among Users

As shown in Figure 4.7, although obviously the proportional fairness is not achieved, the pseudo-proportional fairness is obtained in some sense. In other words,

the average share of the channel for every user is close to its proportional portion according to the expectations of traffic loads of four users, i.e., 3/8, 2/8, 2/8 and 1/8 respectively. Since we use the order of the users to break the tie sometimes in the dynamic bandwidth allocation, the average throughput of user 2 is always a little higher than that of user 3 despite that they have same traffic loads. A random tiebreak rule can be adopted instead of using the fixed user index.

4.4. Conclusions

In Chapter 3, we describe a slotted TDMA protocol more suitable for providing flexible access in a space relay topology with a high data rate downlink. To provide optimally or near-optimally efficient utilization and fair allocation of bandwidth of this downlink channel while guaranteeing specific QoS requirements for different service classes, we propose a two-level bandwidth allocation scheme in this chapter. The long-term bandwidth allocation is implemented to provide per-flow/per-user QoS guarantees and shape the average behavior. In our time-varying short-term bandwidth allocation with threshold regulation, a dynamic allocation is performed by solving an optimal timeslot scheduling problem according to the requests and other parameters. Through simulation results, the performance of the suitable MAC protocol with two-level bandwidth allocation is analyzed and compared with that of the existing static fixed-assignment scheme in terms of ETE delay and successful throughput. We also study the fairness among all the users under a special scenario and find that the pseudo-proportional fairness is achieved for our hybrid protocol. More details can be found in our publications [66, 67, 68, 69].

5. Rate-Control System with Time-varying Delays

Real-time rate-based flow control with feedback is broadly used to avoid queue overflow by adjusting the variable data rates assigned to all the flows. In wide-area networks, however, the time associated with the adaptive processes for feedback-based rate control is in the order of the large propagation delays. The problem is more severe considering the high speed in some wide-area networks, for example, in broadband satellite communication networks. But feedback-based rate control is still very suitable for broad classes of bursty applications, whose bandwidth demands will persist for comparable time durations to the time of adaptive processes. Also, it provides the feedback information to allow users/flows to take full advantage of the allocated bandwidth. In this chapter, we focus on feedback-based rate control in our broadband IP-based satellite communication networks.

In broadband IP-based satellite communication networks, the propagation delays are not only significantly large, but also different among users due to their different geographical locations. Moreover, when LEO/MEO/HEO or other moving objects are used as source nodes or intermediate nodes, the propagation delays are varying over time. Besides, the queuing delays in the source and intermediate nodes are also time-varying. So, we need to formulate rate-control system models with heterogeneously time-varying large propagation delays for our broadband satellite communication networks, and study the stability and the time-varying behavior of the bandwidth (rate) allocations and the on-board queue.

The rest of this chapter will be organized as follows: Section 5.1 describes our network models of rate control systems with time-varying propagation delays, and presents brief literature reviews directly related to our models. Section 5.2 lists recent work on rate control problems with time-varying delays from Kelly's framework. Section 5.3 gives the general algorithms for feedback-based rate control systems. Section 5.4 and 5.5 formulates the fluid models for a single flow and multiple flows, and studies their stability and time-varying behavior, respectively. Finally Section 5.6 summarizes this chapter.

5.1. Network Models

We first focus on a class of rate control algorithms with feedback to the users in the form of single bits within broadband satellite communication networks. The feedback information provided by the single bit is whether the instantaneous queue size at the distant location is beyond a threshold or not. The inter-arrival time between two adjacent feedbacks is approximately the one-way propagation delay since other communication delays are very small when compared with it.

Figure 5.1 shows the considered one-hop network model with various propagation delays among different flows. These flows could originate from LEOs or moving vehicles located at various geographical sites on the surface of the Earth or other planets. A distant queue has the service rate μ and the queue threshold Q_T, and could be located at the LEOs, the relay satellite or the ground station on Earth. For simplicity, the forward delay and feedback delay for a specific flow are always equal to the one-way propagation delay because the propagation delay is far larger than the other components of the transport delay; and the service discipline at the queue is

First-Come-First-Serve (FIFS). Depending on the locations of the flows and the distant queue, the propagation delay could be fixed or time-varying. Assume that the size of the packet is fixed. Also, the service rate in the satellite system is time-varying due to the time-varying characteristics of the satellite/wireless links, i.e., $\mu = \mu(t)$. It is worth noting that any network model with two or more than two hops can be decomposed and converted to the combination of one-hop network models as shown in Figure 5.1. So we focus on the dynamics of adaptation and the on/off of the flows in the one-hop model.

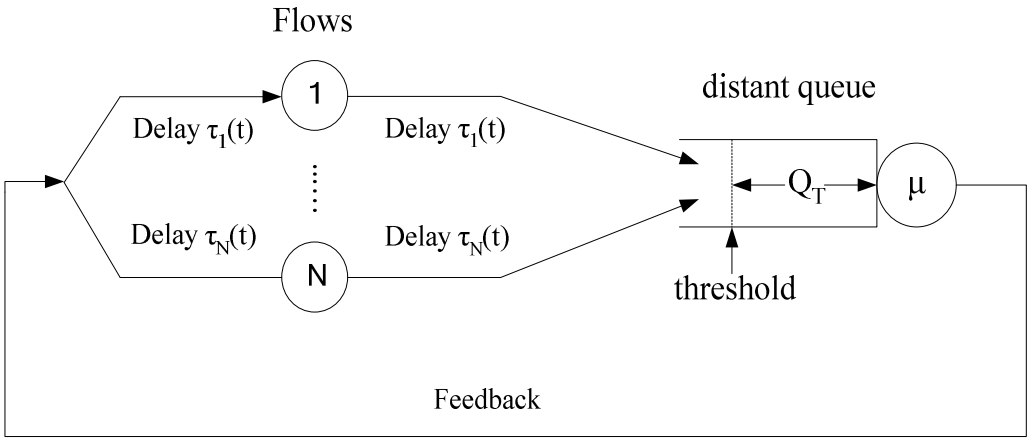

Figure 5.1: Network Models

Each flow is associated with two nonnegative parameters, v_j and σ_j, for flow j. v_j is the minimum bandwidth and σ_j is the nonnegative weight assigned to flow j to determine its best-effort share of the available bandwidth. According to their different types, the flows may be assigned appropriate values of these two parameters. CBR flows are only assigned minimum bandwidth because they demand fast delivery with zero toleration of the transfer delays. So $\sigma_j = 0$. Real-time (rt) and non real-time (nrt) Variable Bit Rate (VBR) traffics with minimum QoS guarantees are assigned

different v_j and σ_j for their requirements. For rt-VBR and nrt-VBR traffics without minimum QoS guarantees, $v_j = 0$, while σ_j are similar as before.

We briefly review some prior work directly related to our models here. A network model with large propagation delays in wide-area networks is presented in [70], and the dynamics of this model is fully investigated via both analytic ways and simulations. This network model is very similar to our one-hop network model except that both propagation delays and service rates are fixed. A fundamental theory of response-time based adaptations for large propagation delays is developed in [71]. The damping and gain parameters are selected for the delay-differential equations to optimize transient behavior. A basic symmetric algorithm, called Mitra-Seery (MS), and its design rules are given in [70], while an asymmetric algorithm, called Jacobson-Ramakrishnan-Jain (JRJ), is introduced in [72]. We also draw ideas for the model formulation, fluid models approximation and behavior analysis from [73, 74].

In the rest of this chapter, we will first present a literature overview on rate-control problems derived from Kelly's framework in Section 5.2. Section 5.3 gives the general algorithms for feedback-based rate control for our generalized one-hop network model, where both propagation delays and service rates are time-varying. Section 5.4 and Section 5.5 introduce and analyze the fluid models for single and multiple flows respectively. Our goal is to take full advantage of the network bandwidth among the active flows according to their allocation parameters and the fairness criterion. Section 5.6 draws our conclusions.

5.2. Recent Work on Rate-Control Problems from Kelly's Framework

We have described Kelly's framework in Section 4.1 and then derived a long-term bandwidth allocation algorithm from it thereafter. In this section we will briefly review previous work on the rate control system from Kelly's framework with fixed or time-varying communication delays.

Two simpler optimization problems based on Problem (4.1) are proposed and rate-based algorithms are presented to solve the system optimization problem in [63]. Then the convergence of these algorithms is established in [75] without consideration of feedback delays. The system of differential equations in [75] is as follows:

$$\frac{d}{dt}x_i(t) = \kappa_i \left[w_i(t) - x_i(t) \sum_{l \in r_i} \mu_l(t) \right]. \tag{5.1}$$

Here, $w_i(t)$ and $x_i(t)$ are user i's willingness to pay per unit time and rate allocation at time t, respectively. And k_i, $k_i > 0$ is the gain parameter for user i. Also $\mu_l(t) = p(x(t))$, where $p(x)$ is the price per unit flow charged by the resource when the rate is x. Most detailed notations are described in Section 4.1.

Recent work has been done on studying the system with fixed delays [76, 77, 78, 79, 80, 81, 82]. In [76], a single-flow single-resource case with a fixed feedback delay is analyzed and the condition of stability was shown under some assumptions on the price function. [80] gives the sufficient condition for the stability of the single-flow single-resource system with more general utility functions and fixed delay. The case with homogeneous fixed round-trip delay and utility function given by $w\log(.)$ is studied in [79] concerning stability and convergence rate. [78] provides a sufficient

condition for the stability of a single-resource multiple-flows system with fixed queuing delay.

The stability of a single-flow single-resource with state-dependent time-varying queuing delay is considered in [83]. It is shown that the stability conditions for a fixed delay are sufficient for a time-varying delay for this case. Analysis on the stability of a multiple-flows multiple-resources system with time-varying delays is presented in [76]. The stability of this system is established with a family of popular utility and price functions. It is also shown that the stability conditions for a fixed homogeneous delay are sufficient for time-varying delays.

In [81], a class of rate-control systems with time-varying propagation delays is analyzed under an optimization framework, with the delay modeled using a Gamma distribution. A sufficient condition for global stability of the considered rate-control system is proved, using the method based on contraction mapping by bounding the solution trajectory. In [82], heterogeneous time-varying delays are taken into consideration for the primal/dual distributed algorithms that solve the network flow optimization problems. Lyapunov-Krasovskii functionals are used to obtain the stability conditions for these algorithms, which is only dependent on the upper bound of delays.

The research in [76] gives us a very good viewpoint to study the dynamics for a system with time-varying delay. The network model mentioned in Section 5.1 and shown in Figure 5.1, is a multiple-flows single-resource system with heterogeneous time-varying propagation delays, which is a special case of the system studied in [76]. However, in our case, the variations of the propagation delays and themselves are

significantly larger so that it could be necessary to re-evaluate the sufficient and necessary conditions for stability for a family of time-varying propagation delays. Another reason is that we want to investigate performance and dynamic behaviors when the system does not have stationary solutions.

An alternative view of our proposed rate control problem can be derived from equations (10) and (11) in [76]. For $i = 1, \ldots, N$, the end user dynamics are given by

$$\frac{d}{dt}x_i(t) = \kappa_i \left[x_i(t)U_i'(x_i(t)) - p\big(x_i(t-\tau_i(t))\big)\right]. \tag{5.2}$$

Here, $\tau_i(t)$ is the round-trip delay of user i at time t. The other notations are the same as before. The queue dynamics can be represented by the following differential equations:

$$\frac{d}{dt}q(t) = \begin{cases} \sum_i x_i(t-\tau_i(t)) - \mu(t), & \text{if } 0 < q(t) < B \\ \left[\sum_i x_i(t-\tau_i(t)) - \mu(t)\right]^+, & \text{if } q(t) = 0 \\ \left[\sum_i x_i(t-\tau_i(t)) - \mu(t)\right]^-, & \text{if } q(t) = B \end{cases}, \tag{5.3}$$

where B is the finite buffer size, $[.]^+ = \max(., 0)$, and $[.]^- = \min(., 0)$.

Equations (5.2) and (5.3) could provide another viewpoint of the rate control system proposed and investigated in the rest of this chapter. Recall from Section 4.1.1 that the utility $U_i(x_i)$ is an increasing, strictly concave and continuously differentiable function of x_i over the range $x_i \geq 0$ (i.e., elastic traffic).

5.3. Algorithms for Feedback-based Rate-Control System

In this section, we give general asynchronous and synchronous versions for feedback-based rate-control systems. We introduce fluid models to approximate the

single flow and multiple flows, and study their stability and dynamic behavior in Section 5.4 and 5.5, respectively.

In what follows below, we first give the asynchronous algorithm, which is a modified version of (2.1) in [70] to incorporate time-varying service rates and propagation delays.

$$R_j(t) = \begin{cases} R_j(t-\tau_j(t)) - \gamma_j(u_j(t)) \cdot \tau_j(t) \cdot [R_j(t-\tau_j(t)) - \nu_j] + a_j(u_j(t)) \cdot \tau_j(t) \cdot u_j(t), & \text{if } j \in U(t) \\ R_j(t-0) & \text{if } j \notin U(t) \end{cases} \quad (5.4)$$

In equation (5.4), $R_j(t)$ denotes the rate allocation to the j^{th} flow right after an update at time t. $\tau_j(t)$ denotes the propagation delay associated with the j^{th} flow at the receiving time t. $U(t)$, a subset of $\{1, 2, \ldots, N\}$, denotes the set of flows which have their rates updated at t. Here N is the total number of flows. $u_j(t) \in \{-1, 1\}$ is the received feedback at the j^{th} flow right before time t. An update is triggered by the receipt of feedback information here but could be triggered by other events too. The binary value of $u_j(t)$ is determined by the size of the distant queue at time $(t - \tau_j(t))$ as follows: $u_j(t) = \text{sgn}[Q_T - Q(t - \tau_j(t))]$. Here $\gamma_j(.)$, $\gamma_j(.) \geq 0$ is the damping function while $a_j(.)$, $a_j(.) \geq 0$ is the gain function.

Let $\Delta_j(n)$ denote the interval between n^{th} and $(n+1)^{th}$ updates of the rate allocation for the j^{th} flow, and $R_j(n)$ denote the n^{th} update of the rate allocation. Also $u_j(n)$ denotes the n^{th} feedback. Then we have a synchronous version of equation (5.4) as follows:

$$R_j(n) = R_j(n-1) - \gamma_j(u_j(n)) \cdot \Delta_j(n) \cdot [R_j(n-1) - \nu_j] + a_j(u_j(n)) \cdot \Delta_j(n) \cdot u_j(n). \quad (5.5)$$

The window control problem can be easily formulated from equations (5.4) and (5.5) by replacing $R_j(t)$ and $\nu_j(t)$ with $K_j(t)$ and $K_{j,\,min}$, respectively. Here, $K_j(t)$ denotes the window of the j^{th} flow at time t and $K_{j,\,min}$ is the minimum window of the j^{th} flow.

5.4. Models for a Single Flow

In this section we focus on the case of only one flow, i.e., $N = 1$, hence the flow index j is suppressed. We then derive the approximate fluid model from equation (5.5) and start the study from the following damping and gain functions:

$$\gamma(u(t)) = \begin{cases} \gamma^+, \text{if } u(t) > 0 \\ \gamma^-, \text{if } u(t) < 0 \end{cases} \qquad \text{and} \qquad a(u) = \begin{cases} a^+, \text{if } u(t) > 0 \\ a^-, \text{if } u(t) < 0 \end{cases}$$

The model for a single flow with time-varying delay and bandwidth is:

$$\frac{d}{dt}\varphi(t) = \begin{cases} -\Gamma^+[\varphi(t) - \nu] + A^+ u(t) & \text{if} \quad u(t) > 0 \\ -\Gamma^-[\varphi(t) - \nu] + A^- u(t) & \text{if} \quad u(t) < 0 \end{cases} \qquad \text{(a)}$$

$$\frac{d}{dt}q(t) = \begin{cases} [\varphi(t - \tau(t)) - \mu(t)] & \text{if} \quad q(t) > 0 \\ [\varphi(t - \tau(t)) - \mu(t)]^+ & \text{if} \quad q(t) = 0 \end{cases} \qquad \text{(b)} \qquad (5.6)$$

Here, $\varphi(t)$ is the flow rate in term of the throughput of packets at time t. Γ^+, Γ^-, A^+, A^- are nonnegative parameters. Also $u(t) = \text{sgn}[Q_T - q(t - \tau(t))]$, and $[.]^+ = \max(., 0)$. To guarantee the minimum bandwidth, the admission control needs to ensure that $\nu \le \rho \cdot \mu$, where ρ is the average channel utilization and belongs to (0, 1). The steady state throughput is approximated by the long-term time average: $\lim_{t\to\infty} 1/t \int_0^t \varphi(s)ds$.

The correspondence between equations (5.4) and (5.6) leads to the following results: $\varphi(t) \approx R(t)$, $\Gamma^+ \approx \gamma^+$, $\Gamma^- \approx \gamma^-$, $A^+ \approx a^+$, $A^- \approx a^-$. Hence the design of algorithms for rate control in equation (5.6) is independent of the propagation delays $\tau(t)$.

Obviously it is difficult to directly solve equation (5.6) or study its dynamic behavior. So we will start our analysis from two cases mentioned in Section 5.1: time-varying propagation delay while fixed service rate; fixed propagation delay while time-varying service rate.

5.4.1. Case 1 – Time-varying Delays with Fixed Service Rate

The model for a single flow with time-varying propagation delay but fixed bandwidth is

$$\frac{d}{dt}\varphi(t) = \begin{cases} -\Gamma^{+}[\varphi(t)-\nu] + A^{+}u(t) & \text{if} \quad u(t) > 0 \\ -\Gamma^{-}[\varphi(t)-\nu] + A^{-}u(t) & \text{if} \quad u(t) < 0 \end{cases} \qquad \text{(a)}$$

$$\frac{d}{dt}q(t) = \begin{cases} [\varphi(t-\tau(t))-\mu] & \text{if} \quad q(t) > 0 \\ [\varphi(t-\tau(t))-\mu]^{+} & \text{if} \quad q(t) = 0 \end{cases} \qquad \text{(b)} \qquad (5.7)$$

In this case, the time-varying propagation delay does not affect the existence of stationary solutions. Consider stationary solutions that satisfy $d\varphi(t)/dt = dq(t)/dt = 0$ in equation (5.7). The only two possibilities are $u \equiv 1$ and $u \equiv -1$. When $u \equiv -1$, $q > Q_T > 0$, and $\varphi > \mu > \nu$ from the admission control. But for $d\varphi(t)/dt = 0$ with $u \equiv -1$, we have $\varphi = \nu - A^{-}/\Gamma^{-} < \nu$, which leads to contradiction. Hence, $u \equiv 1$, $\varphi = \nu + A^{+}/\Gamma^{+}$ and $\varphi < \mu$. Therefore, the stationary solution exists provided that $\nu + A^{+}/\Gamma^{+} < \mu$. This is the same as the system with fixed propagation delay and fixed bandwidth. We have the same results with the (i) and similar results with (ii) of Proposition 3.2 in [70].

Proposition 5.1: Suppose $\nu + A^{+}/\Gamma^{+} < \mu$ holds. The system in equation (5.7) has a stationary solution: $\varphi \equiv \nu + A^{+}/\Gamma^{+}$ and $q \equiv 0$. Also:

1. If $\varphi(t_1) \le \nu + A^+/\Gamma^+$ for any t_1, then $\varphi(t) \le \nu + A^+/\Gamma^+$ for all $t \ge t_1$. If $\varphi(t_0) > \nu + A^+/\Gamma^+$, then there exists t_2, $t_2 > t_0$, s.t. $\varphi(t)$ decreases monotonically when $t_2 > t > t_0$, and $\varphi(t_2) = \nu + A^+/\Gamma^+$.

2. Assume $\tau(t) \in S_T \subset R$ and S_T is compact. Denote its bounds as τ_{min} and τ_{max}. There exists t_3, s.t. for all $t \ge t_3$, $q(t) < Q_T$, $\varphi(t) \to \nu + A^+/\Gamma^+$ at the exponential rate Γ^+.

Proof: (1) If $\varphi(t) \le \nu + A^+/\Gamma^+ < \mu$, from equation (5.7b), $dq(t)/dt \le 0$ and $q \le Q_T$, hence $u \equiv 1 \ge 0$. From equation (5.7a), $d\varphi(t)/dt \ge 0$ holds until the stationary solution is achieved. So, we have $\varphi(t) \le \nu + A^+/\Gamma^+$ for all $t \ge t_1$.

If $\varphi(t) > \nu + A^+/\Gamma^+$, from equation (5.7a), we have:

$d\varphi(t)/dt \le \max\left(-\Gamma^+[\varphi(t) - \nu] + A^+,\ -\Gamma^-[\varphi(t) - \nu] - A^-\right) < 0$, i.e., $\varphi(t)$ decreases monotonically until the stationary solution.

(2) If $\varphi(t_1) \le \nu + A^+/\Gamma^+$ for any $t \ge t_1$, then $\varphi(t - \tau(t)) \le \nu + A^+/\Gamma^+ < \mu$ for $t \ge (t_1 + \tau_{max})$, and from (5.7b), $dq(t)/dt \le 0$ and $q \le Q_T$. Hence, after $t \ge (t_1 + \tau_{max})$, $q(t)$ decreases monotonically till the queue is empty and it remains empty thereafter. So, there exists t_3, s.t. for all $t \ge t_3 \ge (t_1 + \tau_{max})$, $q(t) < Q_T$, and $u \equiv 1 \ge 0$, which from (5.7a) leads to:

$$\varphi(t) = \nu + A^+/\Gamma^+ + e^{-\Gamma^+ \cdot (t - t_3)}\left[\varphi(t_3) - \nu - A^+/\Gamma^+\right].$$

□

From the proof of Proposition 5.1, we also have the following remarks when $\nu + A^+/\Gamma^+ < \mu$ holds:

Remark 5.1: The first property of Proposition 5.1 does not require bounded $\tau(t)$. We will show that the second property holds even for unbounded $\tau(t)$ if (1) $0 < \tau(t) < t$

and (2) $(t - \tau(t))$ is (not necessarily monotonically) increasing to $+\infty$. The conditions can be satisfied when the system is always in connection during the considered time window and based on FIFO.

Proof: If $\varphi(t_1) \le \nu + A^+/\Gamma^+$ for any $t \ge t_1$, there exists t_4, such that $t - \tau(t) \ge t_1$ for any $t \ge t_4$. This directly comes from the condition $0 < t - \tau(t) \to \infty$. Hence for any $t \ge t_4$, we have $\varphi(t - \tau(t)) < \mu$, and from equation (5.7b), $dq(t)/dt \le 0$ and $q \le Q_T$. Hence, after $t \ge t_4$, $q(t)$ decreases monotonically till the queue is empty and it remains empty thereafter. So, there exists t_3, s.t. for all $t \ge t_3 \ge t_4$, $q(t) < Q_T$, and $u \equiv 1 \ge 0$, which from (5.7a) leads to the same results in the second property of Proposition 5.1.

□

Remark 5.2: Recall that Γ^+, Γ^-, A^+, A^- are nonnegative parameters. Further assume that Γ^+, $\Gamma^- > 0$. The system in equation (5.7) is then globally asymptotically stable with exponential rate.

Proof: Define $\psi(t) \equiv \varphi(t) - \left(\nu + A^+/\Gamma^+\right)$. Also denote $\Gamma_M \equiv \min\left(\Gamma^+, \Gamma^-\right) > 0$ and $A_M \equiv \max\left(0,\ A^- - \dfrac{\Gamma^-}{\Gamma^+} \cdot A^+\right)$. From equation (5.7a), we have

$$\frac{d}{dt}\psi(t) = \begin{cases} -\Gamma^+ \cdot \psi(t), & \text{if} \quad u(t) > 0 \\ -\Gamma^- \cdot \psi(t) + \left(A^- - \dfrac{\Gamma^-}{\Gamma^+} \cdot A^+\right), & \text{if} \quad u(t) < 0 \end{cases} \tag{5.8}$$

Apparently its unique equilibrium point is $\psi(t) = 0$ since $\nu + A^+/\Gamma^+ < \mu$. Consider the upper right-hand derivative $D^+|\psi(t)|$, where $D^+v(t)$ is defined in [84] as:

$$D^+v(t) = \limsup_{h \to 0^+} \frac{v(t+h) - v(t)}{h}.$$

From equation (5.8) we have

$$
\begin{aligned}
D^+|\psi(t)| &= \mathrm{sgn}[\psi(t)]\cdot\frac{d}{dt}\psi(t) \\
&= \begin{cases} -\Gamma^+\cdot|\psi(t)|, & \text{if } u(t)>0 \\ -\Gamma^-\cdot|\psi(t)|+\mathrm{sgn}[\psi(t)]\cdot\left(A^- - \dfrac{\Gamma^-}{\Gamma^+}\cdot A^+\right), & \text{if } u(t)<0 \end{cases} \\
&\le -\Gamma_M\cdot|\psi(t)|+A_M
\end{aligned}
\tag{5.9}
$$

Hence, the system in equation (5.7) is globally asymptotically stable with exponential rate Γ_M.

□

Observe that equations (5.8) and (5.9) hold regardless of whether $\nu + A^+/\Gamma^+ < \mu$ is satisfied or not. Therefore, for any t_0 and $t > t_0$,

$$
|\psi(t)| \le A_M/\Gamma_M + \left[|\psi(t_0)| - A_M/\Gamma_M\right]\cdot\exp\left[-\Gamma_M(t-t_0)\right]. \tag{5.10}
$$

This property is very useful when studying the solutions in the fluctuation region where $\nu + A^+/\Gamma^+ < \mu$ does not hold.

5.4.2. Case 2 – Fixed Delays with Time-varying Service Rate

The model for a single flow with fixed delay but time-varying bandwidth is:

$$
\frac{d}{dt}\varphi(t) = \begin{cases} -\Gamma^+[\varphi(t)-\nu]+A^+u(t) & \text{if } u(t)>0 \\ -\Gamma^-[\varphi(t)-\nu]+A^-u(t) & \text{if } u(t)<0 \end{cases} \qquad \text{(a)}
$$

$$
\frac{d}{dt}q(t) = \begin{cases} [\varphi(t-\tau)-\mu(t)] & \text{if } q(t)>0 \\ [\varphi(t-\tau)-\mu(t)]^+ & \text{if } q(t)=0 \end{cases} \qquad \text{(b)} \tag{5.11}
$$

Now the admission control needs to ensure that $\nu \le \rho\cdot\overline{\mu}$, where ρ is the average channel utilization and belongs to (0, 1), $\overline{\mu}$ is the expectation of $\mu(t)$. Using the same method as in Case 1, when $u \equiv -1$, $q > Q_T > 0$, and $\varphi \ge \mu(t)$, which leads to $\varphi \ge \overline{\mu} > \nu$ from admission control. But for $d\varphi(t)/dt = 0$ with $u \equiv -1$,

$\varphi = \nu - A^-/\Gamma^- < \nu$, which leads to contradiction. Hence, $u \equiv 1$, $\varphi = \nu + A^+/\Gamma^+$ and $\varphi < \mu(t)$. With the time-varying service rate, it is not easy to even find the existence of stationary solutions except under the following special condition.

Proposition 5.2: Suppose that $\nu + A^+/\Gamma^+ < \inf_{t>t_0} \mu(t)$ for a finite time t_0. Then the system in equation (5.11) has a stationary solution: $\varphi \equiv \nu + A^+/\Gamma^+$ and $q \equiv 0$.

However, it is worth noting that in broadband satellite communication networks, the service rate is time-varying, but slowly compared with the time horizon of the system dynamic behavior due to the heterogeneous propagation delay. The service rate is even fixed for many other rate control systems. Hence, in the rest of this chapter, we focus on the rate control system with time-varying propagation delays while the service rate is fixed (Case 1 in Section 5.4.1), unless stated otherwise.

5.4.3. Solutions in the Fluctuation Region

According to Proposition 5.1, no stationary solution exists in the fluctuation region, where $\nu + A^+/\Gamma^+ < \mu$ does not hold for the system specified in equation (5.7). In this section we focus on the dynamic system behavior in the fluctuation region and expect that the system has fluctuating solutions with small amplitude in some sense through careful system designs. The assumptions in this section are listed below:

- $\nu + A^+/\Gamma^+ > \mu$. The system does not have any equilibrium point.
- A^+, $A^- \geq 0$ and Γ^+, $\Gamma^- > 0$. This is also the condition that the system is globally asymptotically stable with exponential rate when $\nu + A^+/\Gamma^+ < \mu$ holds.
- $\varphi(t)$ and $q(t)$ are piece-wise continuous and differentiable functions.

- $\tau(t) \in S_T \subset R$, where S_T is a compact set with nonnegative lower and upper bounds τ_{min} and τ_{max}, respectively.

In Remark 5.1, it has been shown that the propagation delays need not be bounded for Proposition 5.1 to hold, provided that $\tau(t) \geq 0$, $t - \tau(t) \geq 0$, and $t - \tau(t)$ goes to $+\infty$. In the fluctuation region, however, since the demand $(\nu + A^+/\Gamma^+)$ is even higher than the service rate μ, unbounded delays may eventually lead to forced dropping of incoming packets in the system. Figure 5.2 shows three typical solutions under different system conditions. Note that the presented solutions in all figures of this chapter are deterministic; however, our analyses are valid for non-deterministic cases.

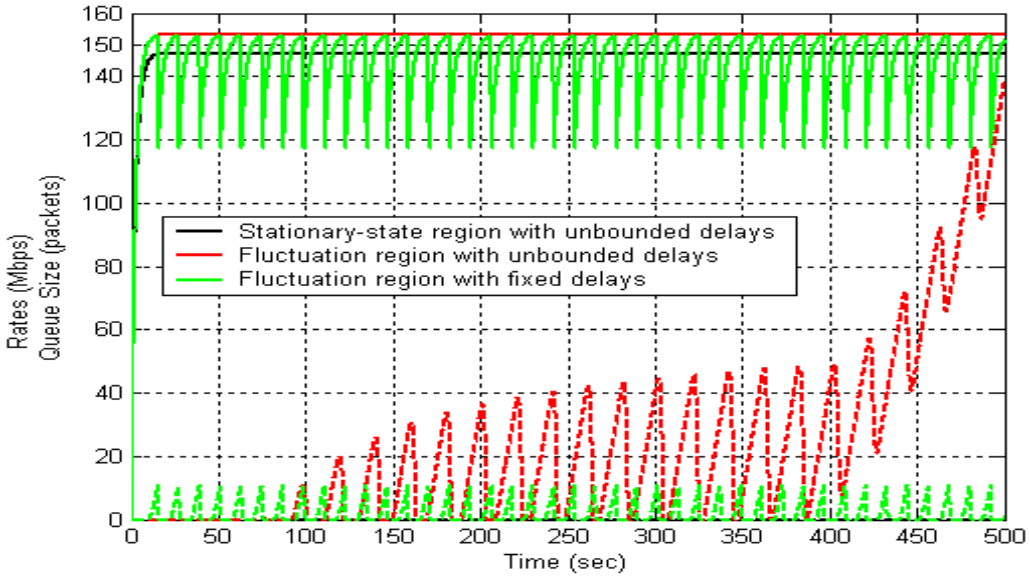

μ = 150 Mbps, ν = 30 Mbps, $A^+ = A^-$ = 48.1 Mbps, Δ = 0.05 s, Q_T = 10 packets.
Stationary-state region: $\Gamma^+ = \Gamma^-$ = 0.41; Fluctuation region: $\Gamma^+ = \Gamma^-$ = 0.39. Fixed delays: $\tau(t) \equiv$ 0.1 sec; Unbounded time-varying delays: $\tau(t) = t \cdot [0.928 + 0.06 \cdot \sin(\pi \cdot t / 10)]$.

Figure 5.2: Rate-Control System for a Single Flow with Unbounded Delays

As shown in Figure 5.2, each solid line represents the rates of the rate control system and the dash line of the same color depicts the corresponding queue behavior. In the system with unbounded delays, clearly $\tau(t) \geq 0$, $t - \tau(t) = t \cdot [0.072 - 0.06 \cdot \sin(\pi \cdot t/10)] \geq 0.012 \cdot t \geq 0$, and goes to infinity. In the stationary-state region when

$\nu + A^+/\Gamma^+ \approx$ 147.3 Mbps, even with unbounded delays, the system is stable at the equilibrium point with an empty queue. However, in the fluctuation region when $\nu + A^+/\Gamma^+ \approx$ 153.3 Mbps, the system with the same unbounded delays attempts to serve the flow at the rate of 153.3 Mbps, and hence with a finite buffer it will have to start dropping incoming packets if the service time is long enough. This dropping of packets is not desirable in satellite communication networks because satellite capacity is a scarce resource. Finally as a reference only, we show the system with fixed delays in the fluctuation region when $\nu + A^+/\Gamma^+ \approx$ 153.3 Mbps. It has been originally shown in [70, 85] that the system with fixed delays will have periodic solutions when no stationary solutions exist. In Figure 5.2, this periodic solution fluctuates in the range of 117 ~ 153 Mbps with a period of about 12 sec and an average rate of 144.5 Mbps.

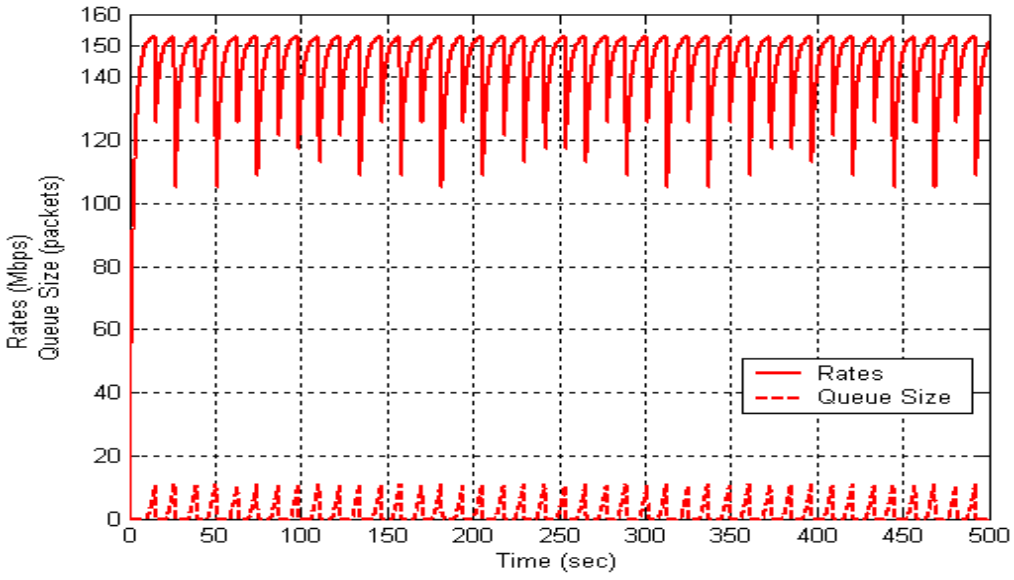

μ = 150 Mbps, ν = 30 Mbps, $A^+ = A^- =$ 48.1 Mbps, $\Gamma^+ = \Gamma^- =$ 0.39, Δ = 0.05 s, Q_T = 10 packets, $\tau(t) = 0.1 + 0.05 \cdot \sin(\pi \cdot t / 11)$.

Figure 5.3: Rate-Control System for a Single Flow with Bounded Delays

Unlike the system with fixed delays, with bounded time-varying delays, the rate-control system does not have equiripple periodic solutions in the fluctuation region, as shown in Figure 5.3. Here as an example we use a sinusoidal function to model the time-varying propagation delay. Let $\tau(t) = T_0 + \alpha sin(2\pi\beta t)$, where T_0 is a fixed delay, and α, β are parameters with $\alpha > 0$. Set $T_0 = 0.1$ s, $\alpha = 0.05$ s and $\beta \approx 0.0455$ Hz.

As shown in Figure 5.3, the single-flow system with bounded time-varying delays has (periodic or aperiodic) fluctuating solutions. With the same average delay as the system with fixed delays in Figure 5.2, this system with time-varying delays also has similar average rate (144.2 Mbps) and average "period" (12.1 sec). Despite of its larger amplitude compared with the fixed-delay case, the fluctuation is relatively small (<1/3) compared with the maximum rate (153 Mbps); and it could be even less with careful design of parameters.

Now we study the dynamic behavior of the system with general time-varying delay in the fluctuation region. Since v can be absorbed by $\varphi(t)$ and μ in equation (5.7), we set $v = 0$ in the rest of this section. And we use the Mitra-Seery (MS) algorithm in [70] where $\Gamma^+ = \Gamma^- = \Gamma$ and $A^+ = A^- = A$. At time 0, $\varphi(0) = q(0) = 0$.

Phase 1: $t \in (t_0, t_1)$, where $t_0 \equiv \inf\{t \geq 0: \varphi(t) = \mu\}$, $t_1 \equiv \inf\{t \geq t_0: q(t - \tau(t)) = Q_T\}$. We have $\varphi(t_0) = \mu$ and $q(t_0) = 0$. Clearly, in Phase 1, $u(t) = \text{sgn}[Q_T - q(t - \tau(t))] \equiv 1$, $\varphi(t)$ overshoots μ and always increases; $q(t)$ stays positive and increases except a subset of $(t_0, t_0 + \tau_{max})$. Assuming $t_0 + \tau_{max} << t_1$ and ignoring this small transition subset, the governing equations for Phase 1 are

$$\begin{aligned} \frac{d}{dt}\varphi(t) &= -\Gamma\varphi(t) + A \\ \frac{d}{dt}q(t) &= \varphi(t-\tau(t)) - \mu \end{aligned} \tag{5.12}$$

Hence $\varphi(t)$ is similar to previous discussions of equations (5.8) and (5.9):

$$\varphi(t) = A/\Gamma - (A/\Gamma - \mu)\cdot\exp\left[-\Gamma\cdot(t-t_0)\right],\ t \in (t_0, t_1)\,. \tag{5.13}$$

It is straightforward from (5.12) and (5.13) that $\mu \le \varphi(t_1) \le A/\Gamma$.

Note that equation (5.13) can be extended to $t \in (t_0 - \tau_{\max},\ t_0)$ during which $u(t) \equiv 1$ always holds and hence the governing equation for $\varphi(t)$ is exactly the same with the assumption $\tau_{max} << t_0$. Also, $\varphi(t-\tau_{\max}) \le \varphi(t-\tau(t)) \le \varphi(t-\tau_{\min})$ holds for any $t \in (t_0 - \tau_{\max}, t_0)$ due to the finite bounds of $\tau(t)$ and the monotonically increasing property of $\varphi(t)$.

Define two (bounds) trajectories at $t \in (t_0, t_1)$: $\breve{q}_l(t)$, $\hat{q}_l(t)$ that satisfy equation (5.12) with fixed delay as τ_{max} or τ_{min}, respectively, with the same initial state as $q(t)$ at time t_0, i.e., $\breve{q}_l(t_0) = \hat{q}_l(t_0) = q(t_0) = 0$. So, we have

$$\frac{d}{dt}\breve{q}_l(t) = \varphi(t-\tau_{\max}) - \mu \ \le\ \frac{d}{dt}q(t) \ \le\ \frac{d}{dt}\hat{q}_l(t) = \varphi(t-\tau_{\min}) - \mu,\ t \in (t_0, t_1),$$

and hence $\breve{q}_l(t) \le q(t) \le \hat{q}_l(t)$ for $t \in (t_0, t_1)$. So these two trajectories $\breve{q}_l(t)$, $\hat{q}_l(t)$ are called left-sided lower and upper bound curves, respectively.

We can then obtain the solutions of $\breve{q}_l(t)$, $\hat{q}_l(t)$, $t \in (t_0, t_1)$ from equation (5.13):

$$\begin{cases} \breve{q}_l(t) = (A/\Gamma - \mu)\cdot\left[(t-t_0) - 1/\Gamma\cdot\exp(\Gamma\cdot\tau_{\max})\cdot(1-\exp(-\Gamma\cdot(t-t_0)))\right] \\ \hat{q}_l(t) = (A/\Gamma - \mu)\cdot\left[(t-t_0) - 1/\Gamma\cdot\exp(\Gamma\cdot\tau_{\min})\cdot(1-\exp(-\Gamma\cdot(t-t_0)))\right] \end{cases}. \tag{5.14}$$

Note that $A/\Gamma - \mu > 0$ in equations (5.13) and (5.14). We can also assume $\varphi(t_0 - \tau(t_0)) > 0$, by satisfying $\exp(-\Gamma \cdot \tau_{\max}) > 1 - \mu \cdot \Gamma / A$ through parameter design.

From equation (5.14), a longer delay (τ_{max}, τ_{min} or $\tau(t)$) leads to a slower increasing of the number of packets in the queue for the corresponding (bound or time-varying queue) trajectory.

The approximations of $(t_1 - t_0)$, denoted as $(\hat{t}_1 - \hat{t}_0)$ and $(\breve{t}_1 - \breve{t}_0)$, can be obtained from these bound trajectories of equation (5.14) by setting $\hat{q}(t_1) = q(t_1)$ and $\breve{q}(t_1) = q(t_1)$, respectively. The relations between these approximations and the true value can be easily shown as $0 \le \hat{t}_1 - \hat{t}_0 \le t_1 - t_0 \le \breve{t}_1 - \breve{t}_0$. Note that $\hat{t}_0 = t_0 = \breve{t}_0$ from the definition of the bound trajectories.

From the lower bound trajectory in equation (5.14), $(\breve{t}_1 - \breve{t}_0)$ satisfies

$$(\breve{t}_1 - \breve{t}_0) - q(t_1)/\left(A/\Gamma - \mu\right) = 1/\Gamma \cdot \exp(\Gamma \cdot \tau_{\max}) \cdot \left[1 - \exp\left(-\Gamma \cdot (\breve{t}_1 - \breve{t}_0)\right)\right]. \qquad (5.15)$$

Denote $\breve{x} \equiv (\breve{t}_1 - \breve{t}_0)$, $\breve{x} \ge 0$. The LHS of equation (5.15) is a linear equation of $\breve{x}$ with a positive slope and a negative *y*-intercept; while the RHS of equation (5.15) is an exponential function of $\breve{x}$. Furthermore, the RHS is strictly monotonically increasing to $1/\Gamma \cdot \exp(\Gamma \cdot \tau_{\max})$ as $\breve{x} \to \infty$.

Figure 5.4 shows the LHS and RHS as functions of $\breve{x}$ in the first quadrant. The exponential curve (RHS) starts from the origin *O* and approaches the horizontal line $y = 1/\Gamma \cdot \exp(\Gamma \cdot \tau_{\max})$. On the other hand, the linear equation (LHS) has a positive *x*-intercept $q(t_1)/\left(A/\Gamma - \mu\right)$ at the point *B* and at the point *D* it crosses the horizontal line $y = 1/\Gamma \cdot \exp(\Gamma \cdot \tau_{\max})$. So, the intersection *J* of the LHS and RHS of equation (5.14) is located at a point between *B* and *D*. With a closer look at the Figure 5.4, one

can further claim that the point J lies between the points C and D by comparing points A, B and C. Hence, the bounds for $(\breve{t}_1 - \breve{t}_0)$ are

$$\frac{q(t_1)}{A/\Gamma - \mu} + \tau_{\max} < (\breve{t}_1 - \breve{t}_0) < \frac{q(t_1)}{A/\Gamma - \mu} + \frac{1}{\Gamma} \cdot \exp(\Gamma \cdot \tau_{\max}). \tag{5.16a}$$

An alternative lower bound can be obtained by considering the point B, E and F. At time $t = q(t_1)/(A/\Gamma - \mu)$, the LHS is zero at the point B while the RHS is Y_E at the point E, where by definition $Y_E \equiv \frac{1}{\Gamma}\exp(\Gamma \cdot \tau_{\max})\left[1 - \exp\left(-\Gamma \cdot \frac{q(t_1)}{A/\Gamma - \mu}\right)\right]$. With a slope of 1, the LHS needs an exact time of Y_E to achieve Y_E at the point F; and the point J lies beyond the point F for sure. Hence this alternative bound is

$$\frac{q(t_1)}{A/\Gamma - \mu} + \frac{1}{\Gamma}\exp(\Gamma \cdot \tau_{\max})\left[1 - \exp\left(-\Gamma \cdot \frac{q(t_1)}{A/\Gamma - \mu}\right)\right] < \breve{t}_1 - \breve{t}_0. \tag{5.16b}$$

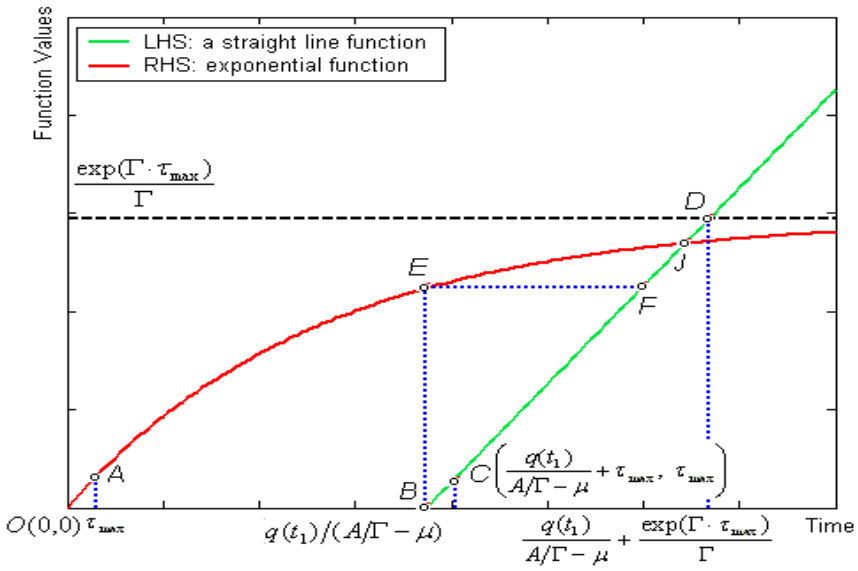

Figure 5.4: Approximation of ($t_1 - t_0$) from the Lower Bound Trajectory

The relative relation between the two lower bounds in (5.16a) and (5.16b) could go either way depending on the design parameters. So, the bounds can be written as

$$\max\left(\tau_{\max},\ \frac{\exp(\Gamma\cdot\tau_{\max})}{\Gamma}\left[1-\exp\left(\frac{-\Gamma\cdot q(t_1)}{A/\Gamma-\mu}\right)\right]\right)<\breve{t}_1-\breve{t}_0-\frac{q(t_1)}{A/\Gamma-\mu}<\frac{\exp(\Gamma\cdot\tau_{\max})}{\Gamma} \tag{5.16c}$$

For two extreme cases, the bounds for $(\breve{t}_1-\breve{t}_0)$ are

$$\begin{cases}\dfrac{\exp(\Gamma\cdot\tau_{\max})}{\Gamma}<\breve{t}_1-\breve{t}_0-\dfrac{q(t_1)}{A/\Gamma-\mu}<\dfrac{\exp(\Gamma\cdot\tau_{\max})}{\Gamma}, & \text{if} \quad A/\Gamma-\mu<<1\\ \tau_{\max}<\breve{t}_1-\breve{t}_0-\dfrac{q(t_1)}{A/\Gamma-\mu}<\dfrac{\exp(\Gamma\cdot\tau_{\max})}{\Gamma}, & \text{if} \quad A/\Gamma-\mu>>1\end{cases} \tag{5.16d}$$

Similarly, we can have the bounds for $(\hat{t}_1-\hat{t}_0)$ from the upper bound trajectory:

$$\max\left(\tau_{\min},\ \frac{\exp(\Gamma\cdot\tau_{\min})}{\Gamma}\cdot\left[1-\exp\left(\frac{-\Gamma\cdot q(t_1)}{A/\Gamma-\mu}\right)\right]\right)<\hat{t}_1-\hat{t}_0-\frac{q(t_1)}{A/\Gamma-\mu}<\frac{\exp(\Gamma\cdot\tau_{\min})}{\Gamma} \tag{5.17}$$

As a summary of equations (5.16) and (5.17), (t_1-t_0) is bounded via:

$$\max\left(\tau_{\min},\ \frac{\exp(\Gamma\cdot\tau_{\min})}{\Gamma}\cdot\left[1-\exp\left(\frac{-\Gamma\cdot q(t_1)}{A/\Gamma-\mu}\right)\right]\right)<t_1-t_0-\frac{q(t_1)}{A/\Gamma-\mu}<\frac{\exp(\Gamma\cdot\tau_{\max})}{\Gamma} \tag{5.18}$$

To move any further from equation (5.18), we need to study the range of $q(t_1)$. Recall the definitions: $t_1\equiv\inf\{t\ge t_0: q(t-\tau(t))=Q_T\}$, $t_0\equiv\inf\{t\ge 0:\varphi(t)=\mu\}$. It can be easily derived from the monotonically increasing property of $\varphi(t)$ in Phase 1 that

$$Q_T\le q(t_1)\le Q_T+(A/\Gamma-\mu)\cdot\tau(t_1)\le Q_T+(A/\Gamma-\mu)\cdot\tau_{\max}. \tag{5.19}$$

Substituting (5.19) into (5.18), we have the following bounds for (t_1-t_0):

$$\begin{aligned}\max\left(\frac{Q_T}{A/\Gamma-\mu}+\tau_{\min},\ \frac{Q_T}{A/\Gamma-\mu}+\frac{\exp(\Gamma\cdot\tau_{\min})}{\Gamma}\cdot\left[1-\exp\left(-\Gamma\cdot\frac{Q_T}{A/\Gamma-\mu}\right)\right]\right)\\ <t_1-t_0<\frac{Q_T}{A/\Gamma-\mu}+\tau_{\max}+\frac{1}{\Gamma}\cdot\exp(\Gamma\cdot\tau_{\max})\end{aligned} \tag{5.20}$$

Again we use the assumption that $t_0 + \tau_{max} << t_1$. From equation (5.20) it is obvious that $(t_1 - t_0)$ is roughly inversely proportional to $\left(A/\Gamma - \mu\right)$ and shaped by the bounds of the delays. Equations (5.18) and (5.20) can be used to provide bounds for the time duration of Phase 1.

For the system without delay, i.e., $\tau_{\min} = \tau_{\max} = 0$, $q(t_1) = Q_T$, $(t_1 - t_0)$ is a solution of $(t_1 - t_0) - Q_T/\left(A/\Gamma - \mu\right) = 1/\Gamma \cdot \left[1 - \exp\left(-\Gamma \cdot (t_1 - t_0)\right)\right]$, which is consistent with equation (5.20).

It is worth noting that alternative bound trajectories can be obtained by evaluating the system behavior in Phase 1 from the right side at time t_1. From this viewpoint, equation (5.13) can be rewritten as

$$\varphi(t) = A/\Gamma - \left(A/\Gamma - \varphi(t_1)\right) \cdot \exp\left[-\Gamma \cdot \left(t - t_1\right)\right],\ t \in (t_0, t_1), \tag{5.21}$$

where $\varphi(t_1) > \mu$ from previous analysis.

Define two trajectories at $t \in (t_0, t_1)$: $\breve{q}_r(t)$, $\hat{q}_r(t)$ that satisfy equation (5.12) with fixed delay as τ_{min} or τ_{max}, respectively, with the same initial state as $q(t)$ at time t_1, i.e., $\breve{q}_r(t_1) = \hat{q}_r(t_1) = q(t_1) > Q_T$. So, we have

$$\frac{d}{dt}\breve{q}_r(t) = \varphi(t - \tau_{\min}) - \mu \ \geq\ \frac{d}{dt}q(t) \ \geq\ \frac{d}{dt}\hat{q}_r(t) = \varphi(t - \tau_{\max}) - \mu,\ t \in (t_0, t_1),$$

and hence $\breve{q}_r(t) \leq q(t) \leq \hat{q}_r(t)$ for $t \in (t_0, t_1)$. So these two trajectories $\breve{q}_r(t)$, $\hat{q}_r(t)$ are called right-sided lower and upper bound curves, respectively.

We can then obtain the solutions of $\breve{q}_r(t)$, $\hat{q}_r(t)$, $t \in (t_0, t_1)$ from equation (5.16):

$$\begin{cases} \breve{q}_r(t) = \left(A/\Gamma - \mu\right) \cdot \left(t - t_1\right) - 1/\Gamma \cdot \exp(\Gamma \cdot \tau_{\min}) \cdot \left(A/\Gamma - \varphi(t_1)\right) \cdot \left[1 - \exp\left(-\Gamma \cdot (t - t_1)\right)\right] + q(t_1) \\ \hat{q}_r(t) = \left(A/\Gamma - \mu\right) \cdot \left(t - t_1\right) - 1/\Gamma \cdot \exp(\Gamma \cdot \tau_{\max}) \cdot \left(A/\Gamma - \varphi(t_1)\right) \cdot \left[1 - \exp\left(-\Gamma \cdot (t - t_1)\right)\right] + q(t_1) \end{cases} \tag{5.22}$$

Similarly approximations for $(t_1 - t_0)$ can be obtained (skipped here).

The following combination of $\breve{q}_l(t)$, $\hat{q}_l(t)$, $\breve{q}_r(t)$, $\hat{q}_r(t)$ leads to tighter bound trajectories: $\breve{q}(t) \equiv \max[\breve{q}_l(t), \breve{q}_r(t)]$, $\hat{q}(t) \equiv \min[\hat{q}_l(t), \hat{q}_r(t)]$, $t \in (t_0, t_1)$. These two trajectories $\breve{q}(t)$, $\hat{q}(t)$ are then called two-sided lower and upper bound curves, respectively. Their formulations can be obtained from equations (5.14) and (5.22); however, for simplicity, the details are skipped here. In the following analysis, we will only elaborate on the left-sided bound trajectories in any other phase; hence the left-sided (right-sided) index *l* (or *r*) is suppressed.

Phase 2: $t \in (t_1, t_2)$, where $t_2 \equiv \inf\{t \geq t_1: q(t - \tau(t)) = Q_T, \varphi(t) < \mu\}$. Clearly, in Phase 2, $u(t) \equiv -1$, so $\varphi(t)$ decreases and passes the line $\varphi(t) = \mu$ based on equations (5.8) and (5.9). $q(t)$ overshoots Q_T in Phase 1 when $t \in (t_1 - \tau(t_1), t_1) \subseteq (t_1 - \tau_{\max}, t_1)$, and remains increasing until $\varphi(t - \tau(t)) < \mu$ again; it decreases thereafter (to a neighborhood of Q_T) in the rest of Phase 2. Hence $q(t)$, $q(t) > 0$ is concave with a (local) maximum value at a time denoted by t_{12}^*, $t_{12}^* \in (t_1, t_2)$. Again we assume $t_1 + \tau_{max} << t_2$.

The governing equations for Phase 2 are

$$\begin{aligned} \frac{d}{dt}\varphi(t) &= -\Gamma\varphi(t) - A \\ \frac{d}{dt}q(t) &= \varphi(t - \tau(t)) - \mu \end{aligned} \tag{5.23}$$

Similarly to Phase 1, we can obtain:

$$\varphi(t) = \left(\varphi(t_1) + A/\Gamma\right) \cdot \exp\left[-\Gamma \cdot \left(t - t_1\right)\right] - A/\Gamma, \; t \in (t_1, t_2), \tag{5.24}$$

where $\varphi(t_1)$ is determined by equation (5.13). In Phase 2, due to the finite bounds of $\tau(t)$ and the monotonically decreasing property of $\varphi(t)$, we have

$\varphi(t-\tau_{\min}) \le \varphi(t-\tau(t)) \le \varphi(t-\tau_{\max})$. Note that $\varphi(t-\tau_{\max}) \le \varphi(t-\tau(t)) \le \varphi(t-\tau_{\min})$ holds in Phase 1, including $t \in (t_1-\tau_{\max}, t_1)$.

Extend the two bound trajectories $\breve{q}(t)$, $\hat{q}(t)$ previously defined for $t \in (t_0-\tau_{\max}, t_1)$ to $t \in (t_1, t_2)$, such that $\breve{q}(t)$, $\hat{q}(t)$ satisfy equation (5.23) and have the same initial state as $q(t)$ at time t_1, i.e., $\breve{q}(t_1) = \hat{q}(t_1) = q(t_1) > Q_T > 0$. Their corresponding delays are denoted as $\breve{\tau}(t)$, $\hat{\tau}(t)$: at $t \in (t_1+\tau_{\max}, t_2)$, $\breve{\tau}(t) \equiv \tau_{\min}$, $\hat{\tau}(t) \equiv \tau_{\max}$; while at $t \in (t_1, t_1+\tau_{\max})$, $\breve{\tau}(t) \equiv t - t_1'$, $\hat{\tau}(t) \equiv t - t_1$, where $t_1' = \arg\min\{\varphi(t): |t-t_1| \le \tau_{\max}\}$. Note that $\varphi(t_1)$ is a (local) maximum value.

For $t \in (t_1, t_2)$, $\varphi(t-\breve{\tau}(t)) - \mu \le \varphi(t-\tau(t)) - \mu \le \varphi(t-\hat{\tau}(t)) - \mu$, and hence we have $\breve{q}(t) \le q(t) \le \hat{q}(t)$ from equation (5.23). So, $\breve{q}(t)$, $\hat{q}(t)$ are the (left-sided) lower and upper bound curves, respectively.

The solution for $\breve{q}(t)$, $t \in (t_1, t_2)$ can be obtained from equations (5.23) and (5.24):

$$\breve{q}(t) = \begin{cases} (\varphi(t_1') - \mu)\cdot(t-t_1) + q(t_1), & t \in [t_1,\ t_1+\tau_{\max}] \\ \dfrac{(\varphi(t_1) + A/\Gamma)\cdot[1-\exp(-\Gamma\cdot(t-t_1-\tau_{\max}))]}{\Gamma\cdot\exp[\Gamma\cdot(\tau_{\max}-\tau_{\min})]} & \\ -\left(\dfrac{A}{\Gamma}+\mu\right)\cdot(t-t_1) + \left(\varphi(t_1') + \dfrac{A}{\Gamma}\right)\cdot\tau_{\max} + q(t_1), & t \in (t_1+\tau_{\max},\ t_2] \end{cases} \tag{5.25}$$

and the solution of $\hat{q}(t)$, $t \in (t_1, t_2)$:

$$\hat{q}(t) = \begin{cases} (\varphi(t_1) - \mu)\cdot(t-t_1) + q(t_1), & t \in [t_1,\ t_1+\tau_{\max}] \\ \dfrac{1}{\Gamma}\cdot(\varphi(t_1) + A/\Gamma)\cdot[1-\exp(-\Gamma\cdot(t-t_1-\tau_{\max}))] & \\ -\left(\dfrac{A}{\Gamma}+\mu\right)\cdot(t-t_1) + \left(\varphi(t_1) + \dfrac{A}{\Gamma}\right)\cdot\tau_{\max} + q(t_1), & t \in (t_1+\tau_{\max},\ t_2] \end{cases} . \tag{5.26}$$

Note that $\breve{q}(t_1) = \hat{q}(t_1) = q(t_1) > Q_T > 0$, $\varphi(t_1) > \mu$ in equations (5.24) – (5.26).

From equations (5.25) and (5.26), a longer delay (τ_{max}, τ_{min} or $\tau(t)$) leads to a quicker increasing of the queue size for the corresponding (bound or time-varying queue) trajectory.

The approximations for $(t_2 - t_1)$, denoted as $(\hat{t}_2 - \hat{t}_1)$ and $(\breve{t}_2 - \breve{t}_1)$, can be obtained from these bound trajectories in equation (5.23) by setting $\hat{q}(t_2) = q(t_2)$ and $\breve{q}(t_2) = q(t_2)$, respectively. The relations between these approximations and the true value can be easily shown as $0 \le \breve{t}_2 - \breve{t}_1 \le t_2 - t_1 \le \hat{t}_2 - \hat{t}_1$. Note that $\hat{t}_1 = t_1 = \breve{t}_1$ from the definition of the bound trajectories. Also note the relations here are different from those in Phase 1.

From the lower bound trajectory shown in equation (5.25), $(\breve{t}_2 - \breve{t}_1)$ satisfies

$$\left(\frac{A}{\Gamma} + \mu\right) \cdot (\breve{t}_2 - \breve{t}_1) - \left[q(t_1) - q(t_2) + \left(\varphi(t_1') + \frac{A}{\Gamma}\right) \cdot \tau_{\max} \right] = \frac{\exp\left(-\Gamma \cdot (\tau_{\max} - \tau_{\min})\right)}{\Gamma} \cdot \left(\varphi(t_1) + \frac{A}{\Gamma}\right) \cdot \left[1 - \exp\left(-\Gamma \cdot (\breve{t}_2 - \breve{t}_1 - \tau_{\max})\right)\right] \quad . \quad (5.27)$$

Denote $\breve{x} \equiv (\breve{t}_2 - \breve{t}_1)$, $\Delta\tau \equiv \tau_{\max} - \tau_{\min}$ and $\breve{a} \equiv \dfrac{q(t_1) - q(t_2) + \left(\varphi(t_1') + A/\Gamma\right) \cdot \tau_{\max}}{A/\Gamma + \mu}$.

Clearly, we have $\breve{x} \ge 0$, $\Delta\tau \ge 0$, and also $\breve{a} \ge \tau_{\max} \ge 0$ since $q(t_1) \ge Q_T \ge q(t_2)$. Equation (5.27) can then be written as:

$$\left(\frac{A}{\Gamma} + \mu\right) \cdot \left(\breve{x} - \breve{a}\right) = \frac{\exp\left(-\Gamma \cdot \Delta\tau\right)}{\Gamma} \cdot \left(\varphi(t_1) + \frac{A}{\Gamma}\right) \cdot \left[1 - \exp\left(-\Gamma \cdot (\breve{x} - \tau_{\max})\right)\right]. \quad (5.27')$$

The above equation is very similar to equation (5.15). Apparently its LHS is a linear equation of $\breve{x}$ with a positive slope (not 1 this time) and a positive *x*-intercept ($\breve{a}$); while its RHS is an exponential function of $\breve{x}$. Furthermore, its RHS is strictly

monotonically increasing to $1/\Gamma \cdot \exp(-\Gamma \cdot \Delta\tau) \cdot (\varphi(t_1) + A/\Gamma)$ as $\breve{x} \to \infty$, and has a positive *x*-intercept ($\tau_{\max}$). Hence, the bounds for $\breve{x} \equiv (\breve{t}_2 - \breve{t}_1)$ are

$$\begin{aligned} \frac{q(t_1) - q(t_2) + (\varphi(t_1') + A/\Gamma) \cdot \tau_{\max}}{A/\Gamma + \mu} &< \breve{t}_2 - \breve{t}_1 \\ &< \frac{q(t_1) - q(t_2) + (\varphi(t_1') + A/\Gamma) \cdot \tau_{\max} + (\varphi(t_1) + A/\Gamma) \cdot 1/\Gamma \cdot \exp(-\Gamma \cdot \Delta\tau)}{A/\Gamma + \mu} \end{aligned} . \quad (5.28a)$$

Similarly to the analysis of equation (5.15), for equations (5.27) and (5.27′), the alternative tighter lower bound can be obtained by considering the time $\breve{a}$, its RHS function value at time $\breve{a}$ (denoted as *f_rhs*($\breve{a}$)) and the slope of its LHS line function. This alternative lower bound is $\breve{a} + f\_rhs(\breve{a})/(A/\Gamma - \mu)$. However, the formulation turns out to be complicated and hence we leave it out from our discussion.

Similarly, from the upper bound trajectory in equation (5.25), $(\hat{t}_2 - \hat{t}_1)$ satisfies

$$(A/\Gamma + \mu) \cdot (\hat{x} - \hat{a}) = 1/\Gamma \cdot (\varphi(t_1) + A/\Gamma) \cdot [1 - \exp(-\Gamma \cdot (\hat{x} - \tau_{\max}))]. \quad (5.29)$$

Where $\hat{x} \equiv (\hat{t}_2 - \hat{t}_1)$, $\hat{a} \equiv \frac{q(t_1) - q(t_2) + (\varphi(t_1) + A/\Gamma) \cdot \tau_{\max}}{A/\Gamma + \mu}$. Clearly $\hat{x} \geq 0$, and also we have $\hat{a} \geq \tau_{\max} \geq 0$ since $q(t_1) \geq Q_T \geq q(t_2)$. Hence, the bounds for $\hat{x} \equiv (\hat{t}_2 - \hat{t}_1)$ are

$$\begin{aligned} \frac{q(t_1) - q(t_2) + (\varphi(t_1) + A/\Gamma) \cdot \tau_{\max}}{A/\Gamma + \mu} &< \hat{t}_2 - \hat{t}_1 \\ &< \frac{q(t_1) - q(t_2) + (\varphi(t_1) + A/\Gamma) \cdot \tau_{\max} + (\varphi(t_1) + A/\Gamma) \cdot 1/\Gamma}{A/\Gamma + \mu} \end{aligned} . \quad (5.30)$$

As a summary of equations (5.28) and (5.30), $(t_2 - t_1)$ are bounded as:

$$\begin{aligned} \frac{q(t_1) - q(t_2) + (\varphi(t_1') + A/\Gamma) \cdot \tau_{\max}}{A/\Gamma + \mu} &< \breve{t}_2 - \breve{t}_1 \leq t_2 - t_1 \leq \hat{t}_2 - \hat{t}_1 \\ &< \frac{q(t_1) - q(t_2) + (\varphi(t_1) + A/\Gamma) \cdot (\tau_{\max} + 1/\Gamma)}{A/\Gamma + \mu} \end{aligned} . \quad (5.31)$$

The range of $q(t_1)$, given in equation (5.19), is listed here for convenience. Considering the definition of t_2: $t_2 \equiv \inf\{t \geq t_1 \colon q(t-\tau(t)) = Q_T,\ \varphi(t) < \mu\}$, the range of $q(t_2)$ can be obtained similarly:

$$\begin{cases} Q_T = q(t_1 - \tau(t_1)) \leq q(t_1) \leq Q_T + (A/\Gamma - \mu)\cdot\tau(t_1) \leq Q_T + (A/\Gamma - \mu)\cdot\tau_{\max} \\ Q_T - (\mu - \varphi(t_2))\cdot\tau_{\max} \leq Q_T - (\mu - \varphi(t_2))\cdot\tau(t_2) \leq q(t_2) \leq q(t_2 - \tau(t_2)) = Q_T \end{cases}. \quad (5.32)$$

To move any further from equation (5.31), we still need to study the range of $\varphi(t_1)$ and $\varphi(t_1')$. It is straightforward from equations (5.12) and (5.13) that $\mu \leq \varphi(t_1) \leq A/\Gamma$. Recall the definition of t_1': $t_1' = \arg\min\{\varphi(t) : |t - t_1| \leq \tau_{\max}\}$. With the assumption that $t_1 + \tau_{max} << t_2$, it is safe to say

$$\varphi(t_2) \leq \mu \leq \varphi(t_1') \leq \varphi(t_1) \leq A/\Gamma. \quad (5.33)$$

Substituting (5.32) and (5.33) into (5.35), we have the bounds of $(t_2 - t_1)$:

$$\tau_{\max} < t_2 - t_1 < \frac{(A/\Gamma - \mu)\cdot\tau_{\max} + 2\,A/\Gamma\cdot(\tau_{\max} + 1/\Gamma)}{A/\Gamma + \mu}. \quad (5.34)$$

Both equations (5.31) and (5.34) can be used to provide bounds for the time duration of Phase 2. From equation (5.34) it is obvious that $t_2 - t_1$ is roughly inversely proportional to $(A/\Gamma + \mu)$ and shaped by the upper bound of delay $\tau_{\max}$. From equation (5.31), $t_2 - t_1$ is highly dependent on the transition behavior at the neighborhoods of t_2 and t_1. And since $\varphi(t_1)$ can be close to μ with parameter design in Phase 1, $t_2 - t_1$ can be bounded roughly in the range of $[\tau_{\max},\ \tau_{\max} + 1/\Gamma]$, which is largely affected by $\tau_{\max}$ and Γ.

Phase 3: $t \in (t_2, t_3)$, where $t_3 \equiv \inf\{t \geq t_2 \colon q(t) = 0,\ \varphi(t) < \mu\}$, i.e., the first time when the queue is emptied. And Phase 4: $t \in (t_3, t_4)$, where $t_4 \equiv \inf\{t \geq t_3 \colon \varphi(t) = \mu\}$.

Clearly, in Phases 3 and 4, $u(t) = \text{sgn}[Q_T - q(t - \tau(t))] \equiv 1$, $\varphi(t)$ always increases but $\varphi(t) < \mu$ holds in Phase 3 and 4; $q(t)$ stays positive in Phase 3 but goes down to zero at time t_3 and thereafter stays in the zero state in Phase 4. Again assume $t_2 + \tau_{max} < t_3$.

The governing equation for $\varphi(t)$ is the same in Phase 3 and 4, which is the reason why they are put together here:

$$\begin{aligned} \frac{d}{dt}\varphi(t) &= -\Gamma\varphi(t) + A \\ \frac{d}{dt}q(t) &= \begin{cases} \varphi(t-\tau(t)) - \mu, & t_2 < t < t_3 \\ 0, & t_3 \le t < t_4 \end{cases} \end{aligned} \tag{5.35}$$

Similarly we can obtain:

$$\varphi(t) = A/\Gamma - \left(A/\Gamma - \mu\right)\cdot \exp\left[-\Gamma\cdot\left(t - t_4\right)\right], \text{ or}$$

$$\varphi(t) = A/\Gamma - \left(A/\Gamma - \varphi(t_2)\right)\cdot \exp\left[-\Gamma\cdot\left(t - t_2\right)\right],\ t \in (t_2, t_4), \tag{5.36}$$

by using $\varphi(t_4) = \mu$, or $\varphi(t_2)$ which is determined by equation (5.24) and $\varphi(t_2) < \mu$. Since $\varphi(t-\tau(t))$ is monotonically increasing in Phases 3 and 4 but decreasing in Phase 2, we have $\varphi(t-\tau_{\min}) \ge \varphi(t-\tau(t)) \ge \varphi(t-\tau_{\max})$ for $t \in (t_2 + \tau_{\max}, t_4)$, while $\varphi(t_2') \ge \varphi(t-\tau(t)) \ge \varphi(t_2)$ for $t - \tau(t) \le t_2$, where $\varphi(t_2)$ is a (local) minimum value and $t_2' = \arg\max\{\varphi(t) :\ |t - t_2| \ \le\ \tau_{\max}\}$.

Since $q(t) \equiv 0$ in Phase 4, we focus on the queue behavior in Phase 3 for $t \in (t_2, t_3)$. Extend the two (right-sided) bound trajectories $\breve{q}(t)$, $\hat{q}(t)$ previously defined in Phase 1 and Phase 2, such that $\breve{q}(t)$, $\hat{q}(t)$ satisfy equation (5.35) for $t \in (t_2, t_3)$ with the same initial state as $q(t)$ at time t_3, i.e., $\breve{q}(t_3) = \hat{q}(t_3) = q(t_3) = 0$. Note that $0 \le q(t_2) \le Q_T$. Their corresponding delays, $\breve{\tau}(t)$, $\hat{\tau}(t)$, are: $\breve{\tau}(t) \equiv t - t_2'$, $\hat{\tau}(t) \equiv t - t_2$ for $t \in (t_2, t_2 + \tau_{\max})$; while at $t \in (t_2 + \tau_{\max}, t_3)$, $\breve{\tau}(t) \equiv \tau_{\min}$, $\hat{\tau}(t) \equiv \tau_{\max}$.

Apparently $d\breve{q}(t)/dt \geq dq(t)/dt \geq d\hat{q}(t)/dt$ holds for any $t \in (t_2, t_3)$. Hence with the right-side end point fixed at time t_3, $\breve{q}(t) \leq q(t) \leq \hat{q}(t)$ holds from equation (5.35). So $\breve{q}(t)$, $\hat{q}(t)$ are still the (right-sided) lower and upper bound curves, respectively.

The solution of $\breve{q}(t), t \in (t_2, t_3)$ can be obtained from equations (5.35) and (5.36):

$$\breve{q}(t) = \begin{cases} \dfrac{\left(A/\Gamma - \varphi(t_2)\right)\cdot\left[1-\exp\left(-\Gamma\cdot(t_3 - t_2 - \tau_{\max})\right)\right]}{\Gamma\cdot\exp\left[\Gamma\cdot(\tau_{\max}-\tau_{\min})\right]} \\ +\left(\varphi(t_2')-\mu\right)\cdot\left(t - t_2 - \tau_{\max}\right) - \left(\dfrac{A}{\Gamma}-\mu\right)\cdot\left(t_3 - t_2 - \tau_{\max}\right), & t \in [t_2,\ t_2+\tau_{\max}] \\ \left(\dfrac{A}{\Gamma}-\mu\right)\cdot\left(t-t_3\right) + \dfrac{\left(A/\Gamma-\varphi(t_2)\right)\cdot\left[\exp\left(\Gamma\cdot(t_3-t)\right)-1\right]}{\Gamma\cdot\exp\left[\Gamma\cdot(t_3-t_2-\tau_{\min})\right]}, & t \in (t_2+\tau_{\max},\ t_3] \end{cases} \tag{5.37}$$

and the solution of $\hat{q}(t)$, $t \in (t_2, t_3)$:

$$\hat{q}(t) = \begin{cases} 1/\Gamma\cdot\left(A/\Gamma - \varphi(t_2)\right)\cdot\left[1-\exp\left(-\Gamma\cdot(t_3 - t_2 - \tau_{\max})\right)\right] \\ +\left(\varphi(t_2)-\mu\right)\cdot\left(t - t_2 - \tau_{\max}\right) - \left(\dfrac{A}{\Gamma}-\mu\right)\cdot\left(t_3 - t_2 - \tau_{\max}\right), & t \in [t_2,\ t_2+\tau_{\max}] \\ \left(\dfrac{A}{\Gamma}-\mu\right)\cdot\left(t-t_3\right) + \dfrac{\left(A/\Gamma-\varphi(t_2)\right)\cdot\left[\exp\left(\Gamma\cdot(t_3-t)\right)-1\right]}{\Gamma\cdot\exp\left[\Gamma\cdot(t_3-t_2-\tau_{\max})\right]}, & t \in (t_2+\tau_{\max},\ t_3] \end{cases} \tag{5.38}$$

Note that $0 < q(t_2) < Q_T$, $\varphi(t_2) < \varphi(t_3) < \mu$ in equations (5.36) – (5.38).

Again, $(t_3 - t_2)$ can be approximated from the bound trajectories in equations (5.37) and (5.38). These approximations, denoted as $(\hat{t}_3 - \hat{t}_2)$ and $(\breve{t}_3 - \breve{t}_2)$, are obtained by setting $\hat{q}(t_2) = q(t_2)$ and $\breve{q}(t_2) = q(t_2)$, respectively. It can be easily shown that $0 \leq \hat{t}_3 - \hat{t}_2 \leq t_3 - t_2 \leq \breve{t}_3 - \breve{t}_2$. It is worth noting that $\hat{t}_3 = t_3 = \breve{t}_3$.

From equation (5.37), the approximation $(\breve{t}_3 - \breve{t}_2)$ satisfies:

$$\left(A/\Gamma-\mu\right)\cdot\left(\breve{t}_3-\breve{t}_2\right)+q(t_2)-\tau_{\max}\cdot\left(A/\Gamma-\varphi(t_2')\right)\ =$$
$$\left(A/\Gamma-\varphi(t_2)\right)\cdot\frac{\left[1-\exp\left(-\Gamma\cdot(\breve{t}_3-\breve{t}_2-\tau_{\max})\right)\right]}{\Gamma\cdot\exp\left[\Gamma\cdot(\tau_{\max}-\tau_{\min})\right]} \quad . \tag{5.39}$$

Since $\varphi(t_2)<\mu<A/\Gamma$, the LHS of equation (5.39) is a linear equation with a positive slope, and its RHS is an exponential function with the following properties at [0, +∞): strictly monotonically increasing, positive after the zero point $\tau_{\max}$, and approaching the maximum value as $(\breve{t}_3-\breve{t}_2)\to+\infty$. Therefore, if the linear equation (LHS) and the exponential function (RHS) have an intersection in the first quadrant, its upper bound will satisfy equation (5.39) by letting $(\breve{t}_3-\breve{t}_2)\to+\infty$ in the RHS. So, we have

$$\left(A/\Gamma-\mu\right)\cdot\left(\breve{t}_3-\breve{t}_2\right)+q(t_2)-\tau_{\max}\cdot\left(A/\Gamma-\varphi(t_2')\right)\ \le$$
$$\left(A/\Gamma-\varphi(t_2)\right)\cdot 1/\Gamma\cdot\exp\left[-\Gamma\cdot(\tau_{\max}-\tau_{\min})\right] \tag{5.40}$$

And finally we find the upper bound of $(\breve{t}_3-\breve{t}_2)$:

$$\breve{t}_3-\breve{t}_2\le\frac{\tau_{\max}\left(A/\Gamma-\varphi(t_2')\right)-q(t_2)+\left(A/\Gamma-\varphi(t_2)\right)\cdot 1/\Gamma\cdot\exp\left[-\Gamma\cdot(\tau_{\max}-\tau_{\min})\right]}{A/\Gamma-\mu} \tag{5.41}$$

The necessary condition for the existence of the positive solution in equation (5.39) is that the denominator in equation (5.41) is positive, i.e.,

$$\tau_{\max}\cdot\left(A/\Gamma-\varphi(t_2')\right)-q(t_2)+\left(A/\Gamma-\varphi(t_2)\right)\cdot 1/\Gamma\cdot\exp\left[-\Gamma\cdot(\tau_{\max}-\tau_{\min})\right]\ge 0\,. \tag{5.42}$$

Under the condition that the inequality (5.42) does not hold, equation (5.39) does not have a positive solution and hence $q(t)$ stays positive in Phases 3 and 4. In other words, the design of parameters leads to a non-empty queue even when the rate $\varphi(t)$ reaches μ at time t_4.

Similarly, the lower bound of $(\breve{t}_3 - \breve{t}_2)$ can be obtained by letting $\Gamma \cdot (\breve{t}_3 - \breve{t}_2) \to 0^+$ in the RHS of equation (5.39). With our previous assumption $\tau_{\min} < \tau_{\max} < \breve{t}_3 - \breve{t}_2$, we have: $\exp(\Gamma \cdot \tau_{\min}) \approx 0$, $\exp(-\Gamma \cdot \tau_{\max}) \approx 1 - \Gamma \cdot \tau_{\max}$. The lower bound is

$$\breve{t}_3 - \breve{t}_2 \geq \frac{q(t_2) - \tau_{\max} \cdot \left(A/\Gamma - \varphi(t_2')\right)}{\mu - \varphi(t_2)} \tag{5.43}$$

From equation (5.38), the approximation $(\hat{t}_3 - \hat{t}_2)$ satisfies:

$$\begin{aligned} &\left(A/\Gamma - \mu\right) \cdot \left(\hat{t}_3 - \hat{t}_2\right) + q(t_2) - \tau_{\max} \cdot \left(A/\Gamma - \varphi(t_2)\right) = \\ &\qquad 1/\Gamma \cdot \left(A/\Gamma - \varphi(t_2)\right) \cdot \left[1 - \exp\left(-\Gamma \cdot (\hat{t}_3 - \hat{t}_2 - \tau_{\max})\right)\right] \end{aligned} \tag{5.44}$$

Since $\varphi(t_2) < \mu < A/\Gamma$, the LHS of equation (5.44) is a linear equation with a positive slope, and its RHS is an exponential function with the following properties at [0, +∞): strictly monotonically increasing, positive after the zero point $\tau_{\max}$, and approaching the maximum $1/\Gamma \cdot \left(A/\Gamma - \varphi(t_2)\right)$ as $(\hat{t}_3 - \hat{t}_2) \to +\infty$. So, the upper bound of $(\hat{t}_3 - \hat{t}_2)$ can be obtained by letting $(\hat{t}_3 - \hat{t}_2) \to +\infty$ in the RHS of (5.44):

$$\hat{t}_3 - \hat{t}_2 \leq \frac{A/\Gamma - \varphi(t_2)}{A/\Gamma - \mu} \cdot \left(\tau_{\max} + 1/\Gamma\right) - \frac{q(t_2)}{A/\Gamma - \mu} \tag{5.45}$$

The necessary condition for the existence of a positive solution of $(\hat{t}_3 - \hat{t}_2)$ is

$$q(t_2) \leq \left(A/\Gamma - \varphi(t_2)\right) \cdot \left(\tau_{\max} + 1/\Gamma\right) \leq \left(A/\Gamma - \mu\right) \cdot \left(\tau_{\max} + 1/\Gamma\right) \tag{5.46}$$

Again, with the design of parameters that cannot satisfy inequality (5.46), the system will not achieve empty queue in Phase 3 and Phase 4. In fact, if it happens, the critical point (t_3) between Phase 3 and Phase 4 needs to be redefined as the time when the minimum queue size is achieved.

Similarly, the lower bound for $(\hat{t}_3 - \hat{t}_2)$ can be obtained by letting $\Gamma \cdot (\hat{t}_3 - \hat{t}_2) \to 0^+$ in the RHS of equation (5.44):

$$\hat{t}_3 - \hat{t}_2 \geq \frac{q(t_2) - \tau_{\max} \cdot \left(A/\Gamma - \varphi(t_2)\right)}{\mu - \varphi(t_2)}, \tag{5.47}$$

where we use $\exp\left[-\Gamma \cdot (\hat{t}_3 - \hat{t}_2)\right] \approx 1 - \Gamma \cdot (\hat{t}_3 - \hat{t}_2)$ and $\exp(\Gamma \cdot \tau_{\max}) \approx 0$.

As a summary of equations (5.41) and (5.47), the bounds of $(t_3 - t_2)$ are:

$$\begin{aligned} &\frac{q(t_2) - \tau_{\max} \cdot \left(A/\Gamma - \varphi(t_2)\right)}{\mu - \varphi(t_2)} \leq t_3 - t_2 \\ &\leq \frac{\tau_{\max} \cdot \left(A/\Gamma - \varphi(t_2')\right) - q(t_2) + \left(A/\Gamma - \varphi(t_2)\right) \cdot 1/\Gamma \cdot \exp\left[-\Gamma \cdot (\tau_{\max} - \tau_{\min})\right]}{A/\Gamma - \mu} \end{aligned} \tag{5.48}$$

Equation (5.48) gives the bounds of the time duration of Phase 3. For the case when the system will not achieve empty queue in Phase 3 (and Phase 4), the upper bound of $(t_3 - t_2)$ should be even more tight.

To move any further from equation (5.48), we need the ranges of $q(t_2)$, $\varphi(t_2)$ and $\varphi(t_2')$, which are obtained and listed below:

$$\begin{cases} 0 \leq \varphi(t_2) \leq \varphi(t_2') \leq \mu \\ Q_T - \left(\mu - \varphi(t_2)\right) \cdot \tau_{\max} \leq q(t_2) \leq Q_T \end{cases} \tag{5.49}$$

Substituting (5.49) into (5.48), we have

$$\begin{aligned} &\frac{Q_T - \tau_{\max} \cdot \left(A/\Gamma - \varphi(t_2)\right)}{\mu - \varphi(t_2)} - \tau_{\max} \leq \frac{q(t_2) - \tau_{\max} \cdot \left(A/\Gamma - \varphi(t_2)\right)}{\mu - \varphi(t_2)} \leq t_3 - t_2 \\ &\leq \frac{\left(A/\Gamma - \varphi(t_2)\right) \cdot \left(\tau_{\max} + 1/\Gamma \cdot \exp\left[-\Gamma \cdot (\tau_{\max} - \tau_{\min})\right]\right) + \left(\mu - \varphi(t_2)\right) \cdot \tau_{\max} - Q_T}{A/\Gamma - \mu} \\ &< \frac{A/\Gamma \cdot \left(\tau_{\max} + 1/\Gamma \cdot \exp\left[-\Gamma \cdot (\tau_{\max} - \tau_{\min})\right]\right)}{A/\Gamma - \mu} \end{aligned} \tag{5.50}$$

Both equations (5.48) and (5.50) can provide bounds for $t_3 - t_2$, the time duration of Phase 3. Its upper bound is roughly inversely proportional to $(A/\Gamma - \mu)$ and shaped by the bounds of delay. And it is also dependent on the transition behavior in the neighborhoods at time t_2.

The time duration of Phase 3 and 4, $t_4 - t_2$, can be directly determined by equation (5.36) along with the bounds:

$$t_4 - t_2 = \frac{1}{\Gamma} \cdot \ln\left[\frac{A/\Gamma - \varphi(t_2)}{A/\Gamma - \mu}\right], \qquad \text{(a)}$$

$$0 \le t_4 - t_2 \le \frac{1}{\Gamma} \cdot \ln\left[\frac{A/\Gamma}{A/\Gamma - \mu}\right]. \qquad \text{(b)} \qquad (5.51)$$

Phase 1 – 4 together form a "cycle" of the fluctuations in the system working in the fluctuation region. The time durations of phases vary in different "cycles". Clearly in each "cycle" $\varphi(t)$ achieves a local maximum value at t_1 and a local minimum value at t_2, denoted as $\Phi_{max} \equiv \varphi(t_1)$ and $\Phi_{min} \equiv \varphi(t_2)$, respectively. We have already established their ranges in equation (5.33) as

$$0 \le \Phi_{\min} \le \mu \le \Phi_{\max} \le A/\Gamma\,. \qquad (5.52)$$

In each "cycle" $q(t)$ also achieves a local maximum value $Q_{\max}$ at t_{12}^* in Phase 2. Starting from $\dot{q}(t_{12}^*) = 0$, equations (5.23) and (5.24), we have t_{12}^*:

$$t_{12}^* - \tau(t_{12}^*) = t_1 + \frac{1}{\Gamma} \cdot \ln\left[\frac{A/\Gamma + \varphi(t_1)}{A/\Gamma + \mu}\right]. \qquad (5.53)$$

Hence, t_{12}^* can be bounded as either

$$\tau_{\min} \le t_{12}^* - t_1 - \frac{1}{\Gamma} \cdot \ln\left[\frac{A/\Gamma + \varphi(t_1)}{A/\Gamma + \mu}\right] \le \tau_{\max}\,. \qquad (5.54a)$$

or

$$\tau_{\min} \le t_{12}^{*} \le t_1 + \frac{1}{\Gamma} \cdot \ln\left[1 + \frac{A/\Gamma - \mu}{A/\Gamma + \mu}\right] + \tau_{\max} < t_1 + \frac{1}{\Gamma} \cdot \ln 2 + \tau_{\max}. \tag{5.54b}$$

The maximum value $Q_{\max}$ at t_{12}^{*} can be bounded according to equation (5.54):

$$\begin{aligned} q(t_{12}^{*}) - Q_T &\le \left[\varphi(t_1) - \mu\right] \cdot \left(t_{12}^{*} - t_1 + \tau_{\max}\right) \\ &\le \left[\varphi(t_1) - \mu\right] \cdot \left(\frac{1}{\Gamma} \cdot \ln\left[\frac{A/\Gamma + \varphi(t_1)}{A/\Gamma + \mu}\right] + 2\tau_{\max}\right). \\ &\le \left(\frac{A}{\Gamma} - \mu\right) \cdot \left(\frac{1}{\Gamma} \cdot \ln\left[1 + \frac{A/\Gamma - \mu}{A/\Gamma + \mu}\right] + 2\tau_{\max}\right) \end{aligned} \tag{5.55}$$

From equation (5.55), the bound of the maximum queue size $Q_{\max}$ is roughly proportional to $\left(A/\Gamma - \mu\right)$, and dependent on $1/\Gamma$ and $\tau_{\max}$.

Define the period of an individual fluctuation "cycle" as T, $T \equiv t_4 - t_0$. Note $T = \left(t_1 - t_0\right) + \left(t_2 - t_1\right) + \left(t_4 - t_2\right)$. According to equations (5.20), (5.34) and (5.51), we have the lower bound of T, denoted as $T_{\min}$,

$$T_{\min} \ge \frac{Q_T}{A/\Gamma - \mu} + \tau_{\min} + \tau_{\max} + \frac{1}{\Gamma} \cdot \ln\left[\frac{A/\Gamma - \varphi(t_2)}{A/\Gamma - \mu}\right], \tag{5.56a}$$

$$T_{\min} \ge \frac{Q_T}{A/\Gamma - \mu} + \frac{\exp(\Gamma \cdot \tau_{\min})}{\Gamma} \cdot \left[1 - \exp\left(\frac{-\Gamma \cdot Q_T}{A/\Gamma - \mu}\right)\right] + \tau_{\max} + \frac{1}{\Gamma} \ln\left[\frac{A/\Gamma - \varphi(t_2)}{A/\Gamma - \mu}\right], \tag{5.56b}$$

and the upper bound of T, denoted as $T_{\max}$, is

$$T_{\max} = \frac{Q_T}{A/\Gamma - \mu} + \frac{1}{\Gamma} \exp(\Gamma \cdot \tau_{\max}) + \frac{2\,A/\Gamma \cdot (2\tau_{\max} + 1/\Gamma)}{A/\Gamma + \mu} + \frac{1}{\Gamma} \ln\left[\frac{A/\Gamma - \varphi(t_2)}{A/\Gamma - \mu}\right]. \tag{5.57}$$

Combining equations (5.56b) and (5.57), we have the bounds of T

$$\frac{Q_T}{A/\Gamma-\mu}+\frac{\exp(\Gamma\cdot\tau_{\min})}{\Gamma}\cdot\left[1-\exp\left(\frac{-\Gamma\cdot Q_T}{A/\Gamma-\mu}\right)\right]+\tau_{\max} \quad \le \quad T$$
$$\le \frac{Q_T}{A/\Gamma-\mu}+\frac{1}{\Gamma}\exp(\Gamma\cdot\tau_{\max})+\frac{2A/\Gamma\cdot(2\tau_{\max}+1/\Gamma)}{A/\Gamma+\mu}+\frac{1}{\Gamma}\ln\left(\frac{A/\Gamma}{A/\Gamma-\mu}\right). \quad (5.58)$$

Remark 5.3: From equations (5.52) – (5.58), we have the following remarks for the system working in the fluctuation region:

1. The "period" of fluctuation shows the quality of the responsiveness, including the convergence speed, amplitude fluctuation, etc. For the system with time-varying propagation delays, although the fluctuation is aperiodic, the time duration of each "cycle" is bounded by equation (5.58). In fact, the time duration of each phase is bounded by equations (5.20), (5.34) and (5.51).

2. A larger upper bound $\tau_{\max}$ tends to increase the length of each "cycle period" and its variation from equation (5.58). And this fact also holds for the bounds of time duration of each phase from equations (5.20), (5.34) and (5.51). This remark is straightforward since it is more difficult for the remote user(s) to track the dynamic system behavior with likely larger delays.

3. The parameter designs can significantly affect the dynamic system behavior. The time duration of each "cycle" largely depends on the ratio of A/Γ and its difference from μ. When A/Γ is close to μ, the terms containing $(A/\Gamma-\mu)$ are dominating in equation (5.58). The smaller the difference between A/Γ and μ, the longer the time duration of each "cycle" is. Also, with a fixed ratio A/Γ, the time duration of each "cycle" is affected by Γ, as discussed in the next remark.

4. Amplitude behavior of the rate $\varphi(t)$ is also affected by both the time-varying delays and parameter designs. The introduction of time-varying delays slows down

the dynamic system behavior due to the outdated feedback information. Its effect on the amplitude behavior can be shown in the following equations, which are derived from equations (5.13) and (5.24):

$$\Phi_{\max} \equiv \varphi(t_1) = \left(A/\Gamma - \mu\right) \cdot \left(1 - \exp\left[-\Gamma \cdot \left(t_1 - t_0\right)\right]\right) + \mu\,, \tag{5.59}$$

$$\Delta\Phi \equiv \Phi_{\max} - \Phi_{\min} \equiv \varphi(t_1) - \varphi(t_2) = \left(\varphi(t_1) + A/\Gamma\right) \cdot \left(1 - \exp\left[-\Gamma \cdot \left(t_2 - t_1\right)\right]\right). \tag{5.60}$$

Generally speaking, the longer the delays, the longer the time duration each individual phase lasts. From equation (5.59), this leads to a higher overshoot of $\varphi(t)$ in Phase 1, i.e., the higher $\varphi(t_1)$ (or Φ_{max}). Also, the system has a larger amplitude of $\varphi(t)$, $\Delta\Phi$, according to equation (5.60). In summary, the system with larger delays has longer phases in each "cycle", higher overshoot and larger amplitude.

Now consider the effects of parameter designs for the system with time-varying delays. Let the service rate (bandwidth μ) be a constant. With a fixed ratio of A/Γ, a larger Γ can speed up the dynamic behavior and in some sense compensate the effects of incorrect feedback information due to delays. So the positive overshoot happens earlier, at the same time the queue size increases faster which leads to a shorter Phase 1. Their composite effect results in a higher positive overshoot and larger amplitude, according to equations (5.59) and (5.60). On the other hand, although the system with a smaller Γ has slower behavior, it has a lower positive overshoot. The system with a Γ too small, however, may have such a slow speed that it could stay in Phase 4 (and the 2nd half of Phase 3) for a long time, during which the system degradation likely happens.

5. Obviously the system without delays has no overshoot in the queue size, $q(t)$, i.e., $q(t) \le Q_T$. For the system with time-varying delays, the overshoots always

happen with the maximum queue size ($Q_{\max}$) upper-bounded as shown in equation (5.55). The system with larger delays tends to have higher $Q_{\max}$; so does the system with a larger Γ after careful study of equations (5.59) and (5.55). Given the total available buffer size (B_0) in the remote server and the estimated upper bound of time-varying delays in the system, the sufficient condition to avoid dropping packets is

$$Q_T + \left(A/\Gamma - \mu\right)\cdot\left(1/\Gamma \cdot \ln\left[1 + \frac{A/\Gamma - \mu}{A/\Gamma + \mu}\right] + 2\tau_{\max}\right) \le B_0/\beta,\ \ \beta > 1, \tag{5.61}$$

when designing parameters.

The minimum queue size is zero if the inequality (5.46) holds. Otherwise, the empty queue state is not achievable in Phase 3 and Phase 4. The queue sizes at the turning points of neighboring phases are two-sided bounded in equation (5.32).

6. Similar to equation (5.51a), we can have the exact formula for $t_1 - t_0$, $t_2 - t_1$ according to equations for $\varphi(t)$ in Phase 1 and 2, respectively. Hence T is

$$\begin{aligned} T &= \frac{1}{\Gamma}\ln\left[\frac{A/\Gamma - \mu}{A/\Gamma - \varphi(t_1)}\right] + \frac{1}{\Gamma}\ln\left[\frac{A/\Gamma + \varphi(t_1)}{A/\Gamma + \varphi(t_2)}\right] + \frac{1}{\Gamma}\ln\left[\frac{A/\Gamma - \varphi(t_2)}{A/\Gamma - \mu}\right] \\ &= \frac{1}{\Gamma}\ln\left[\frac{\left(A/\Gamma - \varphi(t_2)\right)\cdot\left(A/\Gamma + \varphi(t_1)\right)}{\left(A/\Gamma + \varphi(t_2)\right)\cdot\left(A/\Gamma - \varphi(t_1)\right)}\right] \end{aligned}. \tag{5.62}$$

From equation (5.62), we can evaluate the possibility of the event that T is unbounded in an individual "cycle":

$$\left\{T \text{ is unbounded}\right\} \overset{(66)}{\Leftrightarrow} \varphi(t_1) \to A/\Gamma \overset{(63)}{\Leftrightarrow} t_1 - t_0 \to +\infty \overset{(24)}{\Leftrightarrow} A/\Gamma \to \mu. \tag{5.63}$$

So, in the parameter design, $\left(A/\Gamma - \mu\right) \to 0^+$ needs to be avoided. Equation (5.63) is also true for the system without delays, for which the formulation is:

$$\varphi(t_1) = \Gamma\cdot\left(A/\Gamma - \mu\right)\cdot\left(t_1 - t_0\right) - \Gamma\cdot Q_T + \mu. \tag{5.64}$$

where, $(t_1 - t_0)$ is a solution of $(t_1 - t_0) - Q_T / (A/\Gamma - \mu) = 1/\Gamma \cdot [1 - \exp(-\Gamma \cdot (t_1 - t_0))]$.

Before the end of this section, we present Figure 5.5 that depicts the "cycles" in the dynamic behavior with fluctuations. In Figure 5.5(a), the parameters and the time duration (0 ~ 500 sec) are the same as those in Figure 5.3. The fluctuations in 5.5(a) are bounded although aperiodic. These 41 different "cycles" (each with 4 phases) can be classified into 6 groups; each group has a set of "cycles" whose trajectories are very close with each other. With an average rate ($\overline{\Phi}$) of 144.2 Mbps, $\varphi(t)$ achieves its maximum 152.96 Mbps and minimum 104.99 Mbps. The maximum queue size is $Q_{\max} = 11.14$ when φ = 134.3 Mbps. The average T, period of "cycles", is about 12.1 sec. Its response time, the time duration from 0 to the time the flow receives the feedback of the remote queue overflow for the first time, is 9.8 sec.

Figure 5.5(b) shows the dynamic behavior of the same system with the same ratio of A/Γ but different A and Γ (1/10) as those in Figure 5.5(a). Compared with Figure 5.5(a), the time duration of each phase and each "cycle" is longer, so within 0 ~ 500 sec there are less number of "cycles" (about 10). These 10 "cycles" can be classified into 5 groups according to their trajectories. Now $\varphi(t)$ has a maximum value of 151.4 Mbps, a minimum value of 143.4 Mbps and an average rate ($\overline{\Phi}$) of 148.7 Mbps. The maximum queue size is $Q_{\max} = 10.59$ when φ = 148.5 Mbps. The average T, period of "cycles", is about 40.2 sec. Compared with Figure 5.5(a), with a fixed ratio of A/Γ, the smaller Γ leads to a lower $\Phi_{\max}$, a much higher $\Phi_{\min}$, a smaller $Q_{\max}$, a longer T and more throughput. The amplitude of rate decreases from 48 Mbps to 8 Mbps; the relative amplitude, $\Delta\Phi/\overline{\Phi}$, decreases from 0.33 to 0.05 accordingly. Therefore, the

system with a smaller Γ has small-amplitude fluctuations, although its response time is 98.2 sec, 10 times the previous value.

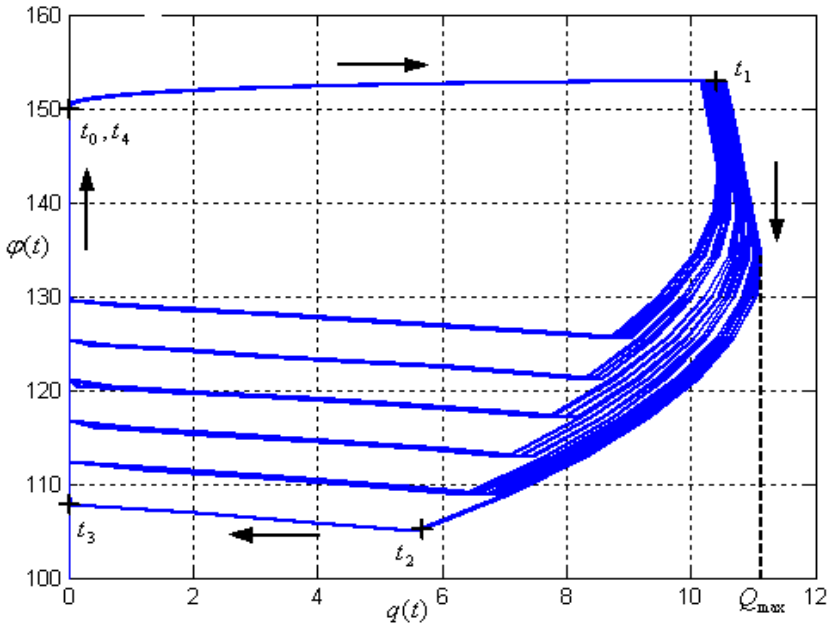

(a) $A^+ = A^- = 48.1$ Mbps, $\Gamma^+ = \Gamma^- = 0.39$

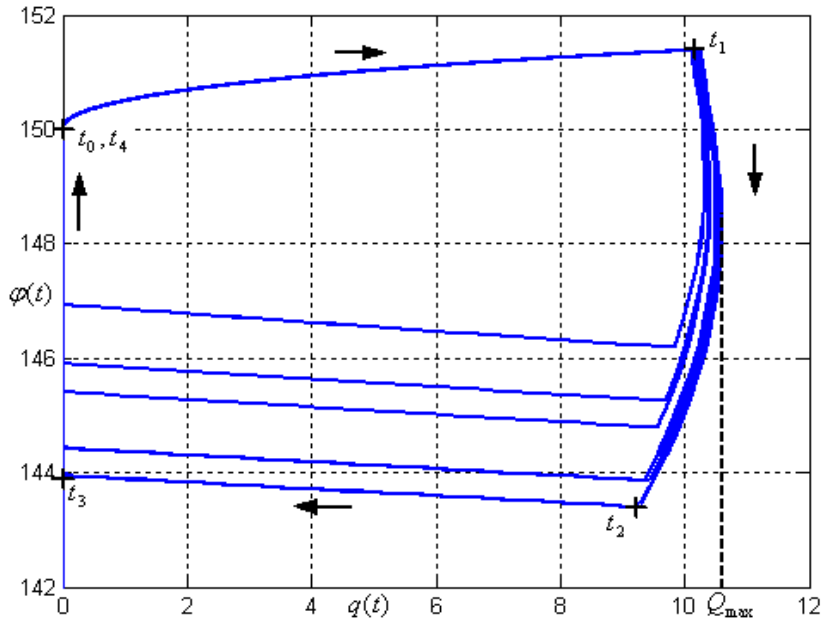

(b) $A^+ = A^- = 4.81$ Mbps, $\Gamma^+ = \Gamma^- = 0.039$

$\mu = 150$ Mbps, $v = 30$ Mbps, $\Delta = 0.05$ s, $Q_T = 10$ packets, $\tau(t) = 0.1 + 0.1 \cdot \sin(\pi t/11)$.

Figure 5.5: Bounded "Cycles" in the Fluctuation Region of Single-Flow Systems

5.5. Models for Multiple Flows

We have made some extensive analysis of the single-flow model, and will follow the same methodology to deal with the multiple-flows model here. We need to point out that fairness is always one of the important issues in the design of algorithms for multiple flows.

We extend the single-flow model (5.7) to the multiple-flows model as follows:

$$\frac{d}{dt}\varphi_j(t) = \begin{cases} -\Gamma_j^+[\varphi_j(t) - v_j] + A_j^+ u_j(t) & \text{if } u_j(t) > 0 \\ -\Gamma_j^-[\varphi_j(t) - v_j] + A_j^- u_j(t) & \text{if } u_j(t) < 0 \end{cases} \quad \text{(a)}$$

$$\frac{d}{dt}q(t) = \begin{cases} \sum_j \varphi_j\left(t - \tau_j(t)\right) - \mu, & \text{if } q(t) > 0 \\ \left[\sum_j \varphi_j\left(t - \tau_j(t)\right) - \mu\right]^+, & \text{if } q(t) = 0 \end{cases}. \quad \text{(b)} \qquad (5.65)$$

Here $\Gamma_j^+, \Gamma_j^-, A_j^+, A_j^-$ are nonnegative parameters associated with the j^{th} flow, j = 1, 2, …, N, and the feedback for the j^{th} flow at time t is $u_j(t) = \text{sgn}[Q_T - q(t - \tau_j(t))]$.

Before the analysis, we list some key issues here for the multiple-flows model:

1. Transient behavior. As an important dynamic property, it shows the quality of the responsiveness, including the convergence speed, amplitude fluctuation, etc.
2. The effect of heterogeneous time-varying propagation delays. The flows with longer propagation delay will typically be discriminated against according to prior research [70, 73]. The various time-varying delays may cause instability for the system and also demand more robustness for parameters in the algorithm designs.
3. Fairness in short-term and long-term behavior. For start-up flow, it is always difficult to obtain its share of the bandwidth from existing flows. The design of

algorithms needs to consider the tradeoff of short-term and long-term fairness and show some sense of flexibility.

4. Arbitrary bandwidth allocations to all the flows.

We will start from the analysis of the system with multiple flows under the condition that stationary solutions exist and are stable. The system that satisfies this condition is stated as the system in the stationary-state region.

5.5.1. Solutions in the Stationary-State Region

Similarly to the analysis of the single-flow model in equation (5.7), we have the following results regarding the existence of stationary solution and the stability:

Proposition 5.3: Suppose $\sum_j \left(\nu_j + A_j^+ / \Gamma_j^+\right) < \mu$. The system in equation (5.65) has a stationary solution: $\varphi_j \equiv \nu_j + A_j^+ / \Gamma_j^+, \forall j = 1, \ldots, N$ and $q \equiv 0$. Furthermore:

1. For a given t_1, if $\varphi_j(t_1) \le \nu_j + A_j^+ / \Gamma_j^+$ $(j = 1, \ldots, N)$, the same inequality also holds for all flows when $t \ge t_1$. If for a flow k at time t_0, $\varphi_k(t_0) > \nu_k + A_k^+ / \Gamma_k^+$, there exists t_2, $t_2 > t_0$, s.t. $\varphi_k(t)$ decreases monotonically when $t_2 > t > t_0$, and $\varphi_k(t_2) = \nu_k + A_k^+ / \Gamma_k^+$.

2. For a flow k, assume $\tau_k(t) \in S_T^k \subset R$ and S_T^k is compact. Denote its bounds by $\tau_{\min}^k$ and $\tau_{\max}^k$. Then there exists t_3, s.t. for all $t \ge t_3$, $q(t) < Q_T$, $\varphi_k(t) \to \nu_k + A_k^+ / \Gamma_k^+$ at the exponential rate Γ^+.

Proof: can be extended from the proof of Proposition 5.1 in the natural way.

□

We also have the following remarks when $\sum_j \left(\nu_j + A_j^+ / \Gamma_j^+\right) < \mu$ holds.

Remark 5.4: The first property does not require $\tau_j(t)$ to be bounded. The second property also holds for unbounded $\tau_j(t)$, given $0 < \tau_j(t) < t$ and $t - \tau_j(t)$ goes to $+\infty$ (not necessarily monotonically). The conditions can be satisfied when the system is always in connection during the considered time window and based on FIFO.

Proof: Similar to Remark 5.1 and skipped.

□

Remark 5.5: Recall that Γ_j^+, Γ_j^-, A_j^+, A_j^-, $j = 1, ..., N$, are nonnegative. Further assume Γ_j^+, $\Gamma_j^- > 0$. The system in equation (5.65) is then globally asymptotically stable with exponential rate.

Proof: Define $\psi_j(t) \equiv \varphi_j(t) - \left(\nu_j + A_j^+ / \Gamma_j^+\right)$. Denote $\Gamma_j^M \equiv \min\left(\Gamma_j^+, \Gamma_j^-\right) > 0$ and $A_j^M \equiv \max\left(0, A_j^- - \frac{\Gamma_j^-}{\Gamma_j^+} \cdot A_j^+\right)$.

Following the reasoning in the proof of Remark 5.2, it can be shown that the system in equation (5.65) is globally asymptotically stable with exponential rate Γ_j^M for the flow j.

□

And similar to equation (14), regardless of whether $\sum_j \left(\nu_j + A_j^+ / \Gamma_j^+\right) < \mu$ holds or not, for any t_0 and $t > t_0$,

$$\left|\psi_j(t)\right| \le A_j^M / \Gamma_j^M + \left[\left|\psi_j(t_0)\right| - A_j^M / \Gamma_j^M\right] \cdot \exp\left[-\Gamma_j^M (t - t_0)\right], \tag{5.66}$$

for any flow j. Basically this property shows that even though the system only has fluctuating solutions in the fluctuation region beyond $\sum_j \left(\nu_j + A_j^+ / \Gamma_j^+\right) < \mu$, this fluctuating behavior is bounded for each flow.

5.5.2. Solutions in the Fluctuation Region

In this section we will study the fluctuating but bounded dynamic behavior in the fluctuation region where $\sum_j \left(\nu_j + A_j^+ / \Gamma_j^+\right) > \mu$. According to our discussion in previous sections for the single flow system, we expect that the multiple-flow system can also have small-amplitude fluctuating solutions through careful system parameter designs. The assumptions in this section are listed below ($\forall j = 1, \ ..., \ N$):

- $\sum_j \left(\nu_j + A_j^+ / \Gamma_j^+\right) > \mu$. The system does not have any equilibrium point.
- $A_j^+, A_j^- \geq 0$ and $\Gamma_j^+, \Gamma_j^- > 0$. This is also the condition that the system is globally asymptotically stable with exponential rate when $\sum_j \left(\nu_j + A_j^+ / \Gamma_j^+\right) < \mu$ holds.
- $\Gamma_j^+ = \Gamma_j^- = \Gamma_j$ and $A_j^+ = A_j^- = A_j$, i.e., mainly consider the MS algorithm.
- $\nu_j = 0$, since ν_j can be absorbed by $\varphi_j(t)$ and μ in equation (5.65).
- $\varphi_j(t)$ and $q(t)$ are piece-wise differentiable functions with $\varphi_j(0) = q(0) = 0$.
- $\tau_j(t) \in S_T \subset R$, where S_T is a compact set with the lower bound $\tau_j^{\min}$ and the upper bound $\tau_j^{\max}$. $0 \leq \tau_j^{\min} \leq \tau_j^{\max}$. Also denote $\tau_{\min} \equiv \min_j \tau_j^{\min}$, $\tau_{\max} \equiv \max_j \tau_j^{\max}$.

With the above assumptions, the multiple-flows model (5.65) can be rewritten as

$$\frac{d}{dt}\varphi_j(t) = -\Gamma_j \cdot \varphi_j(t) + A_j \cdot u_j(t) \qquad \text{(a)}$$

$$\frac{d}{dt}q(t) = \begin{cases} \sum_j \varphi_j\left(t - \tau_j(t)\right) - \mu, & \text{if } q(t) > 0 \\ \left[\sum_j \varphi_j\left(t - \tau_j(t)\right) - \mu\right]^+, & \text{if } q(t) = 0 \end{cases}. \qquad \text{(b)} \qquad (5.67)$$

where the feedback for the j^{th} flow at time t is $u_j(t) = \text{sgn}[Q_T - q(t - \tau_j(t))]$. It is worth noting that different flows have different $u_j(t)$, and that all flows are coupled in equation (5.67b).

Using a similar approach to the analysis of the single-flow system, we will study the dynamic behavior of the multiple-flow system with general time-varying delay in the fluctuation region. Particularly, we focus on Phase 1 which determines not only the response time of each flow, but also in some sense represents the effect of heterogeneous time-varying delays and parameter designs.

We first summarize the denotations for our analysis of Phase 1. $\forall j = 1, ..., N$, $\tau_j^{\min}$, $\tau_j^{\max}$ are the delay bounds of the j^{th} flow. $\tau_{\min}$, $\tau_{\max}$ are the global delay bounds for the system. Denote t_j^1 as the time when the j^{th} user receives the overflow feedback of the remote queue and hence starts reducing its flow rate $\varphi_j(t)$. i.e., t_j^1 can be written as: $t_j^1 \equiv \inf\{t > 0 : q(t - \tau_j(t)) = Q_T\}$. t_j^1 is also called the response time of the j^{th} flow. Generally $\{t_j^1\}_{j=1}^N$ forms a time sequence. Among different flows, the response time decreases with the feedback delay due to their sharing of a common queue. In other words, if one flow always has less delay than another flow at any time, it will also have a longer response time. Denote the bounds of the time sequence $\{t_j^1\}_{j=1}^N$ as $t_{\min}^1 \equiv \min_j t_j^1$ and $t_{\max}^1 \equiv \max_j t_j^1$.

Now consider Phase 1 where $t \in (0, t_{\max}^1)$. For the j^{th} flow, we have $\varphi_j(0) = 0$, and clearly its feedback control $u_j(t)$ in Phase 1 is: $u_j(t) \equiv 1$ for $t \in (0, t_j^1)$; $u_j(t) \equiv -1$

for $t \in (t_j^1,\ t_{\max}^1)$. Here if $t_{\max}^1 = t_j^1$ we have $(t_j^1,\ t_{\max}^1) = \Phi$ (empty set) by convention. So, the governing equation of $\varphi_j(t)$ for Phase 1 is

$$\frac{d}{dt}\varphi_j(t) = \begin{cases} -\Gamma_j \cdot \varphi(t) + A_j, & t \in (0,\ t_j^1) \\ -\Gamma_j \cdot \varphi(t) - A_j, & t \in (t_j^1,\ t_{\max}^1) \end{cases} \tag{5.68}$$

Hence $\varphi_j(t)$ first increases before $t = t_j^1$ and decreases thereafter, which is similar to previous results in Phase 1 and Phase 2 of the single-flow system. $\varphi_j(t)$ is written as

$$\varphi_j(t) = \begin{cases} A_j/\Gamma_j \cdot \left[1 - \exp\left(-\Gamma_j \cdot t\right)\right], & t \in (0,\ t_j^1) \\ A_j/\Gamma_j \cdot \left[2 \cdot \exp\left(-\Gamma_j \cdot (t - t_j^1)\right) - \exp\left(-\Gamma_j \cdot t\right) - 1\right], & t \in (t_j^1,\ t_{\max}^1) \end{cases}. \tag{5.69}$$

Apparently $\varphi_j(t)$ achieves a local maximum $\varphi_j^{\max}$ at $t = t_j^1$:

$$\varphi_j^{\max} = A_j/\Gamma_j \cdot \left(1 - \exp(-\Gamma_j \cdot t_j^1)\right). \tag{5.70}$$

$\varphi_j^{\max}$ is determined by the ratio A_j/Γ_j, Γ_j and the response time t_j^1. Note that for two flows *j*, *k*, the relative relation of their response times depends only on their time-varying delays since all flows use the common queue in the remote server.

Now consider the queue behavior in Phase 1 during which $q(t)$ first stays zero and then increases. Its governing equation is described in equation (5.67b). Denote t_0 as the time when the queue starts buffering incoming packets, i.e.,

$$t_0 \equiv \inf\left\{t > 0 : \sum_j \varphi_j(t - \tau_j(t)) = \mu\right\}. \tag{5.71}$$

Clearly $q(t_0) = 0$, and $0 \le t_0 < t_j^1,\ \forall j$, or equivalently $0 \le t_0 < t_{\min}^1$. We assume $t_0 \ge \tau_{\max}$ for convenience.

For $t \in (t_0,\ t_{\min}^1 + \tau_{\min})$, the queue behavior can be described by equation (5.72a):

$$\frac{d}{dt}q(t)=\sum_j \varphi_j\left(t-\tau_j(t)\right)-\mu \qquad \text{(a)}$$

$$\frac{d}{dt}\hat{q}(t)=\sum_j \varphi_j\left(t-\tau_j^{\min}\right)-\mu\,. \qquad \text{(b)} \qquad (5.72)$$

$$\frac{d}{dt}\breve{q}(t)=\sum_j \varphi_j\left(t-\tau_j^{\max}\right)-\mu \qquad \text{(c)}$$

Equations (5.72b) and (5.72c) govern two reference (bound) queues, denoted as $\hat{q}(t)$ and $\breve{q}(t)$. Their initial states are specified as $\hat{q}(t_0)=\breve{q}(t_0)=q(t_0)=0$. So we have $\breve{q}(t)\le q(t)\le \hat{q}(t)$ for $t\in(t_0,\ t_{\min}^1+\tau_{\min})$. According to our previous analysis, $\hat{q}(t)$ and $\breve{q}(t)$ are the (left-sided) upper and lower bound curves, respectively.

Substituting (5.69) into (5.72b) and (5.72c), we obtain

$$\begin{cases}\hat{q}(t)=\left(\sum_j \dfrac{A_j}{\Gamma_j}-\mu\right)\cdot(t-t_0)-\sum_j\left(\dfrac{A_j}{\Gamma_j}\cdot\dfrac{\exp(\Gamma_j\cdot\tau_j^{\min})}{\Gamma_j}\cdot\left[1-\exp\left(-\Gamma_j\cdot(t-t_0)\right)\right]\right)\\ \breve{q}(t)=\left(\sum_j \dfrac{A_j}{\Gamma_j}-\mu\right)\cdot(t-t_0)-\sum_j\left(\dfrac{A_j}{\Gamma_j}\cdot\dfrac{\exp(\Gamma_j\cdot\tau_j^{\max})}{\Gamma_j}\cdot\left[1-\exp\left(-\Gamma_j\cdot(t-t_0)\right)\right]\right)\end{cases}. \quad (5.73)$$

Before the further analysis of $\left\{t_j^1\right\}_{j=1}^N$ and of the queue behavior, we investigate the time t_0 defined in equation (5.71) and rewrite it as $\sum_j \varphi_j(t_0-\tau_j(t_0))=\mu$. Substituting equation (5.69) and the delay bounds of each flow into it, we have

$$\sum_j\left[\frac{A_j}{\Gamma_j}\exp\left(-\Gamma_j\cdot(t_0-\tau_j^{\min})\right)\right]\le\left[\sum_j\frac{A_j}{\Gamma_j}\right]-\mu\le\sum_j\left[\frac{A_j}{\Gamma_j}\exp\left(-\Gamma_j\cdot(t_0-\tau_j^{\max})\right)\right]. \quad (5.74)$$

Thus far we have not addressed the topic of fairness. Recall in the network model of Section 5.1 that each flow (say flow *j*) is associated with two parameters, (ν_j,σ_j),

where ν_j is its minimum bandwidth requirement and σ_j is its relative weight. These two parameters are used for the bandwidth allocation.

Fairness: it is desired to have the following fairness constraint among flows:

1. For any flow *j*, there exists time $t_j \geq 0$, such that $\varphi_j(t) \geq \nu_j$ when $t \geq t_j$.

2. For any two flows *j* and *k*, $\frac{\varphi_j(t) - \nu_j}{\sigma_j} = \frac{\varphi_k(t) - \nu_k}{\sigma_k}$ when $t \geq \max(t_j,\ t_k)$.

In practice, an approximation to the above proportional fairness is also desirable. Note that $\{\sigma_j\}$ are not necessarily normalized. For convenience ν_j is set as zero.

For the above fairness criteria we consider the following parameter design:

$$\forall j = 1,\ 2,\ ...,\ N, \quad A_j = A \cdot \sigma_j, \quad \Gamma_j = \Gamma, \text{ and let } \sigma \equiv \sum_j \sigma_j . \tag{5.75}$$

With the above design rule, the system fluctuation region $\sum_j A_j / \Gamma_j > \mu$ can be rewritten as $A/\Gamma > \mu/\sigma$. Note that σ is not necessarily equal to 1.

It has been shown in [70] that for the system with heterogeneous fixed delays, the above design rule achieves "pointwise fairness": the divergences from the proportional fairness vanish monotonically as $t \to \infty$.

Substituting (5.75) into (5.70), we obtain

$$\varphi_j^{\max} = A/\Gamma \cdot \sigma_j \cdot \left(1 - \exp(-\Gamma \cdot t_j^1)\right). \tag{5.76}$$

Remark 5.5: Consider the design rule (5.75). The (local) maximum rate of the j^{th} flow ($\varphi_j^{\max}$) is determined by A/Γ, Γ, σ_j and its response time t_j^1. Furthermore, $\varphi_j^{\max}$ increases with σ_j and t_j^1 (or in fact the time-varying delays). For a pair of flows (*j*, *k*), only their relative weights (σ_j, σ_k) and times (t_j^1, t_k^1) (based on the time-

varying delays of the j^{th} and k^{th} flows, respectively) are distinct from each other. It is also worth noting that $\varphi_j^{\max}$ could, but does not necessarily overshoot μ.

Substituting (5.75) into (5.74) for the purpose of bounding the time t_0:

$$\begin{cases} \sigma - \dfrac{\mu \cdot \Gamma}{A} \geq \sum\limits_j \left[\sigma_j \cdot \exp\left(-\Gamma \cdot (t_0 - \tau_j^{\min})\right)\right] & (a) \\ \sum\limits_j \left[\sigma_j \cdot \exp\left(-\Gamma \cdot (t_0 - \tau_j^{\max})\right)\right] \geq \sigma - \dfrac{\mu \cdot \Gamma}{A} & (b) \end{cases} \tag{5.77}$$

The following results provide bounds for the time t_0, which are useful for our further analysis of $\left\{t_j^1\right\}_{j=1}^N$ and the queue behavior:

Proposition 5.4: Suppose $A/\Gamma > \mu/\sigma$, and the design rule (5.75) is adopted. t_0 is the time when the queue starts buffering, as defined by equation (5.71). Assume $t_0 \geq \tau_{\max}$. We have the following lower and upper bounds:

(1) $\tau_{\min} + \dfrac{1}{\Gamma} \cdot \ln \dfrac{A/\Gamma}{A/\Gamma - \mu/\sigma} \leq t_0 \leq \tau_{\max} + \dfrac{1}{\Gamma} \cdot \ln \dfrac{A/\Gamma}{A/\Gamma - \mu/\sigma}$.

(2) $t_0 \geq \dfrac{\mu}{A \cdot \sigma} + \sum\limits_j \left(\dfrac{\sigma_j}{\sigma} \tau_j^{\min} \right)$.

(3) $\dfrac{1}{\Gamma} \cdot \ln \left[\sum\limits_j \dfrac{\sigma_j \exp(\Gamma \cdot \tau_j^{\min})}{\sigma} \right] \leq t_0 - \dfrac{1}{\Gamma} \cdot \ln \dfrac{A/\Gamma}{A/\Gamma - \mu/\sigma} \leq \dfrac{1}{\Gamma} \cdot \ln \left[\sum\limits_j \dfrac{\sigma_j \exp(\Gamma \cdot \tau_j^{\max})}{\sigma} \right]$.

Proof: (1) Equation (5.77b) can be rewritten as follows when we further loosen the upper delay bounds of each flow:

$$\sum_j \left[\sigma_j \cdot \exp\left(-\Gamma \cdot (t_0 - \tau_j^{\max})\right)\right] \geq \sigma - \frac{\mu \cdot \Gamma}{A} > 0$$

$$\Rightarrow \quad \sum_j \left[\sigma_j \cdot \exp\left(-\Gamma \cdot (t_0 - \tau_{\max})\right)\right] \geq \sigma - \frac{\mu \cdot \Gamma}{A}$$

$$\Leftrightarrow \quad t_0 \le \tau_{\max} + \frac{1}{\Gamma} \cdot \ln \frac{A/\Gamma}{A/\Gamma - \mu/\sigma}. \tag{5.78}$$

Similarly the lower bound of t_0 can be obtained from equation (5.77a).

(2) The following property of the exponential function is used for the proof:

$\forall x \in R,\ e^x \ge 1 + x$, with the equality achieved if and only if $x = 0$.

So using the above property in equation (5.77a), we have:

$$\sigma - \frac{\mu \cdot \Gamma}{A} \ge \sum_j \left[\sigma_j \cdot \exp\left(-\Gamma \cdot (t_0 - \tau_j^{\min})\right)\right] \ge \sum_j \left[\sigma_j \cdot \left(1 - \Gamma \cdot (t_0 - \tau_j^{\min})\right)\right]$$

$$\Leftrightarrow \quad \sigma \cdot t_0 - \sum_j \left[\sigma_j \cdot \tau_j^{\min}\right] \ge \frac{\mu}{A}$$

$$\Leftrightarrow \quad t_0 \ge \frac{\mu}{A \cdot \sigma} + \sum_j \left(\frac{\sigma_j}{\sigma} \tau_j^{\min}\right). \tag{5.79}$$

(3) A tight upper bound can be obtained from equation (5.77b) directly:

$$\sum_j \left[\sigma_j \cdot \exp\left(-\Gamma \cdot (t_0 - \tau_j^{\max})\right)\right] \ge \sigma - \frac{\mu \cdot \Gamma}{A} > 0$$

$$\Leftrightarrow \quad \exp(-\Gamma \cdot t_0) \cdot \sum_j \left[\sigma_j \cdot \exp(\Gamma \cdot \tau_j^{\max})\right] \ge \sigma - \frac{\mu \cdot \Gamma}{A}$$

$$\Leftrightarrow \quad t_0 \le \frac{1}{\Gamma} \cdot \ln \frac{A/\Gamma}{A/\Gamma - \mu/\sigma} + \frac{1}{\Gamma} \cdot \ln \left[\sum_j \frac{\sigma_j \cdot \exp(\Gamma \cdot \tau_j^{\max})}{\sigma}\right]. \tag{5.80}$$

The tight lower bound is derived from equation (5.77a) similarly. It is also worth noting that the second term in the right-hand side is always positive except for the system without feedback delays.

□

Proposition 5.4 along with equations (5.78) – (5.80) gives the lower and upper bounds for the time t_0. The important role of the difference between A/Γ and μ/σ

can be clearly observed. The system with $A/\Gamma > \mu/\sigma$ but with only a small difference is at the edge of the fluctuation region; and it has a much longer response time due to large upper and lower bounds for the time t_0. Also, when A/Γ is fixed in such a system, to compensate for the long response time, either a large Γ or a large σ can be adopted (or both). In addition, the distributions of feedback delays affect the time t_0, which can be adjusted by the design of relative weights.

As an extensive analysis of time t_0, we have the following results directly from equation (5.74) for the generalized system without the specific design rule.

Remark 5.6: For the system in equation (5.67), suppose $\sum_j \left(A_j/\Gamma_j\right) > \mu$ and $t_0 \geq \tau_{\max}$. t_0 defined in equation (5.71) has the following bounds:

(1) $\tau_{\min} + \dfrac{1}{\max_j \Gamma_j} \cdot \ln \dfrac{\sum_j \left(A_j/\Gamma_j\right)}{\sum_j \left(A_j/\Gamma_j\right) - \mu} \leq t_0 \leq \tau_{\max} + \dfrac{1}{\min_j \Gamma_j} \cdot \ln \dfrac{\sum_j \left(A_j/\Gamma_j\right)}{\sum_j \left(A_j/\Gamma_j\right) - \mu}$.

(2) $t_0 \geq \dfrac{\mu + \sum_j \left(A_j \cdot \tau_j^{\min}\right)}{\sum_j A_j}$.

Proof: (1) Equation (5.74) can be rewritten as follows when we further loosen the lower delay bounds of each flow:

$$\sum_j \left[\frac{A_j}{\Gamma_j} \cdot \exp\left(-\Gamma_j \cdot (t_0 - \tau_j^{\min})\right)\right] \leq \sum_j \left(\frac{A_j}{\Gamma_j}\right) - \mu$$

$$\Rightarrow \quad \sum_j \left[\frac{A_j}{\Gamma_j} \cdot \exp\left(-\Gamma_j \cdot (t_0 - \tau_{\min})\right)\right] \leq \sum_j \left(\frac{A_j}{\Gamma_j}\right) - \mu$$

$$\Rightarrow \quad \sum_j \left(\frac{A_j}{\Gamma_j}\right) \cdot \exp\left[-\left(\max_j \Gamma_j\right) \cdot (t_0 - \tau_{\min})\right] \leq \sum_j \left(\frac{A_j}{\Gamma_j}\right) - \mu$$

$$\Leftrightarrow \qquad t_0 \geq \tau_{\min} + \frac{1}{\max_j \Gamma_j} \cdot \ln \frac{\sum_j \left(A_j / \Gamma_j\right)}{\sum_j \left(A_j / \Gamma_j\right) - \mu}. \tag{5.81}$$

Similarly the upper bound of t_0 can be obtained from equation (5.74).

(2) Again we use the property of the exponential function: $\forall x \in R,\ e^x \geq 1 + x$ with equality achieved if and only if $x = 0$. From (5.74), we have:

$$\sum_j \left(\frac{A_j}{\Gamma_j}\right) - \mu \geq \sum_j \left[\frac{A_j}{\Gamma_j} \cdot \exp\left(-\Gamma_j \cdot (t_0 - \tau_j^{\min})\right)\right]$$

$$\Rightarrow \qquad \sum_j \left(\frac{A_j}{\Gamma_j}\right) - \mu \geq \sum_j \left[\frac{A_j}{\Gamma_j} - A_j \cdot (t_0 - \tau_j^{\min})\right]$$

$$\Leftrightarrow \qquad t_0 \geq \frac{\mu + \sum_j \left(A_j \cdot \tau_j^{\min}\right)}{\sum_j A_j}. \tag{5.82}$$

The property (2) in Proposition 5.4 can be easily obtained by substituting the design rule (5.75) into equation (5.82).

□

The above results for the time t_0 are useful for our further analysis of $\left\{t_j^1\right\}_{j=1}^N$ and the queue behavior. Substituting the design rule (5.75) into equation (5.73) we obtain

$$\begin{cases} \hat{q}(t) = \left(\sigma \cdot \dfrac{A}{\Gamma} - \mu\right) \cdot (t - t_0) - \dfrac{A}{\Gamma} \cdot \sum_j \left(\sigma_j \cdot \dfrac{\exp(\Gamma \cdot \tau_j^{\min})}{\Gamma} \cdot \left[1 - \exp\left(-\Gamma \cdot (t - t_0)\right)\right]\right) \\ \breve{q}(t) = \left(\sigma \cdot \dfrac{A}{\Gamma} - \mu\right) \cdot (t - t_0) - \dfrac{A}{\Gamma} \cdot \sum_j \left(\sigma_j \cdot \dfrac{\exp(\Gamma \cdot \tau_j^{\max})}{\Gamma} \cdot \left[1 - \exp\left(-\Gamma \cdot (t - t_0)\right)\right]\right) \end{cases}. \tag{5.83}$$

To bound $\left\{t_j^1\right\}_{j=1}^N$, where $t_j^1 \equiv \inf\left\{t > 0 : q(t - \tau_j(t)) = Q_T\right\}$, we define the times $\hat{t}_1$, $\breve{t}_1$ such that $\hat{q}(\hat{t}_1) = \breve{q}(\breve{t}_1) = Q_T$. From our previous discussion, $\breve{q}(t) \leq q(t) \leq \hat{q}(t)$, so

$$\forall j,\ \hat{t}_1 + \tau_j^{\min} \leq t_j^1 \leq \breve{t}_1 + \tau_j^{\max}, \qquad \hat{t}_1 + \tau_{\min} \leq t_{\min}^1 \leq t_j^1 \leq t_{\max}^1 \leq \breve{t}_1 + \tau_{\max}.$$

We have the following results on the bounds for $\left\{ t_j^1 \right\}_{j=1}^N$ and the upper bound for the queue size, using equation (5.83) and the above definitions:

Proposition 5.5: Suppose $A/\Gamma > \mu/\sigma$, and the design rule (5.75) is adopted. $j = 1,\ 2,\ ...,\ N$.

(1) $t_{\min}^1 - t_0 \geq \tau_{\min} + \dfrac{Q_T}{\sigma \cdot A/\Gamma - \mu}$.

(2) $t_{\max}^1 - t_0 \leq \tau_{\max} + \dfrac{Q_T}{\dfrac{A}{\Gamma} \cdot \sum_j \left[\sigma_j \cdot \left(1 - \exp(\Gamma \cdot \tau_j^{\max}) \right) \right] - \mu}$, if the following inequality holds: $\dfrac{A}{\Gamma} \cdot \sum_j \left[\sigma_j \cdot \left(1 - \exp(\Gamma \cdot \tau_j^{\max}) \right) \right] > \mu$.

(3) $t_{\max}^1 - t_0 \leq \tau_{\max} + \dfrac{Q_T + A/\Gamma \cdot 1/\Gamma \cdot \sum_j \left(\sigma_j \cdot \exp(\Gamma \cdot \tau_j^{\max}) \right)}{\sigma \cdot A/\Gamma - \mu}$.

(4) $q(t_j^1) \leq Q_T + \tau_j^{\max} \cdot \left(\sigma \cdot A/\Gamma - \mu \right) \leq Q_T + \tau_{\max} \cdot \left(\sigma \cdot A/\Gamma - \mu \right)$.

Proof: (1) From equation (5.83) we have:

$$Q_T = \hat{q}(\hat{t}_1) = \left(\sigma \cdot \frac{A}{\Gamma} - \mu \right) \cdot \left(\hat{t}_1 - t_0 \right) - \frac{A}{\Gamma} \cdot \frac{1 - \exp\left(-\Gamma \cdot (\hat{t}_1 - t_0) \right)}{\Gamma} \cdot \sum_j \sigma_j \cdot \exp(\Gamma \cdot \tau_j^{\min})$$

$$\Rightarrow \quad \left(\sigma \cdot \frac{A}{\Gamma} - \mu \right) \cdot \left(\hat{t}_1 - t_0 \right) \geq Q_T$$

$$\Rightarrow \quad t_{\min}^1 - t_0 \geq \hat{t}_1 + \tau_{\min} \geq \tau_{\min} + \frac{Q_T}{\sigma \cdot A/\Gamma - \mu}. \tag{5.84}$$

The following inequality also holds:

$$t_j^1 - t_0 \geq \hat{t}_1 + \tau_j^{\min} \geq \tau_j^{\min} + \frac{Q_T}{\sigma \cdot A/\Gamma - \mu}.$$

(2) Using the property of the exponential function: $\forall x \in R,\ e^x \geq 1 + x$ with the equality achieved if and only if $x = 0$, equation (5.83) can be rewritten as follows:

$$Q_T = \breve{q}(\breve{t}_1) = \left(\sigma \cdot \frac{A}{\Gamma} - \mu\right) \cdot (\breve{t}_1 - t_0) - \frac{A}{\Gamma} \cdot \frac{1 - \exp\left(-\Gamma \cdot (\breve{t}_1 - t_0)\right)}{\Gamma} \cdot \sum_j \left(\sigma_j \cdot \exp(\Gamma \cdot \tau_j^{\max})\right)$$

$$\Rightarrow \quad Q_T \geq \left(\sigma \cdot \frac{A}{\Gamma} - \mu\right) \cdot (\breve{t}_1 - t_0) - \frac{A}{\Gamma} \cdot (\breve{t}_1 - t_0) \cdot \sum_j \left(\sigma_j \cdot \exp(\Gamma \cdot \tau_j^{\max})\right)$$

$$\Rightarrow \quad \breve{t}_1 - t_0 \leq \frac{Q_T}{\frac{A}{\Gamma} \cdot \sum_j \left[\sigma_j \cdot \left(1 - \exp(\Gamma \cdot \tau_j^{\max})\right)\right] - \mu}$$

$$\Rightarrow \quad t_{\max}^1 - t_0 \leq \tau_{\max} + \frac{Q_T}{\frac{A}{\Gamma} \cdot \sum_j \left[\sigma_j \cdot \left(1 - \exp(\Gamma \cdot \tau_j^{\max})\right)\right] - \mu}. \qquad (5.85)$$

Note that $\frac{A}{\Gamma} \cdot \sum_j \left[\sigma_j \cdot \left(1 - \exp(\Gamma \cdot \tau_j^{\max})\right)\right] - \mu > 0$ is required for the last two steps.

(3) Alternatively, from equation (5.83),

$$\left(\sigma \cdot \frac{A}{\Gamma} - \mu\right) \cdot (\breve{t}_1 - t_0) = Q_T + \frac{A}{\Gamma} \cdot \frac{1 - \exp\left(-\Gamma \cdot (\breve{t}_1 - t_0)\right)}{\Gamma} \cdot \sum_j \left(\sigma_j \cdot \exp(\Gamma \cdot \tau_j^{\max})\right)$$

$$\Rightarrow \quad \left(\sigma \cdot \frac{A}{\Gamma} - \mu\right) \cdot (\breve{t}_1 - t_0) \leq Q_T + \frac{A}{\Gamma} \cdot \frac{1}{\Gamma} \cdot \sum_j \left(\sigma_j \cdot \exp(\Gamma \cdot \tau_j^{\max})\right)$$

$$\Rightarrow \quad \breve{t}_1 - t_0 \leq \frac{Q_T + A/\Gamma \cdot 1/\Gamma \cdot \sum_j \left(\sigma_j \cdot \exp(\Gamma \cdot \tau_j^{\max})\right)}{\sigma \cdot A/\Gamma - \mu}$$

$$\Rightarrow \quad t_{\max}^1 - t_0 \leq \tau_{\max} + \frac{Q_T + A/\Gamma \cdot 1/\Gamma \cdot \sum_j \left(\sigma_j \cdot \exp(\Gamma \cdot \tau_j^{\max})\right)}{\sigma \cdot A/\Gamma - \mu}. \qquad (5.86)$$

(4) From the definition of t_j^1, we know $q(t_j^1 - \tau_j(t_j^1)) = Q_T$, so

$$
\begin{aligned}
q(t_j^1) &= q(t_j^1 - \tau_j(t_j^1)) + \int_{t_j^1 - \tau_j(t_j^1)}^{t_j^1} \dot{q}(t)dt \\
&= Q_T + \int_{t_j^1 - \tau_j(t_j^1)}^{t_j^1} \left[\sum_j \varphi_j(t - \tau_j(t)) - \mu \right] dt \\
&\le Q_T + \left(\sum_j \varphi_j^{\max} - \mu \right) \cdot \tau_j^{\max}
\end{aligned}
$$

From equation (5.76) and Remark 5.5, $\varphi_j^{\max} = A/\Gamma \cdot \sigma_j \cdot \left(1 - \exp(-\Gamma \cdot t_j^1)\right)$, so

$$
\begin{aligned}
q(t_j^1) &\le Q_T + \tau_j^{\max} \cdot \left(A/\Gamma \cdot \sum_j \left[\sigma_j \cdot \left(1 - \exp(-\Gamma \cdot t_j^1)\right) \right] - \mu \right) \\
&\le Q_T + \tau_j^{\max} \cdot \left(A/\Gamma \cdot \sum_j \sigma_j - \mu \right) \\
&\le Q_T + \tau_j^{\max} \cdot \left(\sigma \cdot A/\Gamma - \mu \right)
\end{aligned}
\quad .
$$

Hence,

$$
q(t_j^1) \le Q_T + \tau_j^{\max} \cdot \left(\sigma \cdot A/\Gamma - \mu \right) \le Q_T + \tau_{\max} \cdot \left(\sigma \cdot A/\Gamma - \mu \right). \tag{5.87}
$$

□

Proposition 5.4 and Proposition 5.5 (1) – (3) in combination give the lower and upper bounds for the sequence of response times $\left\{ t_j^1 \right\}_{j=1}^N$ for the rate-control systems in the fluctuation region ($A/\Gamma > \mu/\sigma$). The difference between A/Γ and μ/σ is one of the most critical factors in bounding $\left\{ t_j^1 \right\}_{j=1}^N$: a smaller difference leads to much longer response times. In general, for a specific flow *j*, the bounds of its response time t_j^1 increase with the feedback delay bounds of the j^{th} flow $\tau_j^{\min}$, $\tau_j^{\max}$. Furthermore, because $\left\{ t_j^1 \right\}_{j=1}^N$ are delayed tracking of a common queue in different flows, the flow with less delay always has the shorter response time. As is well known, the (local) maximum rate $\varphi_j^{\max}$ increases with the corresponding response time t_j^1.

In our parameter design, when A/Γ is fixed in the above system, to compensate for the long response time, either a large Γ or a large σ can be adopted (or both). In addition, for the same purpose, we can adjust the relative weights $\{\sigma_j\}_{j=1}^{N}$ by assigning smaller relative weights to the flows with longer feedback delays.

The fourth item of Proposition 5.5 presents an upper bound of the queue size at the response time of each flow. It is not a (local) maximum queue size although the rate of each flow achieves its (local) maximum at its response time. After the response times of certain flows, the sum of the rates is still higher than the available bandwidth, so the queue size keeps increasing. During this period, however, the rate of each flow always decreases with a higher speed than its increasing speed in Phase 1, according to the governing equation (5.67). Hence, we can obtain an upper bound of the (local) maximum queue size $q_{\max}$:

$$q_{\max} \leq \max_j \left[2 \cdot q(t_j^1) - Q_T\right] \leq \max_j \left[Q_T + 2 \cdot \tau_j^{\max} \cdot \left(\sigma \cdot \frac{A}{\Gamma} - \mu\right)\right]$$

$$\Rightarrow \quad q_{\max} \leq Q_T + 2 \cdot \tau_{\max} \cdot (\sigma \cdot A/\Gamma - \mu). \tag{5.88}$$

Denote the designed buffer size as Q_B. It can be set based on equation (5.88) as $Q_B \equiv \beta_0 \cdot [Q_T + 2 \cdot \tau_{\max} \cdot (\sigma \cdot A/\Gamma - \mu)]$. Here $\beta_0, \beta_0 > 1$ is a safety parameter. Clearly Q_B increases with σ, A/Γ and $\tau_{\max}$. So, a larger A/Γ (or σ) leads to shorter response times and lower maximum rates, with the tradeoff of a larger queue size. On the other hand, a smaller A/Γ (or σ) results in a smaller queue size, with tradeoffs of longer response times and higher maximum rates. In summary, the tradeoffs in the parameter design are necessary to give consideration to both issues of achieving small

response times of all flows and smaller overshoots, if any, with a reasonable queue size.

5.5.3. Simulation Results of the System with Multiple Flows

Extensive simulations have been done for the multi-flows rate-control system with heterogeneous time-varying feedback delays, to demonstrate the issues discussed above, qualitatively and quantitatively. The considered issues were listed at the beginning of this section: transient behavior, parameter design, the effect of time-varying delays, fairness, etc. Particularly we consider the design rule (5.75).

Figure 5.6 shows two flows with the same weight starting at time 0 and 50 s, respectively. Two flows have different time-varying delays with $\tau_1^{\min} = \tau_2^{\min} = 0.05$ s, $\tau_1^{\max} = 0.15$ s and $\tau_2^{\max} = 0.25$ s. For convenience the queue size is measured in units of nominal packets. 1 nominal packet has 6250 bytes, which is the product of 1 Mbps/s and 0.05 s.

In Figure 5.6, for $t < 50$ s the system has only flow 1, $\sigma_1 \cdot A/\Gamma + \nu_1 = 112.22$ Mbps $< \mu$, therefore the system has stationary-state solutions. The rate of flow 1 approaches the steady state exponentially and the queue is always empty. After time 50 s, flow 2 attempts to obtain its share of the bandwidth, $\sum_{j=1,2}\left(\sigma_j \cdot A/\Gamma + \nu_j\right) = 224.44$ Mbps $> \mu$. So the system is in the fluctuation region for $t \geq 50$ s, and the fluctuating behavior in the rates and queue size can be clearly observed in Figure 5.6. With different time-varying delays associated with the two flows, these fluctuations are not periodic and are different for two flows. However, in Figure 5.6, the amplitude and period of the fluctuations are bounded and close to periodic; and the rates of the two flows almost

coincide with each other after the transient period. It follows that fairness (½ to ½) is achieved between two flows almost at any time.

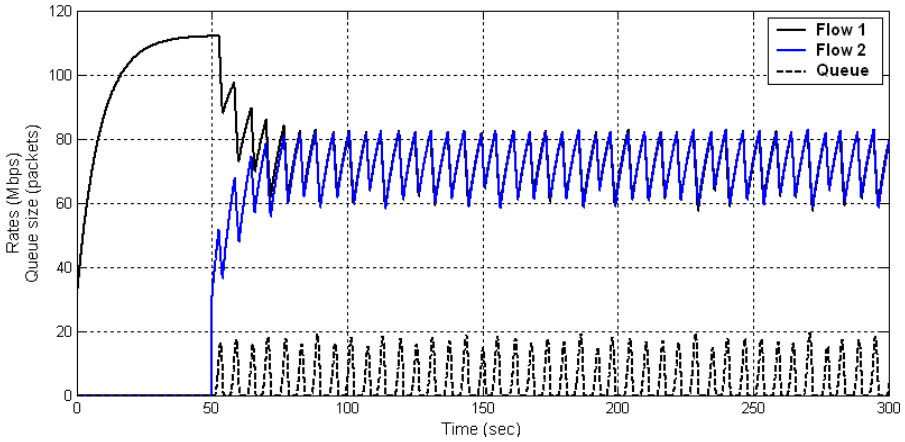

(a) A = 9.62 Mbps, Γ = 0.117

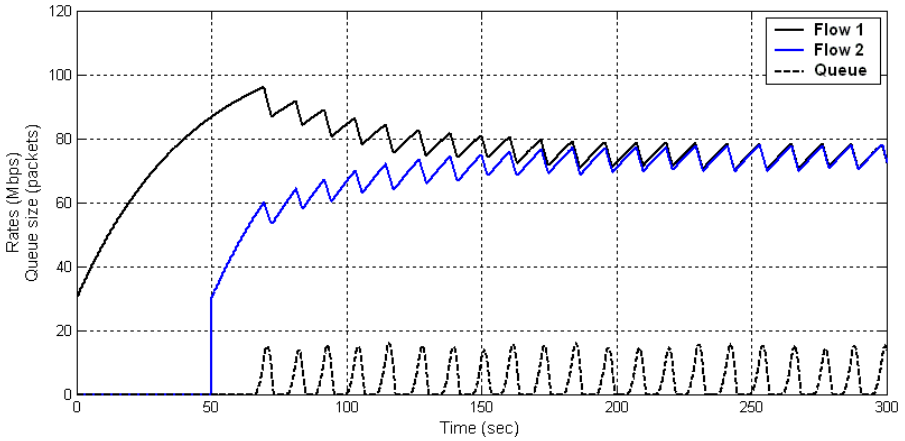

(b) A = 1.924 Mbps, Γ = 0.0234

Flow 1 and 2 starts at 0 and 50 s, respectively. μ = 150 Mbps, $\nu_1 = \nu_2$ = 30 Mbps, Δ = 0.05 s, Q_T = 10 packets, $\sigma_1 = \sigma_2 = 1$, $\tau_1(t) = 0.1 + 0.05 \cdot \sin(\pi t/11)$, $\tau_2(t) = 0.15 + 0.1 \cdot \sin(\pi t/7)$.

Figure 5.6: Multi-Flows: Various Gain and Damping Constants with Fixed Ratio

Two sets of gains and damping constants are used in Figure 5.6 with their ratio fixed: the one in (a) has larger (A , Γ), which leads to shorter response times in both stable and fluctuation regions; while the other set in (b) provides smaller fluctuations and requires less buffer size in the common queue. Either of them could be desirable depending on the specific purpose of parameter design; or it could be any other set in between for further tradeoff among the above performance metrics.

Figure 5.7 presents the results of significantly different feedback delays between two flows. The parameters in Figure 5.7 are the same as those used in Figure 5.6(a), except that the mean of the feedback-delays of flow 2 increases from 0.15 s to 1.15 s. It has been shown in Figure 5.7 as expected that the response times become longer, according to equations (5.78) – (5.80) and (5.84) – (5.86), and that the fluctuations are slower; the amplitude of rates and queue size both increase, from equations (5.76) and (5.88). Also exhibited in Figure 5.7 is the increased difference between two flows, compared with Figure 5.6(a), due to their heterogeneous feedback delays. The delays of flow 1 are roughly 1/10 of those of flow 2 in magnitude.

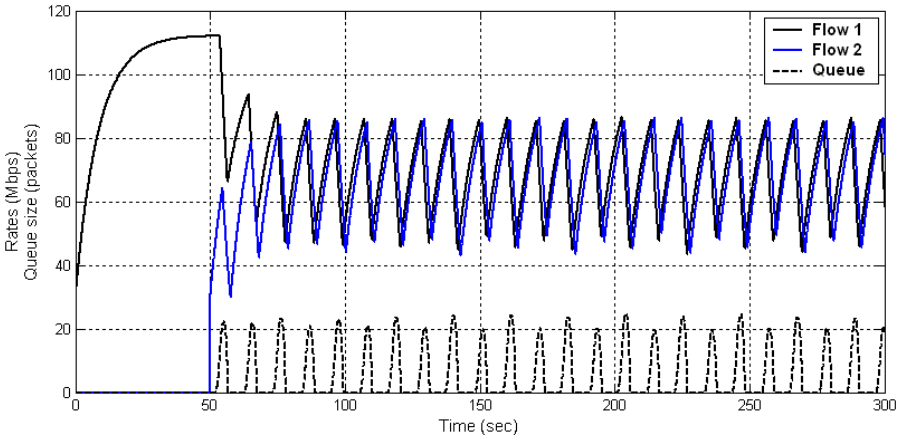

Flow 1 and 2 starts at 0 and 50 s, respectively. A = 9.62 Mbps, Γ = 0.117, μ = 150 Mbps, v_1 = v_2 = 30 Mbps, Δ = 0.05 s, Q_T = 10 packets, $\sigma_1 = \sigma_2 = 1$, $\tau_1(t) = 0.1 + 0.05 \cdot \sin(\pi t/11)$, $\tau_2(t) = 1.15 + 0.1 \cdot \sin(\pi t/7)$.

Figure 5.7: Multi-Flows: The Effect of Various Feedback Delays

Figure 5.8 presents four flows with different minimum bandwidths and equal share (expected) of the remainder of available bandwidth. The rate differences between four pairs of flows (1, 2), (3, 4), (1, 3) and (2, 4) are depicted in Figure 5.8(b). In Figure 5.8(b), there is a 15 Mbps difference in the minimum bandwidth for two flow pairs (1, 2) and (3, 4). From the rates and their difference shown in Figure 5.8(a) and (b), we note that although the fairness is not accurately achieved pointwise,

the curves fluctuate around their average values that closely correspond to the expected sharing under the fairness constraint. For example, in Figure 5.8(b), the rate differences of flow pairs (1, 2) and (3, 4) have a mean of 15 Mbps with its amplitude less than 3 Mbps.

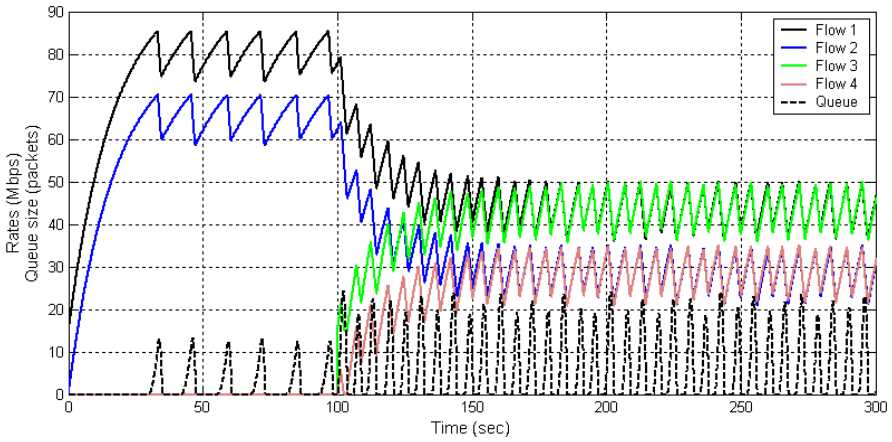

(a) Rates of flows and the queuing behavior

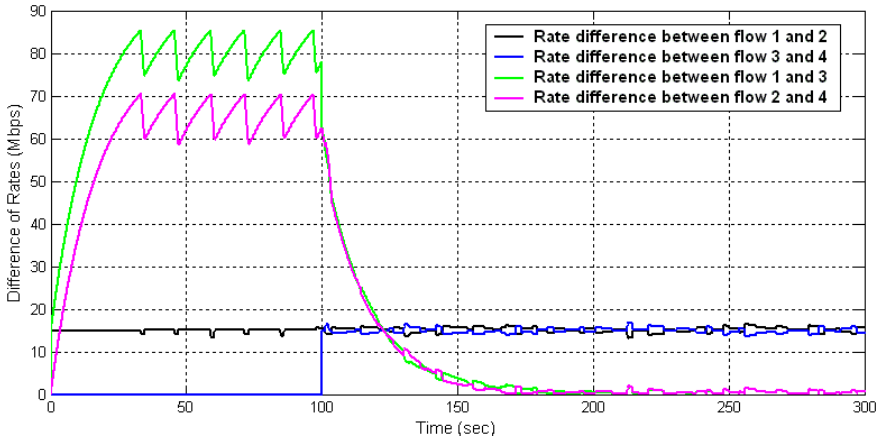

(b) Difference of rates for certain pairs of flows

Flow 1 and 2 starts at 0 s, while Flow 3 and 4 starts at 100 s. A = 4.81 Mbps, Γ = 0.0585, μ = 150 Mbps, $v_1 = v_3$ = 15 Mbps, $v_2 = v_4$ = 0, Δ = 0.05 s, Q_T = 10 packets, σ_j = 1, j = 1, 2, 3, 4. $\tau_1(t) = \tau_4(t) = 0.1 + 0.05 \cdot \sin(\pi t/11)$, $\tau_2(t) = \tau_3(t) = 0.15 + 0.1 \cdot \sin(\pi t/7)$.

Figure 5.8: Multi-Flows: Four Flows with Different Minimum Bandwidths

Figure 5.9 shows the transient behavior of the system with 16 flows as four new flows start at 0, 150, 300 and 450 s, respectively. The rates of all flows are shown in Figure 5.9(a) while the aggregated rate, the average rate per flow and the queue size are shown in Figure 5.9(b).

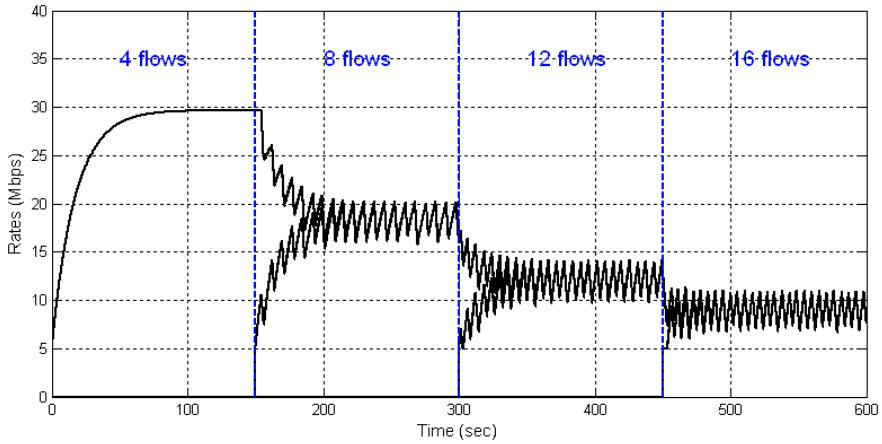

(a) Rates of flows

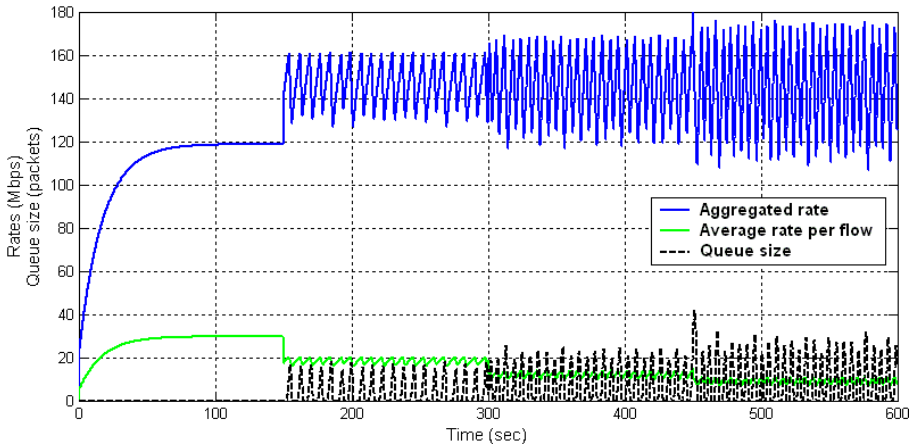

(b) Aggregate rate and queue behavior

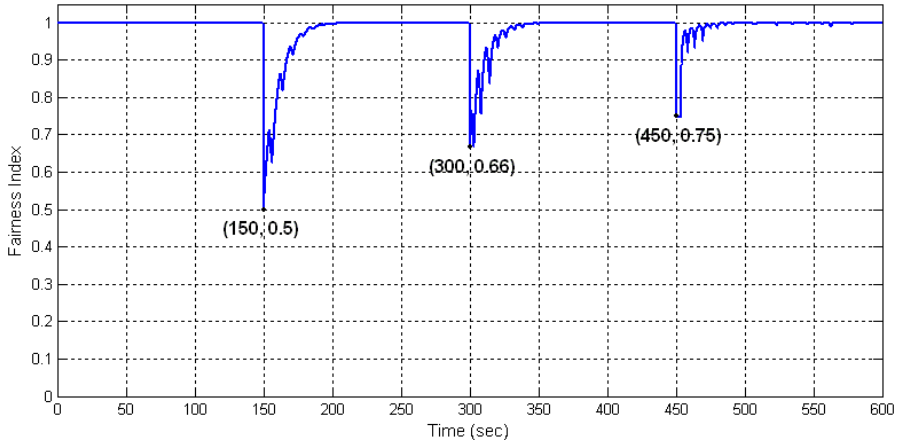

(c) Fairness index

Four new flows start at 0, 150, 300 and 450 s, respectively. A = 4.81 Mbps, Γ = 0.0585, μ = 150 Mbps, Δ = 0.05 s, Q_T = 10 packets, ν_j = 5 Mbps, σ_j = 0.3, j = 1, …, 16. For k = 0, 1, 2, 3, $\tau_{4k+1}(t) = \tau_{4k+4}(t) = 0.1 + 0.05 \cdot \sin(\pi t/11)$, $\tau_{4k+2}(t) = \tau_{4k+3}(t) = 0.15 + 0.1 \cdot \sin(\pi t/7)$.

Figure 5.9: Multi-Flows: The Effect of Increasing Number of Flows

In Figures 5.9(a) and 5.9(b), for $t < 150$ s, the system has stationary solutions with an aggregated rate of 120 Mbps ($< \mu$); for $t \geq 150$ s, the system has fluctuating solutions. Note that the rate fluctuations slow down as the number of flows increases.

A quantitative measure of fairness, Jain's Fairness Index, was proposed first in [86] and has been widely used thereafter. For a system with N competing users, where the i^{th} user receives an allocation x_i, Jain's Fairness Index (FI) is defined as follows:

$$FI = \frac{\left(\sum_{i=1}^{N} x_i\right)^2}{N \cdot \sum_{i=1}^{N} \left(x_i\right)^2} . \tag{5.89}$$

Figure 5.9(c) shows the Jain's Fairness Index (FI) at different times with 4, 8, 12 and 16 active flows, respectively. The minimum bandwidth is not considered in the allocated resource, i.e., $x_i(t) = \varphi_i(t) - \nu_i$, where flow i is an active flow. The perfect fairness ($FI \approx 1$) can be clearly observed except for the transient times when a new group of flows have been just started.

5.6. Conclusions

In this chapter, we focus on feedback-based rate control systems for adaptive bandwidth allocation in broadband IP-based satellite communication networks. The considered feedback is one bit that indicates whether the remote queue is above or below a pre-determined threshold. Each flow in the system has two nonnegative parameters, minimum bandwidth and weight.

Our analyses are based on analytic fluid models composed of first-order delay-differential equations with damping and gain functions. Furthermore, practically and most importantly, the heterogeneous time-varying propagation delays are reflected in the system models. Single-flow and multi-flow system models are analyzed,

respectively, with much attention paid to the symmetrical Mitra-Seery (MS) algorithm.

We present the stationary solutions, existence conditions and convergence speed for the single-flow and multi-flow system models, respectively. And then for the situations under which the systems only have fluctuating solutions, we analyze the dynamic behavior of rates and queue size in detail. Based on the analytic results, we investigate the effect of delays and parameters in terms of fairness, fluctuation (amplitude, period), transient behavior and adaptability, etc. It has been shown, analytically and in simulations, that with proper parameter design the system can achieve stable behavior with close to pointwise proportional fairness among flows.

6. Resource Allocation in 802.16j Multi-hop Relay Systems

Systems based on IEEE 802.16 OFDMA standard (mobile WiMAX, or 802.16e) are among the leading candidates for 4G wireless networks. Mobile WiMAX is designed to provide high data rate to mobile users with QoS; however, initial field trials of mobile WiMAX system have limited coverage and poor service for indoor users as well as users at cell boundaries. Using relay stations (RS) is a well known method to extend the coverage of the base stations (BS) in cellular systems. IEEE 802.16j multi-hop relay standard has been developed as an extension to the 802.16e OFDMA system for coverage extension and capacity enhancement with full backward compatibility to the 802.16e mobile stations (MS). In the 802.16j relay system, relay stations serve as relay nodes between the multihop-relay BS (MR-BS, or BS) and the MSs. The radio link that originates from or terminates at an MS is called access link; while the link between a MR-BS and an RS is called relay link.

Two modes of PHY layer operations are defined in 802.16j: transparent relay mode and non-transparent relay mode. In transparent relay mode, a transparent RS (T-RS) does not transmit control signals including frame-start preamble, FCH, UL/DL-MAP and DCD/UCD. Instead, a MS that access the network through a T-RS depends on the MR-BS for these control signals. The MS is not aware of the T-RS. In non-transparent mode, a non-transparent RS (NT-RS) transmits all the control signals as well as data packets like a regular BS to the MS. T-RS and NT-RS have different and incompatible frame structures and hence present mutually exclusive options:

transparent relay systems and non-transparent relay systems (denoted as T-RS and NT-RS as well). In addition, a NT-RS can operate in either centralized or distributed scheduling mode if the transmission schedule of the RS is generated by the MR-BS (centralized) or the RS itself (distributed). Clearly, a T-RS can only operate in centralized scheduling mode. For NT-RS, in this dissertation we only consider distributed scheduling mode.

It is important to understand the benefits and limits of each option. Based on methodologies specified in [87, 88], a system-level simulator is introduced in [89] for multi-cell 802.16j multi-hop relay systems. Also, performance is compared in [89, 90] through simulations for these options of 802.16j two-hop relay systems, in terms of network coverage and system capacity with various assumptions on relay links for simplification. This chapter describes further work on capacity analysis and resource allocation.

The resource allocation problem in 802.16j relay network has been studied in [91, 92, 93, 94, 95]. It is demonstrated in [91] that in the 802.16j multi-hop relay system, that 1 or 2 RSs per sector can improve the per-cell uplink (UL) throughput (e.g., by 25% or 38% with 90 data users per cell, respectively). RS deployment and resource reuse strategies for 802.16j multi-hop relay system are investigated in [92, 93]. It is shown that using RSs with resource reuse among all RSs can substantially improve the system capacity. In [94], system performance is evaluated for 802.16j multi-hop relay networks with both conventional and its proposed spectrum efficiency based adaptive resource allocation (SEBARA) method. Simulation results show that the SEBARA method outperforms the conventional one in terms of throughput, delay and

packet loss. In [95], several heuristic scheduling schemes for a WiMAX-based OFDMA system have been compared in terms of throughput and delay.

In this chapter, we study and compare the capacity of the two different 16j relay systems through joint resource allocation and user (MS) balancing under the user rate fairness requirement. Special attention is paid to the MS association rule in determining the access station between the MR-BS and the RSs. We carry the study in the downlink (DL) direction of two-hop systems where a MS connects to the MR-BS through at most one RS; the same schemes apply to the UL direction as well. We first propose a system design approach to evaluate the per-user throughput and total system capacity. Then the maximum capacity among different frame partitions is obtained for each type of 802.16j system, and compared with the BS-only system (802.16e) used as a baseline. The effect of increasing the number of deployed RSs per sector, and the usage of SISO or MIMO in the relay links are also investigated. Furthermore, for each 802.16j relay system with rate fairness constraint, two MS association rules are compared with the formulated optimal rule that achieves the maximum capacity among all the association rules and frame partitions. The effective spectrum efficiency (ESE) is used in T-RS networks, and is further modified to account for the aggressive frequency reuse in NT-RS networks.

The chapter is organized as follows: Section 6.1 presents the 802.16j relay frame structures and system configuration. Section 6.2 describes the channel models and simulation results of DL Carrier to Interference-plus-Noise Ratio (CINR). Section 6.3 first gives our proposed system design approach for capacity analysis of each relay system with certain MS association rules under the user rate fairness constraint, and

then evaluates and compares their resulting capacity with respect to different relay systems and/or MS association rules. Section 6.4 draws our conclusions.

6.1. Frame Structure and System Configuration

6.1.1. Frame Structure of Two-hop Relay Networks

Transparent Relay Frame Structure

Figure 6.1 shows the transparent relay frame structure when T-RSs are used [96].

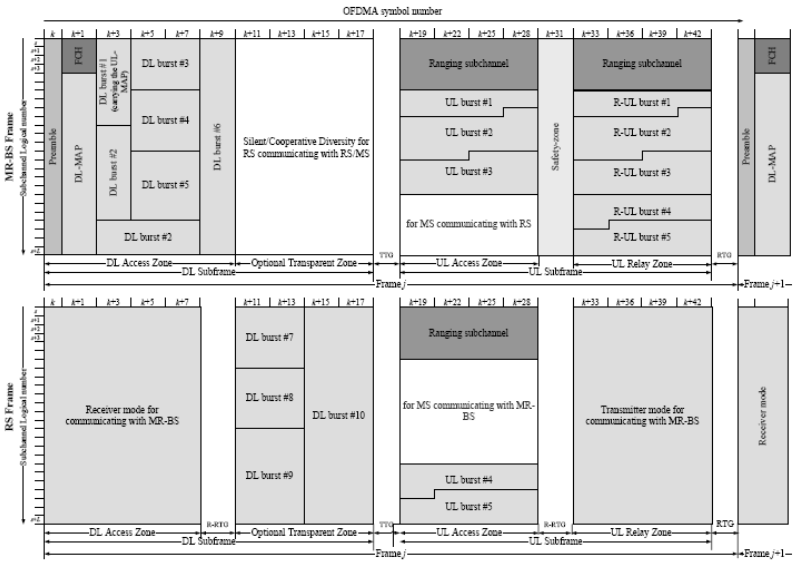

Figure 6.1: Frame Structure for a 2-hop Transparent Relay System [96]

The DL subframe is partitioned into Access Zone and optional Transparent Zone. In Access Zone, BS sends out data bursts to RS and MS, respectively. In Transparent Zone, RS forwards data bursts received from BS in Access Zone to MSs. BS and RS will never transmit simultaneously, therefore no cross interference exists between BS and RS. Because RS needs to switch from receiving mode in Access Zone to transmitting mode in Transparent Zone, BS's Access Zone is 2 symbols longer than that of RS here.

When transmitting to a MS, a transparent RS cannot adjust its TX power arbitrarily. The MS receiver requires the received signal from the RS to match with the received preamble from BS, because it uses the preamble as reference to the data subcarriers in the data bursts. Consequently the data bursts received from a RS can not have higher power than that received from the BS directly, and this eliminates any link budget gain in DL that RS could bring to a MR cell. The transmission power of a RS to a MS has to be individually adjusted so the powers received from the MR-BS and the RS are the same. However, to simulate this requires the detailed transmission schedule to be generated. In order to keep the simulation generic, we make the approximation that a RS always transmits with constant power.

Non-Transparent Relay Frame Structure

Figure 6.2 shows the non-transparent relay frame structure when NT-RSs are used [96].

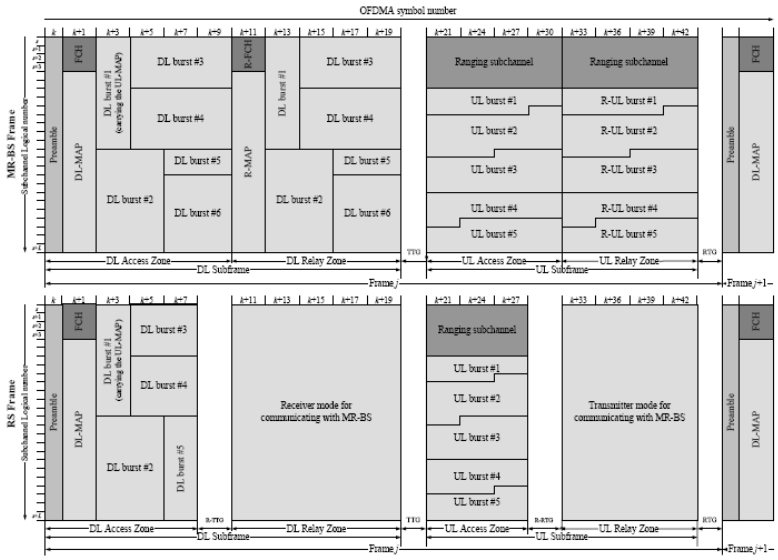

Figure 6.2: Frame Structure for a 2-hop Non-Transparent Relay System [96]

The DL subframe is partitioned into Access Zone and Relay Zone. In Access Zone, BS and RSs simultaneously transmit data bursts and control information to the

MS in each sector; while in Relay Zone, BS sends data bursts to RSs (for forwarding to MSs in the next DL Access Zone). Note that BS's Access Zone is 2 symbols longer than a RS due to the transmission-to-reception transmission gap (R-TTG) of a RS.

6.1.2. Network Configuration

We list the configuration of relay network and DL OFDMA parameters in Table 6.1. One slot is one subchannel by two symbols for DL PUSC (Partial Usage of SubChannels) [12].

Parameters		Value
Number of 3-Sector Cells (staggered)		19
Operating Frequency		2500 MHz
Frequency reuse factor		1/3/3
BS-to-BS Distance		1 km
RS-to-BS Distance		375 m
BS Tx Antenna Gain		16 dBi
BS/RS/MS Height		32 / 10 / 2 m
BS Tx Antenna Power (3 segments)		43 dBm
BS/RS/MS Noise Figure		5 / 6 / 7 dB
RS Tx/Rx Antenna Gain		10 dBi
RS Maximum PA Power		37 dBm
MS Rx Antenna Gain		Omnidirectional, –1 dBi
Implementation Loss at Receiver		5 dB
System Channel Bandwidth		10 MHz
Sampling Frequency (Fp)		11.2 MHz
FFT Size (NFFT)		1024
Sub-Carrier Frequency Spacing		10.9375 kHz
Useful Symbol Time (Tb = 1/f)		91.4 μs
Guard Time (Tg = Tb/8)		11.4 μs
OFDMA Symbol Duration (Ts = Tb + Tg)		102.9 μs
Frame duration		5 ms
Number of Data Symbols		47
Power boosting of Pilot in DL PUSC		2.5 dB
DL PUSC	Null Sub-carriers	184
	Pilot Sub-carriers	120 (40 per sector)
	Data Sub-carriers	720 (240 per sector)
	Sub-channels	30 (10 per sector)

Table 6.1: WiMAX System and DL OFDMA Parameters

RSs are placed evenly in each sector at the ¾ cell radius. The topology of BSs and RSs in T-RS and NT-RS is the same except that a T-RS shares the same frequency segment as its MR-BS; while a NT-RS may use a different segment than its MR-BS and its peers in the same sector. Figure 6.3 shows the frequency patterns in center cell for NT-RS with 1 or 3 RSs per sector. Each color represents a different frequency segment. The DL CINR distribution for MSs in the center cell has been obtained through simulation. Details of the simulation results have been reported in [89] and the related results will be listed in Section 6.2 as well.

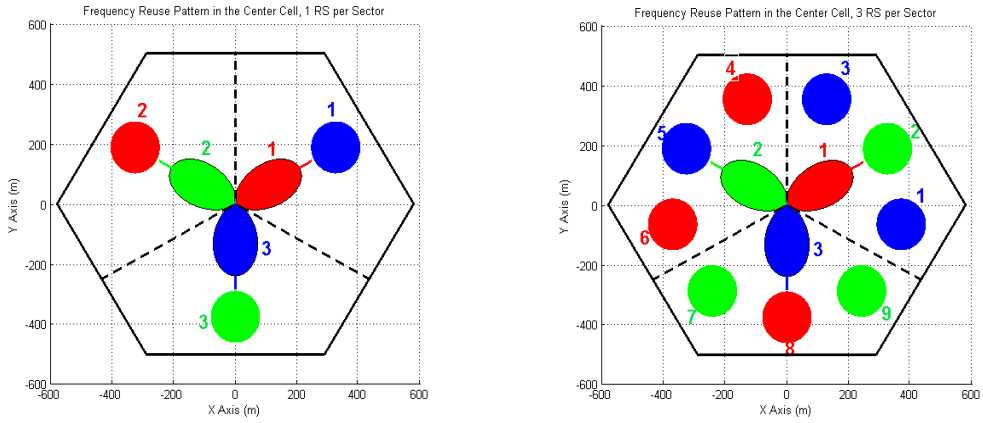

(a). 1 RS per Sector (b). 3 RSs per Sector

Figure 6.3: Topology and Frequency Reuse Pattern in Center Cell in 2-hop Non-Transparent Relay System

6.2. Channel Models and Simulation Results

6.2.1. Channel Models

Path-Loss Model:

The path loss types, usage models [97] and detailed path-loss models [98] are specified in [88].

The modified IEEE 802.16 path-loss model is recommended for Type A/B/C/D links in [98]. Type A, B and C are for macro-cell suburban, where one antenna is mounted above the rooftops (ART) and another is below the rooftops (BRT). Hence they could have a Line-of-Sight (LOS) or Non-Line-of-Sight (NLOS) depending on the distance and obstacles between them. Type D is also for macro-cell suburban but both node antennas are ART so that they have a LOS between them.

In the basic IEEE 802.16 model, three propagation scenarios are categorized as:

- Terrain Type A: Hilly terrain with moderate-to-heavy tree densities
- Terrain Type B: Intermediate path-loss condition
- Terrain Type C: Flat terrain with light tree densities

For Type D, the most benign category (category C) is chosen to allow for the fact that the links in this case are assumed to have been deployed with a good LOS.

Now we present the Modified IEEE 802.16 model as follows:

Modified IEEE 802.16 model:

$$PL\ (dB) = \begin{cases} 20\log\left(\frac{4\pi d}{\lambda}\right) & for\ d \le d_0' \\ A + 10\gamma\log\left(\frac{d}{d_0}\right) + \Delta PL_f + \Delta PL_{ht} & for\ d > d_0' \end{cases} \quad (6.1)$$

Where,

- $A = 20\log\left(\frac{4\pi d_0'}{\lambda}\right)$
- $d_0 = 100\ m$
- $d_0' = d_0 10^{-\left(\frac{\Delta PL_f + \Delta PL_{ht}}{10\gamma}\right)}$

- $\gamma = a - bh_b + \frac{c}{h_b}$
- $\Delta PL_f = 6\log\left(\frac{f(MHz)}{2000}\right)$, correction factor for carrier frequency
- $\Delta PL_{ht} = \begin{cases} -10\log\left(\frac{h_t}{3}\right) & for\ h_t \le 3m \\ -20\log\left(\frac{h_t}{3}\right) & for\ h_t > 3m \end{cases}$, correction factor for receive antenna height
- d = distance between transmitter and receiver
- h_b = height of BS/RS antenna, ART
- h_t = height of RS/MS antenna, BRT for Type A/B/C while ART for Type D
- a, b, c = model parameters

The corresponding model parameters (a, b, c) for each type are given in Table 6.2.

Model Parameter	Type A	Type B	Type C/D
a	4.6	4	3.6
b	0.0075	0.0065	0.005
c	12.6	17.1	20

Table 6.2: Path-Loss Model Parameters

The formula for correction factor for receive antenna height is different depending on whether the receive antenna height is less than 3m. In our simulations, the MS antenna height is 2m while the RS antenna height is 10m, hence their correction factor for receive antenna height are 1.7609 dB and –10.4576 dB, respectively.

Shadow Fading:

According to [87, 88], it is set as 8 dB for BS–MS and RS–MS links, and 3.4 dB for BS–RS links. Spatial correlation distance is set to 20m.

Multi-path fading:

Modified Stanford University Interim (SUI) models [99] are used for BS–RS links with fixed RSs; while ITU models (PA, PB, VA, VB) in [100] are used for BS–MS and RS–MS links with moving MSs.

The implemented 802.16 multi-path fading models derived from SUI models are listed in Table 6.3.

Terrain Type C: Flat terrain with light tree densities							
	SUI-1			**SUI-2**			
	Tap 1	Tap 2	Tap 3	Tap 1	Tap 2	Tap 3	Unit
Delay	0	0.4	0.9	0	0.4	1.1	μs
Power	0	-15	-20	0	-12	-15	dB
K factor	4	0	0	2	0	0	
Doppler	0.4	0.3	0.5	0.2	0.15	0.25	Hz
Terrain Type B: Intermediate path-loss condition							
	SUI-3			**SUI-4**			
	Tap 1	Tap 2	Tap 3	Tap 1	Tap 2	Tap 3	Unit
Delay	0	0.4	0.9	0	1.5	4.0	μs
Power	0	-5	-10	0	-4	-8	dB
K factor	1	0	0	0	0	0	
Doppler	0.4	0.3	0.5	0.2	0.15	0.25	Hz
Terrain Type A: Hilly terrain with moderate-to-heavy tree densities							
	SUI-5			**SUI-6**			
	Tap 1	Tap 2	Tap 3	Tap 1	Tap 2	Tap 3	Unit
Delay	0	4	10	0	14	20	μs
Power	0	-5	-10	0	-10	-14	dB
K factor	0	0	0	0	0	0	
Doppler	2.0	1.5	2.5	0.4	0.3	0.5	Hz

Table 6.3: 802.16 Channel Models Derived from SUI Models

The SUI-1, SUI-2 and SUI-3 models are applicable for LOS condition, and SUI-4, SUI-5 and SUI-6 models are applicable for NLOS condition. When K factor is zero, the corresponding path is a Rayleigh fading process; otherwise it is a Rician fading process.

The implemented 802.16 PDP Channel models are listed in Table 6.4.

PDP Models Case 1: Pedestrian-A (PA), 4 Paths							
	Tap 1	Tap 2	Tap 3	Tap 4			Unit
Delay	0	0.110	0.190	0.410			μs
Relative Power	0	-9.7	-19.2	-22.8			dB
Speed	3, 30, 120						km/h
PDP Models Case 2: Vehicular-A (VA), 6 Paths							
	Tap 1	Tap 2	Tap 3	Tap 4	Tap 5	Tap 6	Unit
Delay	0	0.310	0.710	1.090	1.730	2.510	μs
Relative Power	0	-1.0	-9.0	-10.0	-15.0	-20.0	dB
Speed	30, 120, 250						km/h
PDP Models Case 3: Pedestrian-B (PB), 6 Paths							
	Tap 1	Tap 2	Tap 3	Tap 4	Tap 5	Tap 6	Unit
Delay	0	0.200	0.800	1.200	2.300	3.700	μs
Relative Power	0	-0.9	-4.9	-8.0	-7.8	-23.9	dB
Speed	3						km/h
PDP Models Case 4: Vehicular-B (VB), 6 Paths							
	Tap 1	Tap 2	Tap 3	Tap 4	Tap 5	Tap 6	Unit
Delay	0	0.300	8.900	12.900	17.100	20.000	μs
Relative Power	-2.5	0	-12.8	-10.0	-25.2	-16.0	dB
Speed	30, 120, 250						km/h

Table 6.4: PDP SISO Channel Model Parameters

Table 6.5 lists used propagation, multi-path fading and Log-normal fading models in the following simulation results.

Parameters		**Value**
Propagation Model	BS-RS links	Type D
	BS-MS and RS-MS links	Type B
Multi-path Model	BS-RS links	SUI-2 model
	BS-MS and RS-MS links	VA model (30km/h)
Log-normal Shadowing SD (σ_s)	BS-RS links	3.4 dB
	BS-MS and RS-MS links	8 dB

Table 6.5: Channel Models

6.2.2. DL CINR Calculation and Simulation Results

DL CINR per Subcarrier

In two-hop relay systems, the MS can be served by either the BS or RS with the strongest received CINR. However, in T-RS, it is required for each MS to receive control information, including DL-MAP modulated in QPSK-1/8, from the BS. Hence, an additional requirement for the MS served by the RS is that its received CINR from the BS can support QPSK-1/8. In NT-RS, both control information and data come solely from the BS or RS at the receiver in the MS. Hence the MS could be served by either the BS or the RS in center cell and 2nd-tier cells.

For example, in T-RS, when MS is in Access Zone, the CINR of the m-th subcarrier (γ_m) with consideration of multi-path channels is:

$$\gamma_m = P_{i,j}^{BS} \cdot \left|H_{i,m}^{BS}\right|^2 \Bigg/ \left[\sum_{k=1,\, k\neq i}^{K} \left(P_{k,j}^{BS} \cdot \left|H_{k,m}^{BS}\right|^2\right) + N_0\right]$$
$$P_{i,j}^{BS} = P_{T,BS} G_{i,j}^{BS} \frac{10^{X_i^{BS}/10}}{L_{BS}(d_i)} \tag{6.2}$$

- $P_{i,j}^{BS}$ = received power at MS from sector j of BS i,. j = 1, 2 or 3 in this case.
- K is the number of BS in the system,
- N_0 = noise power,
- $P_{T,BS}$ = the TX power of BS,
- $G_{i,j}^{BS}$ = antenna gain between the MS RX and the sector j of the BS i TX,
- $H_{k,m}^{BS}$ is the instantaneous channel on the subcarrier m from the BS k,
- X_i^{BS} = lognormal shadowing between the MS and BS i,
- $L_{BS}(d_i)$ = path loss from the BS i at distance d_i.

Exponential Effective SIR Mapping (EESM)

We use EESM method to convert the CINR of individual subcarriers to the effective CINR of DL [101]. Its definition is:

$$\gamma_{eff} = SINR_{eff} = -\beta \cdot \ln\left(\frac{1}{N}\sum_{m=1}^{N} e^{-\frac{\gamma_m}{\beta}}\right) \tag{6.3}$$

- N is the number *of* sub-carriers,
- $\beta, \beta \geq 0$, is an EESM parameter.

The parameter β is determined by the system configuration and Modulation and Coding Scheme (MCS), and can be obtained from the extensive training simulations. For the same set of CINR in the subcarriers, different β's lead to different EESM CINR values.

Scheduling Modes

When the MR-BS determines the transmission schedule of its RSs (centralized scheduling), the link quality information between RS and MS has to be forwarded to BS for scheduling, which incurs extra delay. For mobile users, however, instantaneous channel quality is changing rapidly due to Rayleigh fading and this extra delay may lead to obsolete channel quality information (CQI) of MS used by BS for scheduling. How the MR-BS handle this is proprietary. One possible solution is that the BS introduces an extra CINR margin when selecting the MCS for the RS–MS link. In the simulations, an extra CINR margin of 2 dB is used to model this negative effect due to this additional delay.

Simulation Results of DL CINR

The system coverage is defined as the percentage of MSs which have higher effective SINR than a certain threshold. A list of MCS, their required receiver Signal-

to-Noise Ratio (SNR) and β values (from [101]) for DL are shown in Table 6.6. β values of the PB model with speed of 3km/h are used for BS-RS links; while β values of the VA model with speed of 60km/h are used for BS-MS and RS-MS links.

MCS (Repetition: default = 1)		**Spectrum Efficiency**	**Receiver SNR (dB)**	**EESM Beta, β (dB)**	
				PB (3km/h)	*VA (60km/h)*
QPSK	1/2 (4)	0.25	–2.50	2.18	2.12
	1/2 (2)	0.5	0.50	2.28	2.26
	1/2	1	3.50	2.46	2.54
	3/4	1.5	6.50	2.56	2.50
16-QAM	1/2	2	9.00	7.45	7.48
	3/4	3	12.50	8.93	8.93
64-QAM	1/2	3	14.50	11.31	11.43
	2/3	4	16.50	13.80	13.74
	3/4	4.5	18.50	14.71	14.68

Table 6.6: MCS, Required SNR and β values in DL

Table 6.7 lists DL coverage for MS with different MCS in single-hop system and two-hop relay systems. Here Cumulative Mass Function (CMF) is used.

MCS (repetition: default = 1)	**1-Hop System**	**Transparent Relay System**		**Non-Transparent Relay System**	
		1 RS / Sec	*3 RSs / Sec*	*1 RS / Sec*	*3 RSs / Sec*
QPSK ½ (4)	0.757	0.749	0.758	0.822	0.891
QPSK ½ (2)	0.587	0.695	0.736	0.666	0.760
QPSK 1/2	0.338	0.527	0.607	0.408	0.519
QPSK 3/4	0.168	0.371	0.460	0.220	0.302
16QAM 1/2	0.210	0.402	0.490	0.263	0.361
16QAM 3/4	0.102	0.269	0.342	0.140	0.195
64QAM 1/2	0.089	0.244	0.308	0.126	0.177
64QAM 2/3	0.075	0.217	0.279	0.111	0.157
64QAM 3/4	0.050	0.172	0.222	0.080	0.112

Table 6.7: DL Coverage (CMF) for MS in Different Systems

According to Table 6.7, NT-RS has less percentage of MS which are not able to be covered by QPSK 1/8 than any other system; and NT-RS with 3 RSs per sector in distributed mode has the least. The “QPSK ¾" row is always less than the “16QAM ½” row, meaning almost no MS is covered by QPSK ¾ since it is even easier for MS to be covered by 16QAM ½ most of the time through the simulation results. This may

have a negative impact, because when effective CINR feedback is used, the scheduler at BS or RS usually assumes all the MCS level below the MCS signaled by the MS can be supported. It is clear that if the MS signals to BS/RS that its effective CINR is 16QAM ½, there is some possibility that its channel can not support QPSK ¾. In the "64QAM ¾" row, T-RS with either 1 or 3 RSs per sector, performs much better than any other system. The reason is as follows: only MS very close to BS or RS can meet the tough SNR requirement (18.5dB) for 64QAM ¾. It is obvious that the T-RS can provide such chances to more MS compared with the single-hop system; and with no intra-cell interference and much less inter-cell interference, T-RS outperforms NT-RS in the number of MS with absolute high DL SINR values.

Similarly, on the relay link, both SISO and MIMO 2x2 are simulated, producing different spectrum efficiency (SE). The DL CINR distribution of the SISO relay link is shown in Table 6.8, along with the SE for different MCS. Here Probability Mass Function (PMF) is used to represent the DL coverage.

MCS (Rep: default = 1)	**Spectrum Efficiency**	**DL Coverage (PMF)**	
		1 RS per Sec	*3 RSs per Sec*
Not covered	0	0.000	0.005
QPSK ½ (4)	0.25	0.005	0.003
QPSK ½ (2)	0.5	0.004	0.005
QPSK ½	1	0.007	0.023
QPSK ¾	1.5	0.007	0.029
16QAM ½	2	0.028	0.086
16QAM ¾	3	0.024	0.083
64QAM ½	3	0.051	0.115
64QAM 2/3	4	0.070	0.153
64QAM ¾	4.5	0.804	0.498

Table 6.8: DL Coverage of RS in Two-hop Relay Systems, SISO

Note that the same relay link results apply to both T-RS and NT-RS systems. The RS deployed in the center of a sector enjoys better relay link quality than other RSs.

In SISO cases, for 1 or 3 RSs per sector, the SE of the relay link is 4.20 and 3.69 bit/symbol/subcarrier, respectively. In the MIMO 2×2 case, the spectrum efficiency is found to be 1.6-times that of the SISO case [102].

The simulation results shown in this section have been collected as the statistical means over 8660 MSs and 20 ~ 100 frames. The randomness of Log-normal fading with spatial correlations, multi-path channels and subcarrier permutations has been taken into consideration as well. These results are used for the system design and capacity analysis in the rest of this chapter, where no randomness is involved at all.

6.2.3. General Notation

S, x, y and z are the size of a frame, BSMS, RSMS and BSRS zone, respectively. x_i and y_i are the corresponding sizes for MS_i if applicable. The size of each zone can be adjusted to one of all feasible sizes defined by the protocol. DS represents the resource for two symbols. From Table 6.1, $S = 705$, $DS = 30$. M is the number of RSs per sector. N, N_0, N_1, …, N_M are the number of total MSs, MSs served by BS and RS_1, …, RS_M, respectively. I, $I = \{1, 2, \ldots, N\}$, is the set of all MSs. I_0, I_1, …, I_M are the set of MSs served by BS and RS_1, …, RS_M, respectively, which form a partition of I such that $I_0 \bigcap \ldots \bigcap I_M = \Phi$ (empty set) and $I_0 \bigcup \ldots \bigcup I_M = I$. r_i, $r_{i,0}$ and $r_{i,j}$ are the SE of MS_i if $i \in I$, I_0 or I_j, $j = 1, \ldots, M$, respectively. R_j is the SE of RS_j in BSRS zone, $j = 1, \ldots, M$. And s_i is the assigned resource in total for MS_i. The capacity is C, $C = f(r, I_0, I_1, \ldots, I_M)$.

6.2.4. MS Association Rules

The MS association rule determines how a MS chooses its access point (MR-BS or RS). For simplification, each MS can only choose between the MR-BS and at most 1 candidate RS.

Highest MCS scheme

The MR-BS or RS that provides the highest MCS level on the access link to the MS is chosen as the MS's access station.

Highest (Mod) ESE scheme

Each MS picks the MR-BS or RS with the strongest (modified) effective spectrum efficiency (ESE) as its access station.

ESE is defined as the ratio of the end-to-end throughput and consumed resources. For example, consider a 2-hop DL (BS-RS-MS link) in T-RS, where r_{relay} and r_{access} are the SE of BS-RS (relay) and RS-MS (access) link, respectively. Denote s_{relay} and s_{access} as their corresponding total resources. So, the ESE of this 2-hop DL is

$$\text{ESE}_{\text{2-hop}} = \frac{r_{access} \cdot s_{access}}{s_{access} + s_{relay}} = \frac{r_{relay} \cdot s_{relay}}{s_{access} + s_{relay}} = \left(\frac{1}{r_{access}} + \frac{1}{r_{relay}} \right)^{-1}. \tag{6.4}$$

Then, using the notations of Section 6.2.3, the ESE of MS_i in T-RS is

$$r_i^e = \begin{cases} r_{i,0}^e = r_{i,0}, & i \in I_0 \\ r_{i,j}^e = \left(r_{i,j}^{-1} + R_j^{-1} \right)^{-1}, & i \in I_j, j = 1,...,M \end{cases} \tag{6.5a}$$

For NT-RS, in each sector, the same resource is simultaneously used by BS and M RSs to provide access to their serving MSs. The ESE of 2-hop link in NT-RS has to be modified to reflect this aggressive frequency reuse among BS and M RSs. Using the principle of equation (6.4), the modified ESE of 2-hop link in NT-RS is

$$r_{i,j}^{e} = \left[\frac{1}{r_{i,0} + M \cdot r_{i,j}} + \frac{1}{R_j} \right]^{-1} \quad \text{if } i \in I_j, j = 1,...,M \tag{6.5b}$$

The Optimal scheme

It maximizes the system capacity, defined as the total data rate per cell, among all MS association rules under the rate fairness constraint.

6.3. Capacity Analysis in 2-Hop Relay Systems

We now analyze the system capacity under the user data rate fairness constraint. Each MS within the cell is provided with a similar data rate irrespective of its access station. Consequently the total resource used by a MS is inversely proportional to its ESE. The system capacity is then defined as the number of users per cell times the minimal per-user rate.

6.3.1. Capacity in 2-Hop Transparent Relay Systems

Figure 6.4 describes our capacity analysis algorithm in T-RS under the user rate fairness constraint. It can be used to analyze the system condition with arbitrary frame partition or MS association rule, or to search for the optimal point under the user rate fairness constraint. Note that $x \geq DS$, $y \geq 0$ and $z \geq 0$.

The capacity of the cell is given by

$$C = \sum_{i \in I} s_i \cdot r_i^e = \frac{N \cdot S}{\sum_{i \in I} 1 / r_i^e}. \tag{6.6}$$

It is clear that the capacity C is maximized when each MS chooses the access station with the highest ESE.

Input: MS association according to any given rule.

For each feasible RSMS zone size y_p, $p = 1, \ldots, P$ {

Rate per user in RSMS zone:

$$d_p^{RSMS} \equiv y_i \cdot r_i^e = y_p \cdot \left(\sum_{k \notin I_0} 1/r_k^e \right)^{-1} \quad \text{for} \quad i \notin I_0 ;$$

BSRS zone size $z_p = d_p^{RSMS} \cdot \sum_{j \neq 0} N_j / R_j$;

BSMS zone size $x_p = S - y_p - z_p$;

Rate per user when being served by BS in the BSMS zone:

$$d_p^{BSMS} \equiv x_i \cdot r_{i,0} = x \cdot \left(\sum_{k \in I_0} 1/r_{k,0} \right)^{-1} \quad \text{for} \quad i \in I_0 ;$$

};

The optimal frame partition p_s is achieved at:

$$p_s = \arg\max_p \left(\min\left(d_p^{BSMS}, d_p^{RSMS} \right) \right).$$

Figure 6.4: Capacity Analysis Algorithm in T-RS with Rate Fairness Constraint

Figure 6.5 shows the per-user rate in the 1-hop and 2-hop links of T-RS for *Highest MCS scheme* and *Highest ESE scheme*, respectively. Four cases are considered: 1 or 3 RSs per sector, SISO or MIMO in relay links. In Figure 6.5(a), the per-user data rate increases in 2-hop links while decreases in 1-hop links; the MIMO case has slower decreasing speed due to better relay links than the SISO case. Compared with the 1 RS case, the 3 RSs case has worse relay links, better RS-MS links and more MSs under RSs; and their composite effect leads to its lower per-user rate in 2-hop links. Under the user rate fairness constraint, the optimal RSMS zone is determined by the intersection of the user data rate served by 1-hop (BSMS) and 2-hop (BS-RS-MS) links, marked as "o" in Figure 6.5.

Figure 6.5(b) is very similar to Figure 6.5(a) except for the different MS associations in the SISO and MIMO cases in *Highest ESE scheme*. Compared with *Highest MCS scheme*, its resulted per-user rate and system capacity is slightly better, because the MS favors the BS more in *Highest ESE scheme*; however, with a very high SE on the relay links, this only affects fairly small number of MSs for which

both the BS and RSs can support MCS levels higher than QPSK-3/4. From our simulation results of SISO-1RS case, e.g., only 1.4% of MSs falls into this category.

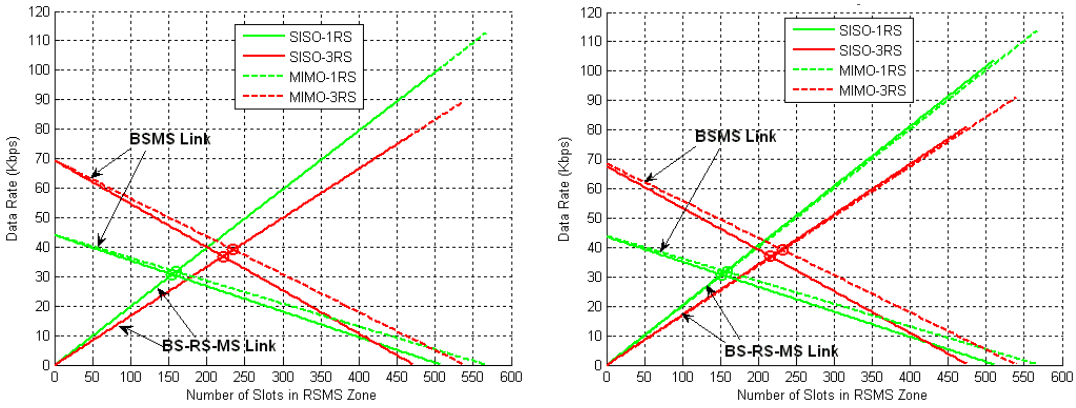

(a). Highest MCS Scheme (b). Highest ESE Scheme (Optimal)

Figure 6.5: Capacity Analysis (Per-user Rate) in T-RS with Rate Fairness Constraint

6.3.2. Capacity in 2-Hop Non-Transparent Relay Systems

In the case of NT-RS, the size of the access zone is almost the same for the BS and the RSs except a 2-symbol difference (*DS*). For those MSs served by RSs, their data rate is the minimal of the rates it gets on the BS-RS link and on the RS-MS link. In order to achieve the maximal system throughput, it is not feasible for the RS-MS zone size to be the bottleneck for these MSs. This is because the system capacity can be improved by simply increasing the size of the access zone in this case. For this reason, the optimal access-zone/relay-zone partition is always achieved when the MSs served by the RSs are limited by relay-zone size and the MSs served by the BSs are limited by the access-zone size. For MS_i served by RS_j, $j = 1, \ldots, M$, let $L_{i,j}$ be the resource it actually consumed in RSMS zone, and $z_{i,j}$ be its assigned resource in BSRS zone by RS_j regardless its usage. Let $L_j = \sum_{i \in I_j} L_{i,j}$, $z_j = \sum_{i \in I_j} z_{i,j}$.

Figure 6.6 describes our capacity analysis algorithm for NT-RS under the rate fairness constraint. Again it can be used to analyze the system condition with arbitrary frame partition or MS association rule, or to search for the optimal point under the user rate fairness constraint. Note that $x, y, z \geq 0$ and $y + z \leq S - DS$.

Input: MS association according to any given rule.
For any feasible BSRS zone size z_p, $p = 1, \ldots, P$ {

$y_p = S - DS - z_p$; % the size of RSMS zone

$AvgR_j(p) = y \Big/ \sum_{i \in I_j} (1/r_i)$; % tentative per user rate

$z_j = z \cdot (N_j / R_j) \Big/ \sum_{k \neq 0} (N_k / R_k)$; % tentative slots

$$d_p^{RSMS} \equiv \min\left(z \Big/ \sum_{k \neq 0} (N_k / R_k),\ AvgR(p)\right)$$
$$= \min\left(z \Big/ \sum_{k \neq 0} (N_k / R_k),\ \min_{j \neq 0} AvgR_j(p)\right);$$

$x = x(p) = S - z(p)$; % the size of BSMS zone

$d_p^{BSMS} \equiv AvgR_0 = x \Big/ \sum_{k \in I_0} (1/r_k)$; % per user data rate.

}
The optimal frame partition p_s is achieved at:

$$p_s = \arg\max_p \left(\min\left(d_p^{BSMS},\ d_p^{RSMS}\right) \right).$$

Figure 6.6: Capacity Analysis Algorithm in NT-RS with Rate Fairness Constraint

Now we want to search for the optimal MS association rule that maximizes the system capacity. By bottleneck-BSRS-zone assumption, the per-user rate in 1-hop links ($AvgR_0$) and 2-hop links by RS j ($AvgR_j$) are

$$\begin{cases} AvgR_0 = r_{i,0} \cdot s_{i,0} = (S - z) \Big/ \sum_{k \in I_0} 1/r_{k,0} \\ AvgR_j = r_{i,j} \cdot L_{i,j} = R_j \cdot z_j / N_j = L_j \Big/ \sum_{k \in I_j} 1/r_{k,j},\ j \neq 0 \end{cases}$$

with: $L_j \leq L_T$, where $L_T \equiv S - DS - z$. For rate fairness among all MSs, $AvgR = \min(AvgR_0, AvgR_1, \ldots, AvgR_M)$.

For any given MS association rule, considering the frame partition under the user rate fairness constraint, let Z_1, Z_2 be the BSRS zone size when the MSs under the BS or the MSs under a most heavily loaded RS is the system wide bottleneck, respectively. Note Z_1, Z_2 are functions of MS association rules.

$$\begin{cases} Z_1 = \dfrac{S \cdot \sum_{k \neq 0} N_k / R_k}{\sum_{i \in I_0} 1/r_{i,0} + \sum_{k \neq 0} N_k / R_k} \\ Z_2 = \dfrac{(S - DS) \cdot \sum_{k \neq 0} N_k / R_k}{\max_{j \neq 0} (\sum_{k \in I_j} 1/r_{k,j}) + \sum_{k \neq 0} N_k / R_k} \end{cases} \tag{6.7}$$

Comparison of Z_1 and Z_2 provides a guidance to switch the MSs between the BS and the RSs in order to relieve the bottleneck and improve the system capacity.

When $Z_1 \leq Z_2$:

The system capacity is:

$$C = N \cdot AvgR_j \Big|_{z=Z_1} = \frac{S \cdot N}{\sum_{i \in I_0} 1/r_{i,0} + \sum_{k \neq 0} N_k / R_k} \tag{6.8}$$

It can be seen from equation (6.8) that switching an MS_i from the MR-BS to RS_j improves the capacity if and only if $r_{i,0} < R_j$. Therefore the optimal rule (*NTRS-Rate-Op-I)* is as follows: $i \in I_0$ *iff* either $r_{i,0} \geq R_j$, or $r_{i,0} > 0$ and $r_{i,j} = 0$, provided $Z_1^0 \leq Z_2^0$ holds for its resulting Z_1^0, Z_2^0. The second condition of *NTRS-Rate-Op-I* means that only the MR-BS can serve MS_i.

When $Z_1 > Z_2$:

So for the frame partition corresponding to the user rate fairness, the system wide bottleneck lies at the MSs under the most heavily loaded RS. The system capacity is:

$$C = N \cdot AvgR_j \Big|_{z=Z_2} = \frac{(S - DS) \cdot N}{\max_{j \neq 0} (\sum_{k \in I_j} 1/r_{k,j}) + \sum_{k \neq 0} N_k / R_k} \tag{6.9}$$

We designed the step-by-step switch-based rule (*NTRS-Rate-Op-II*), shown in Figure 6.7, to approximate the optimal MS association maximizing the system capacity.

Tentatively determine the MS association (MS_A_0) according to *NTRS-Rate-Op-I scheme*.
Calculate its resulting Z_1^0 and Z_2^0 from equation (6.7).
Initially $Z_1 = Z_1^0$, $Z_2 = Z_2^0$.
If $Z_1 \le Z_2$
    MS_A = MS_A_0; % stop
Else { % *NTRS-Rate-Op-II* scheme
    MS_A = MS_A_0; % start from MS_A_0
    While $Z_1 > Z_2$ {
    $k(j) = \arg\min_{i \in I_j}(r_{i,j})$; % RS-MS with the lowest SE
    $I(j) = \arg\max_{k=k(j)}\{r_{k,0}\}$; % BS-MS with the highest SE
    $K = \arg\max_{I(j)}\left(\max_{l\neq 0}(\sum_{k\in I(l)} 1/r_{k,l}) + 1/R_j - \max_{l\neq 0}(\sum_{k\in I_l,\, k\neq I(j)} 1/r_{k,l})\right)$;
    Switch MS K from its RS to BS and update MS_A, Z_1, Z_2.
    }
} % output MS_A and the capacity C by equation (6.8) or (6.9).

Figure 6.7: Optimal Association Rule in NT-RS with Rate Fairness Constraint

A perspective of the optimal rule in Figure 6.7 is: if $Z_1^0 \le Z_2^0$ holds under *NTRS-Rate-Op-I scheme*, the optimum is achieved; otherwise, the selected MSs under RSs are switched to the MR-BS, according to *NTRS-Rate-Op-II scheme*, until $Z_1 \le Z_2$. At each step, it starts from MSs with the lowest MCS levels served by the RSs, and then among them, those with the highest MCS levels from the MR-BS are picked as candidates. Finally the MS, whose switch will incur the maximum capacity among all candidates, is switched to the MR-BS.

Figure 6.8 shows the per-user rate in 1-hop and 2-hop links of the NT-RS with distributed mode in four cases for *Highest MCS*, *Highest Modified ESE* and the

optimal scheme, respectively. In Figure 6.8(a), for each case the two-fold line of 2-hop links results from the minimization of two straight lines for MR-BS–RS and RS–MS links. The turning point (Z_2) marked as the plus, is the change point of bottleneck from BSRS zone to RSMS zone. Its slope before or after the turning point (or the turning region) is roughly $(R+M\cdot r)/(M\cdot r)$ or $(R+M\cdot r)/R$, respectively. Here R and r are the average SE of the relay link and access link in 2-hop links under the rate fairness constraint, respectively, and M is the number of RS per sector. The intersection of 1-hop and 2-hop links (marked by cycle) indicates the optimal BSRS zone size (Z_1) under each MS association rule.

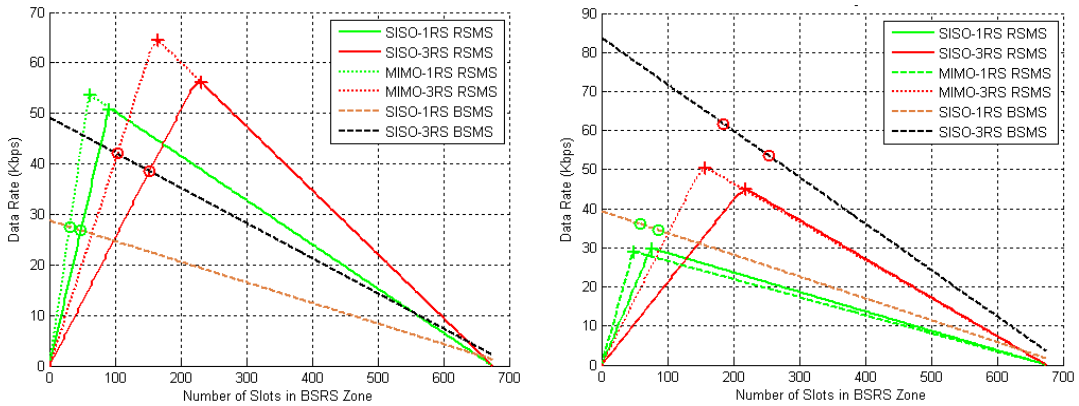

(a) Highest MCS (b) Highest Modified ESE

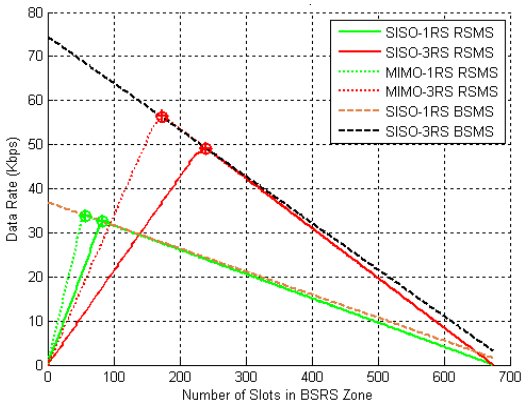

(c) the Optimal Rule

Figure 6.8: Capacity Analysis (Per-user Rate) in NT-RS in Distributed mode with Rate Fairness Constraint

Figures 6.8(a) and (b) show a typical example of MS association rule when $Z_1 \leq Z_2$ and $Z_1 > Z_2$, respectively. As shown in Figure 6.8(c), the resulting optimal rule locates in the critical situation in between. Note that *Highest Modified ESE scheme* has significantly better capacity than *Highest MCS scheme*.

6.3.3. Capacity Comparison of Different 2-Hop Relay Systems

Figure 6.9 shows the system capacity comparison with different association rules under the rate fairness constraint. The system capacity with *Highest* (*Modified*) *ESE scheme* in NT-RS is based on the different per-user rate in 1-hop and 2-hop links due to the fact that no common per-user rate exists in Figure 6.8(b).

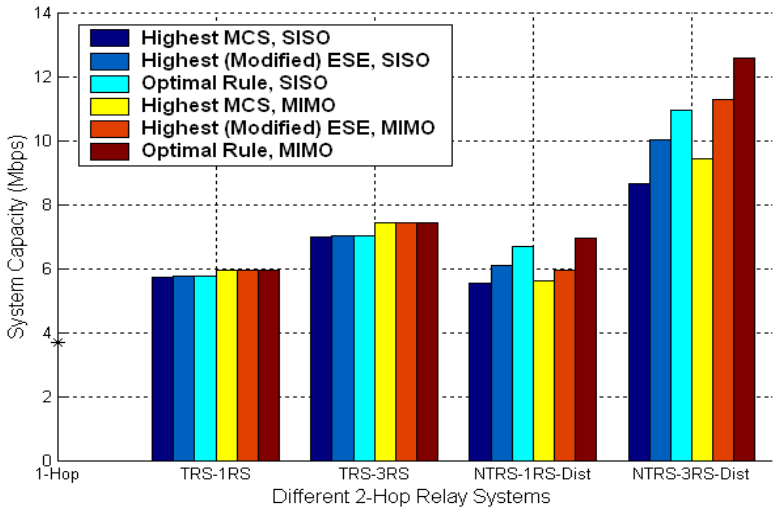

Figure 6.9: System Capacity Comparison with User Rate Fairness Constraint

In Figure 6.9, the capacity improvement brought by the RS, especially with MIMO in the relay link, is clearly visible. With any MS association rule, the highest capacity gain is achieved in NT-RS with 3 RSs per sector in distributed mode and MIMO used in the relay link. This is because the radio resources in the access link in this configuration has the highest reuse factor, therefore the resources saved by

MIMO in the relay link and then assigned to the access link can be used more fully. For example, with *Highest MCS scheme*, system capacity is improved by 133% and 155% over the 1-hop baseline system in SISO and MIMO case, respectively.

In T-RS, *Highest ESE scheme* is optimal with slightly better system capacity than *Highest MCS scheme*. While in NT-RS, *Highest Modified ESE scheme* is suboptimal but has the system capacity close to the optimal rule; it is also always significantly better than *Highest MCS scheme*. And *Highest* (*Modified*) *ESE scheme* requires only information relevant to MS itself and no iterations necessary in the computation. Hence it takes much less computation time compared with the optimal rule.

Highest (*Modified*) *ESE scheme* can be realized as follows: for T-RS, the MR-BS performs the scheduling function with the known access and relay links' qualities; while for the NT-RS in distributed scheduling mode, to calculate the modified ESE, the MR-BS and RSs need to exchange the information: access and relay links' qualities, access station type (MR-BS/RS) and the number of RSs per sector.

6.4. Conclusions

IEEE 802.16j multi-hop relay task standard draft 16jD2 includes two mutually exclusive options: transparent relay system (T-RS) and non-transparent relay system (NT-RS). A system design approach is proposed to compare these different options in term of capacity with rate fairness constraint. The effect of the number of RSs (1 or 3) and different antenna systems (SISO or MIMO) in the MR-BS–RS link are considered. The simulation results show that NT-RS with 3 RSs per sector in distributed mode always achieves the highest system capacity, and that both 3 RSs per sector case and MIMO can improve the system capacity. Furthermore, two

heuristic MS association rules: *Highest MCS scheme* and *Highest* (*Modified*) *ESE scheme* are presented and compared with the formulated optimal rule that maximizes system capacity under user rate fairness constraint. It is shown that *Highest* (*Modified*) *ESE scheme* is optimal in T-RS; and that as a suboptimal rule in NT-RS, it has the system capacity close to the optimal rule with much less information exchange and computation time.

More details of the resource allocation in 802.16j multi-hop relay systems under the user rate fairness constraint can be found in our paper [103]. Considering another popular fairness constraint, the user resource fairness constraint, the capacity analysis and resource allocation are different. With the definition of per-user resource, in our paper [104], we investigate the MS association rules by presenting a reference optimal scheme, proposing a switch-based heuristic optimal scheme, and comparing *Highest MCS scheme* and *Highest* (*Modified*) *ESE scheme* with these two optimal schemes.

A relevant study of frequency assignment schemes in 802.16e systems with femtocell size is presented in our paper [105]. We first investigate the effect of the TX power at femto-BSs (fBSs), cell radius and loading factor in WiMAX femtocells. Furthermore, several heuristic frequency assignment schemes are proposed and compared along with the random assignment scheme that randomly assigns one of three segments for each fBS. The optimal pattern is also presented and serves as a comparison basis. The performance metrics of interest include the average received total interference at an individual fBS, system coverage and capacity.

Bibliography

[1] B. Elbert, "Introduction to Satellite Communication", Artech House, Boston, 1999.

[2] Kul Bhasin, Jeffrey L. Hayden, "Space Internet Architecture and Technologies for NASA Enterprises", 2001 IEEE Aerospace Conference, March 2001.

[3] W. Ivancic, T. Bell, D. Shell, "Deployment Tests of COTS Networking Equipment in STS and ISS", First Space Internet Workshop, NASA Goddard, November 2000.

[4] M. Hadjitheodosiou and A. Nguyen, "Extending IP Services to Space Missions", Proc. 19th AIAA ICSSC, Toulouse, France, April 2001.

[5] James Rash, Keith Hogie, and Ralph Casasanta, "Internet Data Delivery for Future Space Missions", 2002 Earth Science Technology Conference, June 2002.

[6] James Rash, Ron Parise and Keith Hogie, Ed Criscuolo, Jim Langston, Internet technology on spacecraft, Space 2000 Conference, Long Beach, CA, Sep. 21, 2000.

[7] Operating Missions as Nodes on the Internet, (OMNI), NASA GSFC, http://ipinspace.gsfc.nasa.gov.

[8] Phillip E. Paulsen, William D. Ivancic, David Stewart, Terry L. Bell, Lloyd Wood, Dan Shell, Phill Ardire, Brett Conner PhD, Larry Dikeman, Donald Van Drei, Steve Groves, Eric Miller: "Cisco Router in Low Earth Orbit", Draft, http://roland.grc.nasa.gov/~ivancic/papers_presentations/papers.html.

[9] R. Bolla, F. Davoli and M. Marchese, "Adaptive Bandwidth Allocation Methods in the Satellite Environment", Proceedings of ICC 2001, pp. 3183 – 3190, June 2001.

[10] Kul Bhasin and Jeffery L. Hayden, "Developing Architectures and Technologies for an Evolvable NASA Space Communication Infrastructure", Proceedings 22nd AIAA International Communications Satellite Systems Conference & Exhibit 2004 (ICSSC'22), Monterey, California.

[11] IEEE Std 802.16-2004: "Air Interface for Fixed Broadband Wireless Access Systems", Oct. 2004.

[12] IEEE Std 802.16e: "Air Interface for Fixed and Mobile Broadband Wireless Access Systems" with Amendment 2: "Physical and Medium Access Control Layers for Combined Fixed and Mobile Operation in Licensed Bands" and Corrigendum 1.

[13] Ki-Dong Lee, "Throughput-Maximizing Timeslot Scheduling for Interactive Satellite Multiclass Services", IEEE Communications Letters, Vol. 7, No. 6, June 2003.

[14] Marc Emmelmann and Hermann Bischl, "An Adaptive MAC Layer Protocol for ATM-based LEO Satellite Networks", Proc. VTC 2003, Orlando, FL, Oct. 2003.

[15] William Stallings, "Wireless Communications and Networks", Upper Saddle River, NJ: Prentice Hall, 2002.

[16] Theodore S. Rappaport, "Wireless Communications: Principles and Practice", 2nd Edition, Upper Saddle River, NJ: Prentice Hall, 2002.

[17] Dimitri Bertsekas and Robert Gallager, Data Network, 2nd Edition, NJ: Prentice Hall, Upper Saddle River, 1992.

[18] Hui Zhang, “Service Disciplines for Guaranteed Performance Service in Packet-switching Networks”, Proc. IEEE, vol. 83, pp. 1374-1396, Oct. 1995.
[19] L. G. Roberts, “Dynamic allocation of satellite capacity through packet reservation”, AFIPS Conference Proceedings, 1973, Vol.42, pp. 711-716.
[20] W. Szpankowski, “Analysis and Stability Considerations in a Reservation Multiaccess System”, IEEE Trans., 1983, COM-31, pp. 684-692.
[21] N. Celandron, E. Ferro and F. Potorti, “Demand Assignment TDMA Satellite Schemes: Distributed and Centralized Solutions”, Proc. Of IEEE International Conference on Communications: Converging Technologies for Tomorrow’s Applications, Dallas, Texas, USA, Jun. 1996, pp. 911-914.
[22] D. A. Dyson and Z. J. Haas, “The Dynamic Packet Reservation Multiple Access Scheme for Multimedia Traffic”, ACM/Baltzer Journal of Mobile Networks and Applications, 1999.
[23] E. Hossain and V. K. Bhargava, “A Centralized TDMA-based Scheme for Fair Bandwidth Allocation in Wireless IP Network”, IEEE Journal on Selected Areas in Communications, Vol. 19, pp. 2201-2214, Nov. 2001.
[24] Hui Zeng, Ermos Zimboulakis, Michael Hadjitheodosiou and Brenda Ellis, "Efficient, Flexible and Secure Access for the Future NASA Communications Network", Proc. 22nd AIAA International Communications Satellite Systems Conference & Exhibit 2004 (ICSSC'22), Monterey, California
[25] Hui Zeng and M. Hadjitheodosiou, "Traffic Modeling and Dynamic Access for the Future NASA Communications Network", Proc. 21st AIAA International Communications Satellite Systems Conference, Yokohama, Japan, April 2003.
[26] R. Srinivasan and Arun K. Somani, “On Achieving Fairness and Efficiency in High-Speed Shared Medium Access”, IEEE/ACM Trans. on Networking, Vol. 11, No. 1, February 2003.
[27] Le-Ngoc and S. V. Krishnamurthy, “Performance of combined free/demand assignment multiple-access schemes in satellite communications,” International Journal of Satellite Communication, vol. 14, no. 1, pp. 11–21, Jan./Feb. 1996.
[28] Anthony Hung and Marie-Jose Montpetit, et al., “A Framework for ATM via Satellite”, Proc. IEEE GLOBECOM, London, UK, 1996.
[29] T. Nguyen and T. Suda, “Survey and Evaluation of Multiple Access Protocols in Multimedia Satellite Networks”, pages 408-413, IEEE Southeastcon’90, Session 5D3, 1990.
[30] T. Zein, G. Maral and M. Tondriaux, et al., “A Dynamic Allocation Protocol for a Satellite Network Integrated with B-ISDN”, Proc. 2nd ECSC, pages 15-20, 1991.
[31] T. Zein, G. Maral and T. Brefort, et al., “Performance of Combined/Fixed Reservation Assignment (CFRA) scheme for aggregate traffic”, pages 183-199, COST 226 Integrated Space/Terrestrial Networks Final Symposium, Budapest, Hungary, 10-12 May 1995.
[32] G. Acar and C. Rosenberg, “Algorithms for Bandwidth on Demand”, 5th Ka-band Utilization Conference, Taormina, Italy, October 1999.
[33] G. Acar and C. Rosenberg, “Performance Study of End-to-End Resource Management in ATM Geostationary Satellite Networks with On-Board

Processing", Space Communications Journal, Invited Paper, Vol. 17, No. 1-3 (2001), pp. 89-106.
[34] Dennis Connors, Bo Ryu, Gregory J. Pottie and Son Dao, "A Medium Access Control Protocol for Real Time Video over High Latency Satellite Channels", ACM MONET Journal, 7(1):9-20, 2002.
[35] Paul D. Mitchell, David Grace and Tim Tozer, "Burst Targeted Demand Assignment Multiple-Access for Broadband Internet Service Delivery over Geostationary Satellite", IEEE JSAC, Vol. 22, No. 3, April 2004.
[36] Henry Chan, Jie Zhang and Hui Chen, "A Dynamic Reservation Protocol for LEO Mobile Satellite Systems", IEEE JSAC, Vol. 22, No. 3, April 2004.
[37] Y. Cao and V. O. K. Li, "Scheduling algorithms in broadband wireless networks", Proceedings of the IEEE, Vol. 89, No. 1, pp. 76-87, January 2001.
[38] J. Chen, W. Jiao, H. Wang, "A service flow management strategy for IEEE 802.16 broadband wireless access systems in TDD mode", IEEE ICC 2005, Vol. 5, pp. 3422-3426, May 2005.
[39] S. Shakkottai and R. Sricant, "Scheduling real-time traffic with deadlines over a wireless channel", ACM/Beltzer Wireless Networks Journal, Vol. 8, No. 1, pp. 13-26, 2001.
[40] S. Lu, V. Bharghavan and R. Sirkant, "Fair scheduling in wireless packet networks", IEEE Transactions on Communications Network, Vol. 7, No. 4, pp. 473-489, August 1999.
[41] Y. Liu, S. Gruhl and E. W. Knightly, "WCFQ: an opportunistic wireless scheduler with statistical fairness bounds", IEEE Transactions on Wireless Communications, Vol. 2, No. 5, pp. 1017-1028, September 2003.
[42] T.-D. Nguyen and Y. Han, "A proportional fairness algorithm with QoS provision in downlink OFDMA systems", IEEE Communications Letters, Vol. 10, No. 11, November 2006.
[43] T. S. Eugene Ng, I. Stoica and H. Zhang, "Packet Fair Queueing Algorithms for Wireless Networks with Location-dependent Errors", Proc. INFOCOM 98, pp. 1103-1111, March 1998.
[44] P. Bhagwat, A. Krishna and S. Tripathi, "Enhancing Throughput over Wireless LAN's Using Channel State Dependent Packet Scheduling", Proc. INFOCOM 96, pp. 1133-1140, March 1996.
[45] S. Floyd and V. Jacobson, "Link-sharing and Resource Management Models for Packet Networks", IEEE/ACM Transaction on Networking, Vol. 3, pp. 365-386, August 1995.
[46] C. Fragouli, V. Sivaraman and M. Srivastava, "Controlled Multimedia Wireless Link Sharing via Enhanced Class-Based Queueing with Channel-State Dependent Packet Scheduling", Proc. INFOCOM 98, Vol. 2, pp. 572-580, March 1998.
[47] S. Lu, V. Bharghavan and R. Sirkant, "Fair scheduling in wireless packet networks", IEEE Transactions on Communications Network, Vol. 7, No. 4, pp. 473-489, August 1999.
[48] T. S. Eugene Ng, I. Stoica and H. Zhang, "Packet Fair Queueing Algorithms for Wireless Networks with Location-dependent Errors", Proc. INFOCOM 98, pp. 1103-1111, March 1998.

[49] P. Goyal, H. M. Vin and H. Chen, "Start-time Fair Queueing: A Scheduling Algorithm for Integrated Services", Proc. ACM/SIGCOMM 96, pp. 157-168, Palo Alto, CA, August 1996.
[50] A. Gyasi-Agyer and S. Kim, "Cross-Layer Multiservice Opportunistic Scheduling for Wireless Networks", IEEE Communications Magazine, Vol. 44, No. 6, pp. 50-57, June 2006.
[51] A Jalali, R. Padovani and R. Pankaj, "Data Throughput of CDMA-HDR: A High Efficiency-High Data Rate Personal Communication Wireless System", Proc. IEEE VTC 2000-spring, pp. 1854-1858, Tokyo, Japan, May 2000.
[52] "1xEV: 1x Evolution IS-856 TIA/EIA Standard - Airlink Overview", QUALCOMM Inc. White Paper, Section 2.5, November 2001.
[53] S. J. Golestani, "Congestion-free transmission of real-time traffic in packet networks", in Proc. IEEE INFOCOM '90, San Fransisco, CA, pp. 527-536, 1990.
[54] Paul D. Mitchell, David Grace and Tim C. Tozer, "Analytical model of round-robin scheduling for a geostationary satellite system", Communications Letters, IEEE, Vol. 7, Issue 11, Pages: 546 – 548, Nov. 2003.
[55] Abhay Parekh and Robert Gallager, "A Generalized Processor Sharing Approach to Flow Control in Integrated Services Networks: The Single-Node Case", IEEE/ACM Transactions on Networking, Vol. 1, No. 3, June 1993.
[56] Sanjay Shakkottai and R. Srikant, "Scheduling Real-time Traffic with Deadlines over a Wireless Channel", Proc. 2nd ACM Int. Workshop on Wireless Mobile Multimedia, pp. 35-42, 1999.
[57] "Implementation Guide for the Use of the Internet Protocol Suite in Space Mission Communications", Release 1.0, Sept. 2003, Information Systems Division, NASA Goddard Space Flight Center, Greenbelt, Maryland.
[58] CCSDS 102.0-B-5, "Recommendation for Space Data System Standards: Packet Telemetry, Consultative Committee for Space Data Systems", Blue Book, Nov. 2000.
[59] M. Hadjitheodosiou, E. Geraniotis, "Optimizing TDMA Bandwidth Allocation in Broadband Satellite Networks", 17th AIAA Int. Conf. Sat. Comms Systems, Yokohama, Japan, April 1998.
[60] "TDRSS—Tracking and Data Relay Satellite System" from "Mission and Spacecraft Library", http://msl.jpl.nasa.gov/Programs/tdrss.html.
[61] Space Network Users Guide (SNUG) - Revision 8, June 2002, NASA GSFC, Mission Services Program Office, shttp://msp.gsfc.nasa.gov/tdrss/guide.html.
[62] Lin Lin, "On-Demand Multiple Access for Next-Generation NASA Missions", Master's Thesis, Department of ECE, University of Maryland, College Park 2001.
[63] Frank Kelly, "Charging and Rate Control for Elastic Traffic", European Transactions on Telecommunications, Vol. 8, Pages 33-37, January 1997.
[64] Haïkel Yaïche, Ravi R. Mazumdar and Catherine Rosenberg, "A Game Theoretic Framework for Bandwidth Allocation and Pricing in Broadband Networks", IEEE/ATM Transaction on Network, Vol. 8, No. 5, October 2000.
[65] Michel Minoux, "Mathematical Programming: Theory and Algorithms", Wiley, Chichester, 1986.

[66] Hui Zeng, Michael Hadjitheodosiou and John Baras, "Two-level Dynamic Bandwidth Allocation for a Space-to-Ground Relay Network", IEEE GLOBECOM 2006, San Francisco, California, Nov. 27-Dec. 1, 2006.
[67] Hui Zeng, Michael Hadjitheodosiou and John Baras, "Dynamic Bandwidth Allocation for a Space Relay Communications Network", 2006 IEEE Systems and Information Engineering Design Symposium (SIEDS), Charlottesville, Virginia, April 28, 2006.
[68] Hui Zeng, Michael Hadjitheodosiou and John Baras, "Dynamic Resource Allocation for an IP-based Communications Network Supporting Space Exploration", Proc. 23rd AIAA International Communications Satellite Systems Conference (ICSSC-2005), Rome, Italy, 25-28 Sept. 2005.
[69] Hui Zeng, Alex Nguyen and Michael Hadjitheodosiou, "Flexible Access for a Space Communications Network with IP Functionality", Computer Networks, Volume 47, Special Issue on "Extending the Internet to Space", pp. 679-700, 2005.
[70] Flavio Bonomi, Debasis Mitra and Judith B. Seery. "Adaptive algorithms for feedback-based flow control in high-speed wide-area ATM networks", IEEE Journal on Selected Areas in Communications, 13(7):1267--1283, September 1995.
[71] A. I. Elwalid, "Adaptive rate-based congestion control for high speed wide-area networks: stability and optimal design", Proc. of ICC'95, pp. 1948–1953, San Francisco, CA, 1995.
[72] K. K. Ramakrishnan and R. Jain, "A binary feedback scheme for congestion avoidance in computer networks with a connectionless network layer", Proc. ACM SIGCOMM '88, pp. 303-313.
[73] L. Zhang, "A new architecture for packet switching network protocols", Ph.D. Thesis, MIT, Lab. For computer Science, Cambridge, MA, 1989.
[74] S. Keshav, "Packet-Pair Flow Control", IEEE/ACM Transactions on Networking, February 1995.
[75] Frank Kelly, A. Maulloo, and D. Tan, "Rate control for communication networks: shadow prices, proportional fairness and stability", Journal of the Operational Research Society, 49(3):237-252, March 1998.
[76] Richard J. La and Priya Ranjan, "Stability of rate control system with time-varying communication delays", Technical Report, ISR TR 2004-31, 2004.
[77] F. Mazenc and S.-I. Niculescu. "Remarks on the stability of a class of tcp-like congestion control models", Decision and Control, 2003. Proc. 42nd IEEE Conference on Vol. 6, 9-12, pp. 5591 – 5594, Dec. 2003.
[78] T. Alpcan and T. Basar, "A utility-based congestion control scheme for Internet-style networks with delay", INFOCOM 2003, 22nd Annual Joint Conference of the IEEE Computer and Communications Societies, IEEE Vol. 3, pp. 2039 – 2048, March 30-April 3, 2003,.
[79] R. Johari and D. Tan, "End-to-end congestion control for the Internet: Delays and stability", IEEE/ACM Transactions on Networking, Vol. 9, Issue 6, pp. 818-832, Dec. 2001.
[80] S. Deb and R. Srikant, "Global stability of congestion controllers for the Internet", in Proc. of the 41st IEEE Conference on Decision and Control, Vol. 4, 10-13, pp. 3626-3631, Dec. 2002.

[81] P. Ranjan, R. J. La, and E. H. Abed, "Global Stability in the Presence of Distributed Communication Delays", American Control Conference 2005, Portland, OR, 2005.
[82] Huigang Chen, Ph.D. dissertation, "Network Flow Optimizations and Distributed Control Algorithms", University of Maryland, College Park, MD, 2006.
[83] P. Ranjan, R. J. La, and E. H. Abed, "Global stability in the presence of state-dependent delay for rate control", in Proc. of CISS, Oahu, HI, 2004.
[84] Hassan K. Khalil, "Nonlinear Systems", Prentice Hall, Upper Saddle River, NJ, 2002.
[85] K. W. Fendick, M. A. Rodrigues and A. Weiss, "Analysis of Rate-based Feedback Control Strategy for Long Haul Data Transport", Performance Evaluation, vol. 16, pp. 67-84, 1992.
[86] R. Jain, D. Chiu and W. Hawe, "A Quantitative Measure of Fairness and Discrimination for Resource Allocation in Shared Computer System", Technical Report DEC-TR-301, Digital Equipment Corporation, September 26, 1984.
[87] "WiMAX System Evaluation Methodology", Version 1.0, WiMAX Forum, 01/30/2007.
[88] "Multi-hop Relay System Evaluation Methodology (Channel Model and Performance Metric)", IEEE 802.16 Broadband Wireless Access Working Group, IEEE 802.16j-06/013r3, 02/19/2007.
[89] Hui Zeng and Chenxi Zhu, "System-Level Modeling and Performance Evaluation of Multi-hop 802.16j Systems", International Wireless Communications and Mobiel Computing Conference 2008 (IWCMC 2008), Crete Island, Greece, August 2008.
[90] Masato Okuda, Chenxi Zhu and Dorin Viorel, "Multihop Relay Enabled WiMAX Networks: Overview & Benefits of IEEE Draft P802.16j Standard", Fujitsu Scientific & Technical Journal (FSTJ), special issue on "Fujitsu's Mobile WiMAX Solutions", vol. 44, no. 3, July 2008.
[91] E. Visotsky, Junjik Bae, R. Peterson, R. Berry and M.L. Honig, "On the Uplink Capacity of an 802.16j System", IEEE Wireless Communications and Networking Conference 2008 (WCNC 2008), pp. 2657-2662, March 31– April 3, 2008.
[92] I-Kang Fu, Wern-Ho Sheen and Fang-Ching Ren, "Deployment and Radio Resource Reuse in IEEE 802.16j Multi-hop Relay Network in Manhattan-like Environment", 2007 6th International Conference on Information, Communications & Signal Processing (ICICS 2007), Dec. 10-13, 2007.
[93] Y. Sun, Y.Q. Bian, P. Strauch and A.R. Nix, "Study of radio resource sharing for future mobile WiMAX applications with relays", IEEE Mobile WiMAX Symposium, March 25-29, 2007.
[94] Liu Erwu, Wang Dongyao, Liu Jimin, Shen Gang and Jin Shan, "Performance Evaluation of Bandwidth Allocation in 802.16j Mobile Multi-hop Relay Networks", in Proc. IEEE VTC 2007-Spring, pp. 939-943, April 2007.
[95] Michael Einhaus, Ole Klein and Bernhard Walke, "Comparison of OFDMA Resource Scheduling Strategies with Fair Allocation of Capacity", 2008 5th IEEE Consumer Communications & Networking Conference (CCNC 2008), Las Vegas, NV, January 2008.

[96] IEEE Std 802.16j Baseline: “Air Interface for Fixed and Mobile Broadband Wireless Access Systems, Multihop Relay Specification”. IEEE 802.16j-06/026r4.
[97] “Harmonized Contribution on 802.16j (Mobile Multihop Relay) Usage Models”, IEEE 802.16 Broadband Wireless Access Working Group, IEEE 802.16j-06/015, 09/05/2006.
[98] “Multi-hop Path Loss Model (Base-to-Relay and Base-to-Mobile)”, IEEE C802.16j-6/011, May 2006.
[99] “Channel Models for Fixed Wireless Applications”, IEEE 802.16.3c-01/29r4, July 21, 2001.
[100] “802.20 Channel Models Document for IEEE 802.20 MBWA System Simulations”, IEEE 802.20-PD-08, September 6, 2005.
[101] Beijing University of Post and Telecommunication, “EESM Beta Training in 802.16e System”, WiMAX Forum AATG, August 17, 2007.
[102] V. Erceg, P. Soma, D. Baum and A. Paulraj, “Capacity obtained from MIMO channel measurements in fixed wireless environments at 2.5 GHz”, Proceedings of IEEE ICC 2002, New York, 2002.
[103] Hui Zeng, Chenxi Zhu, “System Design and Resource Allocation in 802.16j Multi-hop Relay Systems under the User Rate Fairness Constraint”, submitted to IEEE ICC 2009, June 2009.
[104] Hui Zeng, Chenxi Zhu, “Resource Allocation in 802.16j Multi-hop Relay Systems with the User Resource Fairness Constraint”, submitted to IEEE WCNC 2009, April 2009.
[105] Hui Zeng, Chenxi Zhu, Wei-Peng Chen, "System Performance of Self-Organizing Network Algorithm in WiMAX Femtocells", invited paper to WICON 2008, Nov. 2008.